



저작자표시-비영리-변경금지 2.0 대한민국

이용자는 아래의 조건을 따르는 경우에 한하여 자유롭게

- 이 저작물을 복제, 배포, 전송, 전시, 공연 및 방송할 수 있습니다.

다음과 같은 조건을 따라야 합니다:



저작자표시. 귀하는 원저작자를 표시하여야 합니다.



비영리. 귀하는 이 저작물을 영리 목적으로 이용할 수 없습니다.



변경금지. 귀하는 이 저작물을 개작, 변형 또는 가공할 수 없습니다.

- 귀하는, 이 저작물의 재이용이나 배포의 경우, 이 저작물에 적용된 이용허락조건을 명확하게 나타내어야 합니다.
- 저작권자로부터 별도의 허가를 받으면 이러한 조건들은 적용되지 않습니다.

저작권법에 따른 이용자의 권리는 위의 내용에 의하여 영향을 받지 않습니다.

이것은 [이용허락규약\(Legal Code\)](#)을 이해하기 쉽게 요약한 것입니다.

[Disclaimer](#)

공학박사 학위논문

도시협곡에서의 바람유동과 오염물질 이송에 관한 수치적 연구

Numerical Simulation of Wind Flow and Pollutant Transport in Urban Street Canyon

2021 년 2 월

서울대학교 대학원

건설환경공학부

Nguyen Thanh Chuyen

Numerical Simulation of Wind Flow and Pollutant
Transport in Urban Street Canyon

지도교수 Van Thinh Nguyen

이 논문을 공학박사 학위논문으로 제출함

2021년 1월

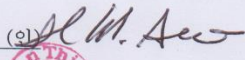


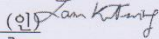
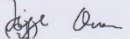
서울대학교 대학원

건설환경공학부

Nguyen Thanh Chuyen

Nguyen Thanh Chuyen의 박사학위논문을 인준함

2021년 1월

위 원 장	서 일 원	(인) 
부 위 원 장	Van Thinh Nguyen	(인) 
위 원	Hermann J. Eberl	(인) 
위 원	Kit Ming Lam	(인) 
위 원	Steven Jige Quan	(인) 

ABSTRACT

In this thesis, a numerical model based on an open source CFD package OpenFOAM is developed in order to investigate the flow pattern and pollutant dispersion in urban street canyons with different geometry configurations. In the new model, the pollutant transport driven by airflow is modelled by the scalar transport equation coupling with the momentum equations for airflow, which are deduced from the RANS (Reynolds Averaged Navier-Stokes) equations. The turbulent flow calculation has been calibrated by various two-equation turbulence closure models, such as standard k - ϵ , RNG k - ϵ , realizable k - ϵ , k - ω , k - ω SST, to select a practical and efficient turbulence model to reasonably capture the flow pattern. There are two approaches for the scalar transport equation to calculate the turbulent scalar flux term: Standard Gradient Diffusion Hypothesis (SGDH) approach and Generalized Gradient Diffusion Hypothesis (GGDH) approach. The GGDH approach shows better results than the SGDH approach, and it overcome the limitation of the SGDH approach caused by time consuming calibration of the turbulent Schmidt number.

The numerical model has been validated against different well-known laboratory experiments in regard to various aspect ratios (a relationship between the building height and the width of street canyon), and different building roof shapes (flat, shed, gable, and round). The comparisons between the numerical simulations and experimental measurements show a good agreement on the flow pattern and pollutant distribution. The numerical model has also provided reasonable agreement with experiment data in three-dimensional problem. It shows the ability of the new numerical model, which can be applied to investigate the wind flow and pollutant dispersion in real urban street area.

Eventually, the numerical model has been applied to a real urban street canyon, the Shinjuku special ward of Tokyo; which contains a large number of skyscrapers,

and poses several interesting wind engineering problems including how the wind shed will affect pedestrians nearby and the microclimate of the surrounding region. The simulation results show that the new model can capture the wind flow in the Shinjuku urban street canyon.

Keyword: Numerical simulation, Wind flow, Pollutant transport, Urban street canyon, OpenFOAM

Student number: 2013-30777

TABLE OF CONTENTS

ABSTRACT	i
TABLE OF CONTENTS	iii
NOMENCLATURE	vi
1. INTRODUCTION.....	1
1.1. Motivation of the work	1
1.2. Necessity and Objectives	5
1.3. Structure of thesis	7
2. LITERATURE REVIEW	9
2.1. Flow characteristics of idealized street canyon	15
2.2. The influence of wind condition.....	18
2.3. Turbulence transfer between a street canyon and the atmosphere.....	20
2.4. Characteristics of pollutant dispersion inside street canyon	21
2.5. The influence of geometry of street canyons	23
2.6. Schmidt number	25
2.7. Three-dimensional modelling.....	26
2.8. CFD modelling of street canyon flow.....	27
3. METHODOLOGY.....	31
3.1. Reynolds-Averaged Navier-Stokes Equation (RANS)	31
3.2. Turbulence models and validation.....	33
3.2.1. The standard $k-\varepsilon$ model.....	34
3.2.2. The RNG $k - \varepsilon$ model	36
3.2.3. The realizable $k-\varepsilon$ model.....	37
3.2.4. The $k-\omega$ model.....	38
3.2.5. The SST $k-\omega$ model	38
3.2.6. Validation of RANS models.....	39
3.3. Scalar transport equation and the implementation of code	44
3.3.1. Standard Gradient Diffusion Hypothesis (SGDH).....	44

3.3.2.	Generalized Gradient Diffusion Hypothesis (GGDH)	46
3.3.3.	Implementation of the scalar transport equation in OpenFOAM....	47
3.3.4.	Validation of the SGD approach.....	50
3.3.5.	Validation of the GGDH approach	51
3.4.	Initial and boundary condition	52
3.4.1.	Boundary type.....	52
3.4.2.	Boundary position.....	53
3.4.3.	Inlet boundary profile.....	54
4.	VALIDATION OF CFD MODELS.....	58
4.1.	Studying the flow characteristics in street canyon with different aspect ratios by comparison to Li (2008)'s experiment	58
4.1.1.	Description of experiment setup	58
4.1.2.	Street canyon of $AR = 1$	60
4.1.3.	Street canyon of $AR = 2$	66
4.1.4.	Street canyon of $AR = 0.5$	71
4.2.	Studying the air dispersion in various roof shapes by validating against Kastner-Klein and Plate (1999)'s experiment	77
4.2.1.	Description of the experiment setup	77
4.2.2.	Validation and discussion.....	80
4.3.	Validation of round-shaped roof against the measurement data from Llaguno-Munitxa et al.'s experiment (2017).....	82
4.4.	Validation against CEDVAL data to study the flow characteristics for 3-D isolated building	85
4.4.1.	Simulation setup	85
4.4.2.	Validation of the isolated rectangular building simulation.....	88
5.	APPLICATION – A CASE STUDY OF AIRFLOW AND POLLUTANT DISPERSION IN SHINJUKU URBAN AREA IN TOKYO	93
6.	CONCLUSIONS AND FUTURE WORK.....	102
6.1.	To develop a reliable and economic tool to study flow in urban street canyon	102
6.2.	To study the impact of various roof shapes and different aspect ratios on air flow and pollutant dispersion in street canyons.	102
6.2.1.	Effect of aspect ratios on flow patterns	102

6.2.2.	Effect of roof shapes on the flow patterns and pollutant distribution	104
6.3.	To develop a method to adjust accurately Schmidt number	106
6.4.	Application to a real urban area.....	107
6.5.	Future work	107
REFERENCE	109
Appendix – Implementation of a solver in OpenFoam	123
초록	138

NOMENCLATURE

Latin symbols

B	street width
C	pollutant concentration
$C_{1\varepsilon}$	model constant in the RANS model
$C_{2\varepsilon}$	model constant in the RANS model
C_μ	model constant in the RANS model
H	building height of idealized buildings
H_1	the height of upstream building in a row of buildings
H_2	the height of downstream building in a row of buildings
I	turbulent intensity
L	building length
L_q	length of emission source
K	non-dimensional pollutant concentration
Re	Reynolds number calculated by free-stream velocity
S	characteristic mean strain rate
Sc_t	turbulent Schmidt number
U	velocity magnitude or x component of velocity
U_0	free-stream velocity
U_{ref}	velocity at reference height
U_i	i components of velocity
k	turbulent kinetic energy
y^+	dimensionless wall-distance calculated by dimensionless velocity near the wall
z	Cartesian coordinate, normal to ground
z_0	roughness length
z_{ref}	reference height

Greek symbols

α	power-law index
β	model constant in the RANS model
η	intermediate quantity in the RNG k- ε equation
η_0	model constant in the RNG k- ε equation
σ_k	turbulent Prandtl number in k-equation
σ_ε	turbulent Prandtl number in ε -equation
δ	boundary layer height
δ_{ij}	Kronecker delta
ρ	density
ε	turbulent dissipation
κ	von Karman constant
μ	dynamic viscosity
ν	kinematic viscosity
ν_t	turbulent kinematic viscosity
ω	specific rate of dissipation

Acronyms

2D	two-dimensional
3D	three-dimensional
ABL	Atmospheric Boundary Layer
AR	Aspect Ratio
CFD	Computational Fluid Dynamics
DNS	Direct Numerical Simulation
TKE	Turbulent Kinetic Energy
LES	Large Eddy Simulation

N-S	Navier-Stokes
RANS	Reynolds-Averaged Navier-Stokes
RNG	Re-Normalization Group
RSM	Reynolds Stress Model
SIMPLE	Semi-Implicit Method for Pressure Linked Equations
SST	Shear Stress Transport

1. INTRODUCTION

1.1. Motivation of the work

As of 2015, more than half of the world's population is living in towns or cities. The number of urban dwellers rose from 729 million in 1950 to 3.9 billion in 2014. By 2050, two out of three humans are expected to be living in urbanized areas (UN, 2014). The United Nations (UN) and the World Bank anticipate a rapid increase of the percentage of the world population living in urban areas within the course of the 21st century (Fig.1.1). This change is expected to occur due to the increase in the number of cities, migration from rural to urban areas and transformation of some rural settlements into urban areas (UN, 2011). Recently, making “cities and human settlements climate resilient and sustainable” is marked as one of the sustainable development goals by the UN (UN, 2015). As a result, research on sustainable habitats and related topics is gaining importance and will continue to do so in the coming years (Martos, 2016). The global tendency towards urbanization deteriorates the urban air quality, thus amplifying the risk of exposure of citizens to discomfort and health hazards.

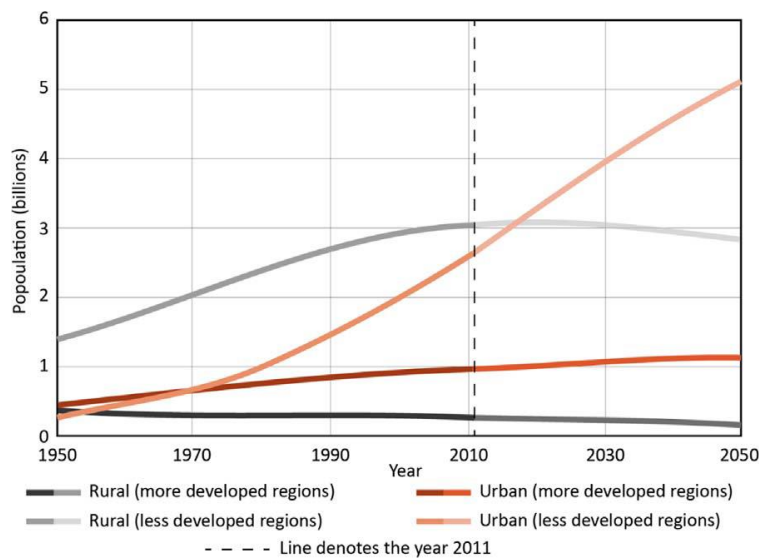


Figure 1.1. World population in urban and rural areas (UN, 2011).

Air pollution can harm human health. According to the U.S Centers for Disease Control and Prevention (CDC), increasing PM_{2.5} air pollution has been linked to cancer, heart disease, pneumonia and low birth weight. Also, it has been noticed that Koreans suffer from mental distress and are at risk of respiratory problems. Korean researchers have suggested an association with Parkinson, cardiovascular illnesses and other neurological diseases (Fifield, 2017). Pollution has been linked to increased illness and deaths in South Korea. For example, exposure to sulfur dioxide causes chronic lung disease and respiratory disorders. Exposure to ozone and particulate matter is associated with respiratory and circulatory diseases and increased mortality (Park, 2015).

In order to provide public health protection and public welfare protection, environment agencies around the world, such as United States Environmental Protection Agency and European Environment Agency, have established regional air quality standards. These standards limit the exceedance of daily and annual levels of several principal pollutants (i.e., carbon monoxide, lead, nitrogen dioxide, ozone and sulfur dioxide) and particulate matters. However, they are not met in many member countries. For example, the UK has been facing up to £300m fines due to failing to meet a key air quality directive for a long time (Johnston, 2014). In Korea, the Korean Government is planning on providing air purification systems for public facilities and schools consisting of air purifiers and air purifying plants (Kim, 2019a). The government has also taken action of improving air quality in the Seoul Capital region by implementing the Special Act on Seoul Metropolitan Air Quality Improvement in 2003 December (Kim, 2019b).

An atmospheric boundary layer is defined as a layer directly influenced by surface friction. It is generally classified into three sub-layers: roughness, inertial, and mixed (Figure 1.2). The turbulence in the roughness sub-layer is fully three-dimensional and significantly depends on the properties of roughness at the surface. The oncoming wind flow is retarded by the ground buildings, parks, and trees. Wind flow inside the roughness sub-layer then becomes three-dimensional and

turbulent. In various climate conditions, the inertial sub-layer will compress the roughness layer. As a result, the roughness boundary could also be called an urban canopy layer. The height-scale of the urban canopy layer is the approximately building height. The flow in the inertial sub-layer mainly depends on the degree of open roughness surface retarding the wind flow. The flow field and pollutant dispersion inside layer will directly influenced by atmospheric stability, which is normally ruled by Monin-Obukhov similarity theory. The turbulence generated by buoyancy effect dominates the mixed layer, while wind-induced shear stress dominates the urban canopy layer and inertial sub-layer (Rotach, 1993; Easong, 2000; Roth, 2000; Bernard et al., 2005).

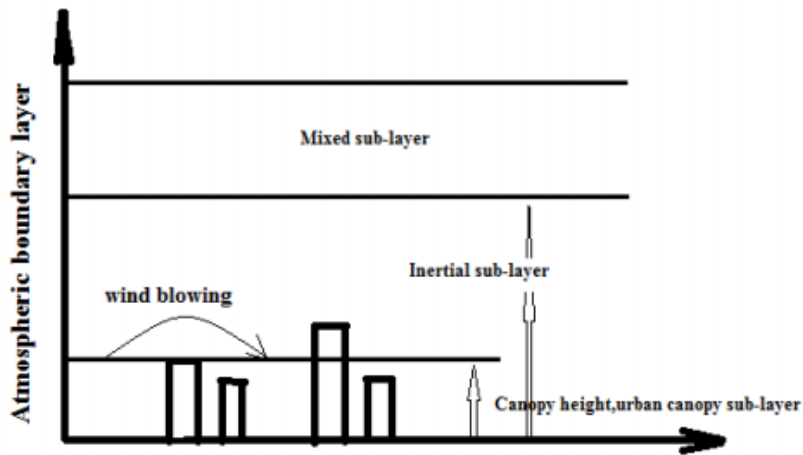


Figure 1.2 Atmospheric boundary layer structure in urban area

Street canyons, where long narrow streets are bordered by a continuous row of buildings on both sides (illustrated in Figure 1.3 below), are known to lead to problems of high pollution and heat accumulation (Oke, 1988). The narrow space between the buildings hinders background wind from penetrating into the street and causes lower wind speed in the street than outside, especially when the background wind is perpendicular to the street (Oke, 1988). Moreover, vortex flow typically forms under the perpendicular wind condition (see Figure 1.1), causing

higher concentration in the leeward side than in the windward side (Kastner-Klein et al., 2004).

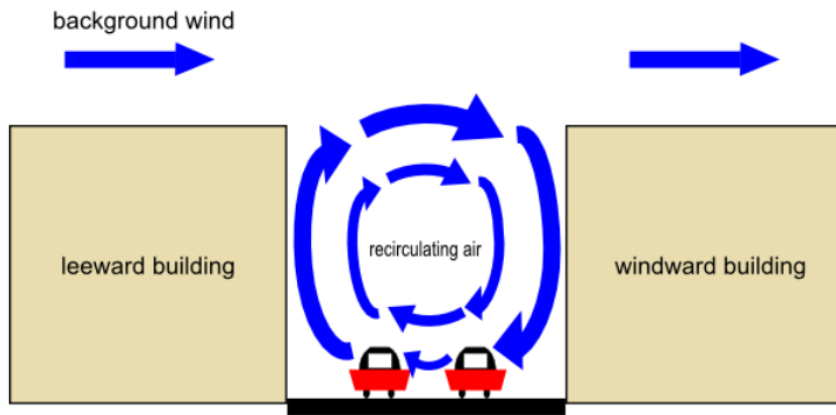


Figure 1.3 A typical two-dimensional street canyon and a typical flow pattern in the street when background wind is perpendicular to the street

According to the pioneer work of Oke (1988), the aspect ratio of building height to street width has the most significant effect on airflow in street canyons: when background wind is oblique or perpendicular to the street, the larger aspect ratio is, the lower velocity is in the street, thus the poorer ventilation is. However, following the trend of urbanization and population growth, it is inevitable to construct taller buildings, resulting in more street canyons and deeper street canyons. Thus, recent researches have focused on studying street geometries, building geometries and local parameters (e.g., traffic motion, tree planting and solar radiation), in order to minimize the problems of high pollution and heat accumulation in street canyon by optimizing detailed building designs and urban planning (Buccolieri et al, 2011; Cheng and Liu, 2011; Sini et al., 1996). Moreover, the recent progress made in the research contributes to improving the accuracy of predicting models (Kastner-Klein et al, 2001).

1.2. Necessity and Objectives

This study is to investigate the impacts of various typical urban geometries on airflow and pollutant dispersion, namely pitched roofs, tall surrounding building, aspect ratio and heterogeneous buildings. It is mainly motivated by four considerations. Firstly, an increase in urbanization takes an effect on air quality of the urban and increases the risk for public health. It is necessary to assess the air quality for sustainable habitats in urban street canyon. Secondly, due to the complicated geometries and boundary layers of urban street canyons, field observations and experimental approaches are very expensive and somehow impossible to observe the flow structures and dispersion processes in urban street canyons, simulation tool becomes an efficient tool can apply to overcome such limitations and capture such complex processes in this region. Thirdly, most numerical studies have been restricted to the building geometry. Therefore, understanding the characteristics of flows and dispersion processes in various roof shapes and different aspect ratios is an important task to improve air quality in urban street canyons. Fourthly, many previous studies proposed various turbulent Schmidt number in scalar transport equation based on the Standard Gradient Diffusion Hypothesis (SGDH) and its value is not universal and very time consuming to validate the Schmidt number. To overcome this limitation, it is essential to develop the Generalized Gradient Diffusion Hypothesis (GGDH) approach as an alternative method for the turbulent Schmidt number.

Based on the four mentioned considerations, four main objectives come into being before or during the research. The first objective is to establish a reliable and economic simulation tool to study flow and pollutant dispersion in urban street canyon. This should be accomplished by choosing available experiment(s) with reliable data observation, creating CFD model(s) and validated against the experimental measurements.

The second objective is to study the impact of various roof shapes and different aspect ratios on airflow and pollutant dispersion in street canyons. Most of previous experiments and models assume flat roofs on all the buildings, which does not represent typical roof structures in many cases (Meroney et al, 1996; Baik et al, 1999; Michioka et al, 2014). Although a few studies have taken pitched roofs into account and have highlighted their profound effects on airflow, all of those studies are based on sharp roof angles which are not commonly seen in the real world (Rafailidis et al, 1997; Yassin, 2011; Takano et al, 2013). Therefore, it is useful to examine various roof shapes and quantify their impacts on ventilation and pollutant removal. In addition, it is planned to test whether various roof shape make consistent impacts under different urban geometries.

The third objective is to develop the Generalized Gradient Diffusion Hypothesis (GGDH) approach for the scalar transport equation to calculate the turbulent scalar flux term more accurately. Up to now, in most CFD models, the turbulent scalar flux term has been approximated by the Standard Gradient Diffusion Hypothesis (SGDH). This approach is based on validating the turbulent Schmidt number. The turbulent Schmidt number is a characteristic feature of the turbulent flow no universal value could be established. The range of the turbulent Schmidt number is so wide from 0.2 to 2.5 (Tominaga et al, 2007; Mokhtarzadeh-Dehghan et al, 2012). The GGDH approach is an alternative approach without validation the turbulent Schmidt number.

The fourth objective is to make a case study of airflow and pollutant dispersion in a real urban area. The real urban area is the Shinjuku sub-central urban area. The Shinjuku special ward of Tokyo contains a large number of skyscrapers which pose several interesting wind engineering problems including how the wind shed will affect pedestrians nearby and the microclimate of the surrounding region. The study will help to identify the pollution issue in this urban area and provide useful guidance for future urban planning.

1.3. Structure of thesis

The content of this thesis is outlined as follows:

Chapter 1 introduces briefly the urban air pollution and its adverse effects. It also gives the definition of the urban street canyon. And this chapter describes the necessities and the objectives of the thesis.

Chapter 2 reviews previous research findings about airflow and pollutant dispersion in street canyons. The review focuses on three parts: the regimes of airflow, the effects of street and building geometries (aspect ratio) and the effect of various roof shapes. The review also concentrates on the limitation of the SGDH approach and the advantage of the GGDH approach. Then, the state of the art in CFD simulation is briefly discussed by comparing with experimental model and field measurement.

Chapter 3 displays the methodology. It derives the Reynolds Averaged Navier-Stokes equation, turbulence models. Different RANS models are calibrated in order to select an appropriate turbulence model for the flow over urban street canyons. It derives the SGDH and GGDH approaches. It describes how to implement the new equation into the original solver in OpenFOAM. Then, it calibrates the turbulence Schmidt number to show the limitation of the SGDH approach and calibrates between SGDH and GGDH approaches to show GGDH better. In addition, this chapter discusses how to specify key CFD modelling settings, such as turbulence model, wall function, boundary conditions and solver settings. A few of them have been agreed in the literature, so those agreed settings are followed; while the others will be tested in the next chapter.

Chapter 4 validates against Li's water channel experiment to study the flow characteristics in the street canyon with different aspect ratios. It validates against Kastner-Klein's wind-tunnel experimental measurements to study the air dispersion

in various roof shapes. It validates against Llaguno-Munitxa's experiment to study the flow characteristics in case of round-shaped roof. It also validates against CEDVAL data to study the flow characteristics for 3-D isolated building. The errors between the model results and the experiment measurements are analyzed through both graphical comparison and statistical approach. They will be used in the following chapters and will be used as initial settings in future work.

Chapter 5 applies for a case study of the flow and dispersion pollutant in Shinjuku urban area.

Chapter 6 summarizes the conclusion and takes a plan for future works.

2. LITERATURE REVIEW

Understanding the flow of the wind through and above the urban area and/or the dispersion of material in that flow (Hanna & Britter 2002) is necessary. We address these issues by considering the problem at different scales. At each of the scales there are observations from the field and the laboratory that are interpreted in terms of various physical (and possibly chemical) processes. These processes, once recognized, are often combined and reformed into mathematical models that can form a hierarchy of complexity or sophistication: Each model has its own regime of applicability and accuracy. A detailed interpretation at one scale is commonly parameterized to assist interpretation at the next larger scale. We use spatial scales to describe the major urban flow features, although the spatial scales can be related to time scales through the $x = ut$ relation. Roughly speaking the timescales are the spatial scales divided by an appropriate advection (wind) velocity. The discussion is broken down into four ranges of length scales: regional (up to 100 or 200 km), city scale (up to 10 or 20 km), neighborhood scale (up to 1 or 2 km), and street scale (less than 100 to 200 m).

The regional scale is affected by the urban area. For example, the urban heat island circulations, any enhanced precipitation, and the urban pollutant plume can extend to these distances. At this scale the mean synoptic meteorological patterns are given and the urban area represents a perturbation, causing deceleration and deflection of the flow, as well as changes to the surface-energy budget and the thermal structure.

The city scale represents the diameter of the average urban area. At these scales the variations in flow and dispersion around individual buildings or groups of similar buildings have been mostly averaged out. Wind flow models developed for this range pay little attention to the details of the flow within the urban canopy layer.

Most of the mass of any pollutant cloud traveling over this distance will be above the height of the buildings.

On the neighborhood scale buildings may still be treated in a statistical way; however, the approach may be different to that on the city scale. At the neighborhood scale we want to know more about the flow within the urban canopy. The wind flow, particularly within the canopy, may also be changing as it moves from one neighborhood to the next. Much of the mass of a pollutant cloud traveling over this distance may remain within the urban canopy.

The street (canyon) scale addresses the flow and dispersion within and near one or two individual streets, buildings, or intersections. This would be of interest when considering turbulence affecting pedestrian comfort and the direct exposure of pedestrians and near-road residences to vehicular emissions. It can be of particular interest when regulatory pollutant monitoring stations are placed within street canyons.

On the regional scale (up to 200 km in the horizontal direction) a large area can be affected by the so-called urban plume – a mixture of primary and secondary pollutants. Tropospheric ozone pollution is a good example for this category. The primary pollutants originate mainly in urban areas while the highest concentrations of ozone – a secondary pollutant that forms in the atmosphere due to photochemical reactions of the primary pollutants – typically occur downwind of urban areas. The transport and mixing of the urban plume is influenced by urban weather modifications. Typical examples for such modifications are urban heat-island effects, and horizontal and vertical flow deflections due to the increased drag in urban areas. When dealing with regional-scale pollution problems, air quality models consequently should account for chemical reactions in the atmosphere and reproduce the urban perturbations on the synoptic-scale weather patterns, but there is no need to resolve the complex flow patterns around individual buildings. However, the flow and turbulence characteristics inside the urban canopy – the

region of the urban boundary layer in which the flow is affected by the local environment (building shapes and densities, type of vegetation etc.) – are key parameters when dealing with neighbourhood or street-scale pollution problems. A good example of pollution problems of this category are emissions from road traffic. These emissions occur near the ground, and dispersion of the exhaust gases is highly affected by the complex flow phenomena inside the urban canopy. Other examples are the dispersion of hazardous material that can be accidentally released in industrial areas. Nowadays, also terrorist attacks with a release of chemical and biological agents are an important concern. In both cases, emergency response personnel must be able to make a fast and reliable prediction of the areas with critical dosages. Flow phenomena around buildings will significantly alter the plume drift and mixing, and must be taken into account in such predictions.

The morphology of urban landscapes is extremely variable and influenced by many factors. Geographical features and the time period of the major city development play important roles. Modern cities are often characterized by clusters of high rise buildings and wider streets, meanwhile older cities often have very narrow streets and densely-packed, few-storey high buildings. Figure 1 shows an example of a complex urban structure of the latter category. The noted differences in the urban morphology strongly impact the urban climate. Thus, if one is interested in predictions of the local air quality in a particular street or neighbourhood of a city, the buildings structure in the area of interest must be resolved in the air quality model in detail. On the other hand, there are many applications when the resources for such detailed studies are not available. Accordingly, attempts have been made to define typical urban buildings structures based on their basic physical properties (built-up area relative to total area, ratio of street width to building height etc.), as it was done in Theurer (1999), and Ratti et al (2002), and to study the principal flow and dispersion characteristics for these different building categories. Also, it is still questionable if presently available numerical models are able to predict the complexity of urban flow and dispersion patterns accurately enough and evaluation

strategies for urban air quality models have been widely discussed (Schatzmann and Leitl, 2002; Chang and Hanna, 2004). Important steps of a model evaluation procedure are comparison studies between model calculations and experimental datasets, and also inter-comparisons of simulations with different models or by different users, see, e.g., Sahm et al (2002) and Ketzel et al (2002). Such studies are typically done for relatively simple building geometries, which can be clearly defined and easily implemented in numerical models. Accordingly, a large number of studies related to urban air quality focus on flow and dispersion in basic urban building configurations.

One urban building category that has been widely investigated during recent years is the street- canyon configuration. A review of modelling air quality in street canyons is given in Vardoulakis et al (2003). Generally, street canyon studies can be classified according to the degree of simplification used in modeling the urban building structure. Figure 2.1 presents an overview of different realizations of street-canyon configurations in air-quality studies:

(a) Isolated 2-D street canyon

This configuration defines the most basic approach to studying street canyon pollution. It has been used in wind-tunnel simulations (e.g., Kastner-Klein and Plate, 1999) and numerical modeling (e.g., Chan et al, 2001) mostly for model evaluation studies. This approach has the advantage that the boundary conditions can be well defined and parameters like the approaching flow direction or the canyon aspect ratio can be easily varied. On the other hand, it has the disadvantage of producing somewhat unrealistic urban flow and dispersion patterns. A typical urban street canyon does not have an undisturbed upwind fetch but, rather, a complicated urban surface, which seriously distorts the flow.

(b) Rows of 2-D street canyons

To address the problems with the single canyon, several studies with extended arrays of streets of the same geometry have been performed like, e.g., the ones of

Meroney et al (1996) and Brown et al (2000). One of the questions of interest in these studies has been, at which row the flow starts to become self-similar and thereby, where street canyon pollution resembles an urban situation. Brown et al (2000) argue that this is the case after about the 6th row. Further upwind, the flow, turbulence, and dispersion conditions are to a large extent determined by the flow separation at the upwind edge of the first building.

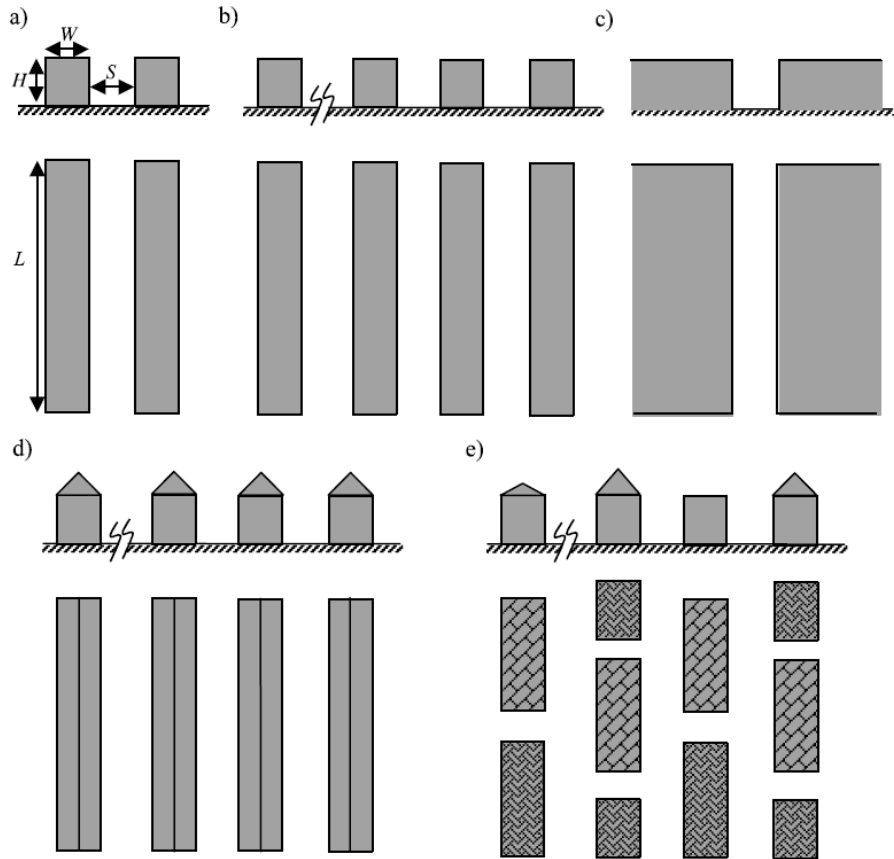


Figure 2.1. Representation of idealized street canyon configurations with increasing complexity from (a) to (e), see text for details.

(c) The cavity

As an intermediate case between street canyons of type a) and b) a cavity has been simulated, see, e.g. Kovar-Panskus et al (2002) and Sahm et al (2002). In this

configuration there is no “first-building effect”, but the upwind “urban” surface is not representative of a rough, irregular building pattern.

(d) Variable roof geometry

Urban buildings do not usually have a simple rectangular geometry and several studies were focused on the influence of different roof shapes on street canyon ventilation, see, e.g., Rafailidis (1997) and Kastner-Klein and Plate (1999). Such studies were done with a simple two building setup, as well as with extended arrays of buildings of the same geometry. Buildings with pitched roofs as well step-down or step-up configurations (upwind building higher or lower than downwind building) were considered.

(e) Nonuniform geometry

The last category of idealized street canyon configurations is the one most closely resembling real urban configurations. Buildings of variable geometry are arranged on staggered or non-staggered arrays, which simulate the rough, irregular pattern of urban landscapes, see, e.g. Cheng and Castro (2002) and Chan et al (2003).

(f) Real urban surfaces

The most realistic modeling approach (not included in Fig. 2.1) for urban street canyons is certainly to reproduce the street geometry in as much detail as possible. This may be attempted in wind-tunnel simulations as well as in numerical experiments. A detailed physical model of an urban building structure that was used in the studies of Kastner-Klein and Rotach (2004) is shown in Fig. 1. Schatzmann and Leitl (2002) also discuss the value of such studies for model evaluation purposes.

This chapter reviews recent progress made in studying street canyon flow. The review covers a few topics that are closely relevant to this thesis. After the review, the state of the art in CFD simulation is briefly discussed from two respects: its advantages and its performance. The structure of this chapter is given as below.

Section 2.1 introduces typical patterns of street canyon flow under perpendicular wind conditions. Section 2.2 introduces the influence of wind condition. Section 2.3 explains the process of turbulent air exchange between street canyon and the atmosphere. Section 2.4 introduces the characteristics of pollutant dispersion inside the street canyon. Section 2.5 discuss how geometry of street canyon effects on flow patterns and pollutant transport in the street canyon. Section 2.6 discusses general advantages and limitations of CFD modelling and evaluates its performance and accuracy according to previous researches.

2.1. Flow characteristics of idealized street canyon

Street canyons define streets with buildings in parallel (Nicholson, 1975). An isolated street canyon can be defined by two parameters: aspect ratio (AR) H/B and length-to-width ratio L/H . Dimensions of H , B , and L respectively represent flat roof height in vertical direction, width of street, and length of upwind buildings in stream-wise and span-wise directions. Depending on the (H/B) , street canyon can be shallow ($H/B < 0.5$), uniform ($H/B = 1$), or deep ($H/B > 2.0$). According to (L/H) , street canyon can be short ($L/H < 3.0$), medium or long ($L/H > 7.0$). In terms of relative height between neighboring buildings, street canyons can be classified into three configurations: step-down, step-up, and even (Figure 2.2). The ratio of relative height H_1/H_2 , is used to describe these configurations. Street canyons without identical heights are asymmetric. Those street canyons with identical heights are symmetric (Ahmad et al., 2005).

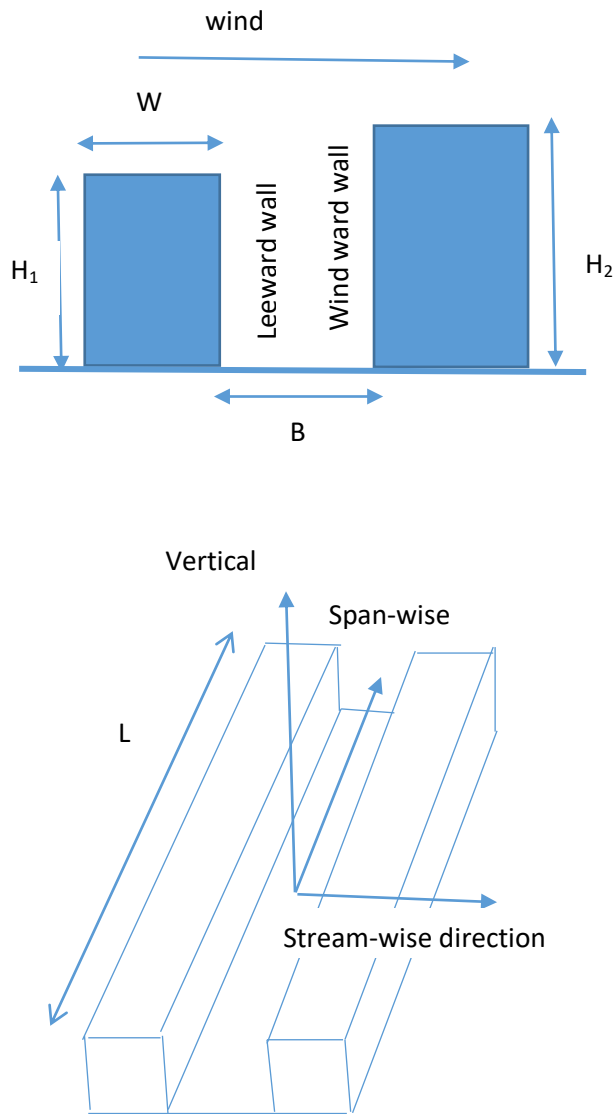


Figure 2.2. Definition of idealized street canyon

There are numerous researches studying street canyon flow. Most of them examine the case of a street subjected to perpendicular background wind condition(s), as this is the worst scenario for ventilation and pollutant removal. Oke (1988) conducted a pioneer work to summarize typical flow under this condition. He classified the flow into three basic regimes (see Figure 2.3) according to the aspect

ratio of building height to street width H/B and the aspect ratio of building length to building height ratio L/H . The following three paragraphs make a summary of his findings in association with the famous schematic diagrams in his work as shown in Figure 2.2 above and Figure 2.3 below.

As can be observed from Figure 2.3 below, the transitions between three basic flow regimes are mainly dependent on the aspect ratio H/B . For wide street canyons ($H/B < 0.3$), the flow behind the leeward building does not interact with the flow in front of the windward building, as illustrated in Figure 2.3(a) below. This type of flow is termed isolated roughness flow. When the street width is intermediate ($0.3 < H/B < 0.7$), the wake behind the leeward building interferes with the recirculation flow in front of the windward building (see Figure 2.3(b) below). This type of flow is termed wake interference flow. When the street is narrow ($H/B > 0.7$), the flow in the street canyon is characterized by a persistent large vortex, as shown in Figure 2.3(c) below. Since the background wind does not easily travel across the narrow space between the buildings, this type of flow is termed skimming flow.

On the other hand, Figure 2.2 above shows that the aspect ratio L/H has a minor effect on the transitions. In general, the critical aspect ratios (H/B) for the transitions are slowly increased with increasing street length.

Amongst the three flow regimes, skimming flow has been confirmed to be the most detrimental for ventilation and pollutant removal. Under this flow regime, the typical velocity in street canyon is usually an order of magnitude lower than the free-stream velocity in the atmosphere. Furthermore, the vortex flow pattern flushes pollutants upwards along the leeward building, causing higher pollutant concentration in the leeward side than in the windward side. It should be mentioned that skimming flow regime also exists in deeper street canyons ($H/W > 2.0$). However, in this case, the flow inside the street canyon is not stable and is sensitive to background wind condition, street canyon geometries and local parameters. For

example, Eliasson et al. (2006) found both single vortex and double counter-rotating vortices (in the upper and lower parts of the street respectively) could exist in the same deep street canyon but at different times. The former persisted in most time, and the latter formed and broke in short terms (Eliasson et al., 2006).

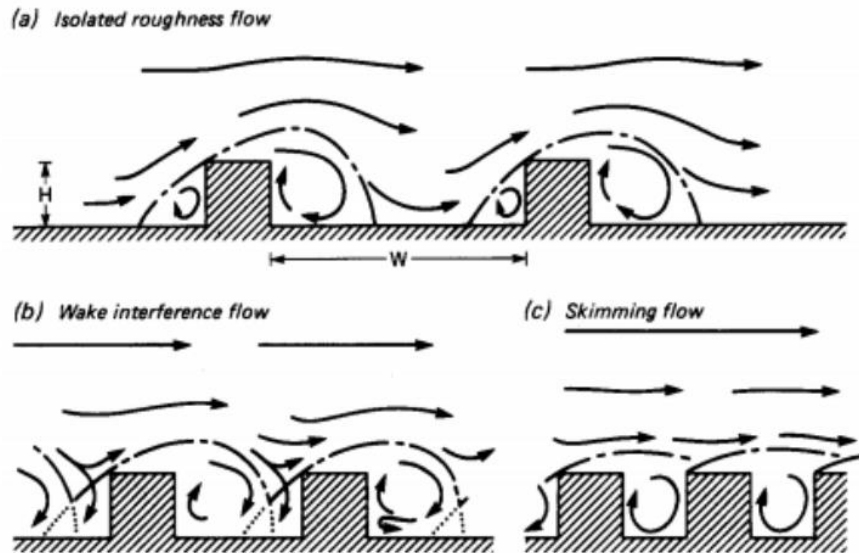


Figure 2.3. Three flows regimes for flow over buildings: (a) isolated roughness flow, (b) wake interfere flow, and (c) skimming flow (Oke, 1988)

2.2. The influence of wind condition

Background wind condition directly affects airflow in street canyon. According to the similarity law of flow, an increase of background wind velocity will lead to proportional increases of velocity components and turbulence statistics in the same street. This is the most straightforward effect made by different background wind velocities.

Background wind direction has profound effects on airflow and pollutant dispersion. Generally, street canyon is more efficiently ventilated when

background is parallel or oblique to the street than when background is perpendicular to the street (Soulhac et al., 2008). Under a parallel background wind condition, street canyon flow shares a similar regime to channel flow (Louka et al., 2000; Yamartino and Wiegand, 1986). As a result, pollutants can be effectively flushed away along the street. For various oblique background wind conditions, Soulhac et al. (2008) showed that the general flow patterns were characterised by complicated combinations of vortex flow and channel flow. Kastner-Klein and Plate (1999) further investigated pollutant distribution under seven wind directions, which had angles of 0° , 15° , 30° , 45° , 60° , 75° , and 90° to the street axis. They confirmed that the perpendicular wind was the worst condition for pollution, and the 30° and 45° winds caused the second-highest concentrations in the street canyon. The parallel wind produced the best pollutant removal performance, as the concentrations at most measuring points were only around 1/3 of those measured concentrations under the perpendicular wind (Kastner-Klein and Plate, 1999).

Once the effects of steady background wind speed and direction were well understood, researchers started to study the effects of time-variant wind conditions.

The variation of background wind velocity mainly affects turbulence in street canyon. Castro and Robins (1977) and Kim and Baik (2003) claimed that the turbulent kinetic energy in street canyon was positively related to the turbulent kinetic energy in the background flow. When the background wind is critically unstable, the flow pattern in the street canyon will become unstable. A good illustration of this type of unstable flow is the existence of both single vortex flow and double counter-rotating vortices in the same deep street canyon but at different times, which has been mentioned before in Section 2.1. In addition, Eliasson et al. (2006) attributed these flow features to the relatively low mean background velocity and the strong fluctuation of background wind condition.

The variation of background wind direction is possible to induce the switch between different flow regimes. Balogun et al. (2010) found that a small change of

the background wind direction altered the in-street flow angle substantially, and the flow near the cross-junction was the most sensitive to the change. With respect to pollutant dispersion, Karra et al. (2011) found more efficient vertical mixing of pollutants during a period that had large changes of wind direction.

The simultaneous variations of background wind velocity and background wind direction have been taken into account in a limited number of studies. Zhang et al. (2011) modelled such effect by importing a real-time wind profile. By using this technique, they found some unique time-variant flow features, such as time-variant expansion and compression of the vortex flow, the flapping of the shear layer above the vortex and the detachment of the shear layer. These features were not found in the control model with the same geometries but modelled by a steady wind profile.

2.3. Turbulence transfer between a street canyon and the atmosphere

The ventilation efficiency of a street canyon relies on not only mean flow but also fluctuating flow or turbulence. The previous section has introduced typical flow patterns under perpendicular background wind condition(s), and this section explains turbulent transfer between street canyon and the atmosphere

For long street canyons, previous studies have demonstrated that the velocity difference between the external flow and the cavity flow will produce a shear layer above the buildings and the street canyons (Salizzoni et al., 2011). The flow in the shear layer is unstable, promoting air exchange between the street canyon and the atmosphere through an intermittent process of turbulent transfer (Cui et al., 2004; Salizzoni et al., 2011).

The turbulent transfer efficiency hinges on the dynamics of the shear layer, which are determined by the local production of turbulence and the turbulent flux from

the external flow (Salizzoni et al., 2011). A good illustration is that the turbulent transfer for an isolated street canyon is usually very efficient, as the flow separation above the first building produces a large amount of turbulence (Kastner-Klein et al., 2001). In this case, air is continuously discharged from the isolated street canyon, and the flow pattern in the street changes over time (Meroney et al., 1996). In contrast, the turbulence transfers for a non-isolated street canyon (e.g., one of consecutive street canyons) is usually much weaker, because flow separation does not happen above the adjacent buildings to the street (Kastner-Klein et al., 2001). This results in a stable vortex flow in the street and an intermittent discharge of air from the street (Meroney et al., 1996).

For short street canyons or building arrays, Salizzoni et al. (2011) found that the unstable shear layer did not form at the roof level. Thus, turbulent transfer plays a less important role compared to long street canyons. According to this finding, it should be made a reconsideration of the representativeness of physical and numerical models, as modelling work usually assumes long streets and homogeneous buildings, while real urban geometries are always made up of short streets, heterogeneous buildings and other complicated geometries.

2.4. Characteristics of pollutant dispersion inside street canyon

Much focus has been given to the pollution dispersion in street canyons, as concentrations of canyon flow directly affect urban air quality. Many empirical models have been developed to predict pollution distribution in street canyons. Two methods have been investigated to evaluate concentration distribution in street canyons: uniform concentration (which perceives street canyon as boxes) and nonuniform concentration. If the canyon volume is a uniform source field, the

variation of concentration in canyon volume related to time is expressed as (Lee and Park, 1994):

$$\frac{dC}{dt} = -\frac{q}{V}C \quad (2.1)$$

where V is canyon volume, C is canyon flow concentration, and q is influx change into canyon. At steady state, the equation solution is

$$C(t) = C_0 e^{-t/\tau} \quad (2.2)$$

where $\tau = V/q$ represents constant. At time $t = \tau$, concentration C of canyon flow will be decrease by e^{-1} . Hoydysh and Dabberdt (1988) studied the impact of wind direction and canyon configuration on flow characteristics and pollutant dispersion. An empirical exponential function was proposed to describe concentration distribution along vertical height:

$$K = ae^{bz/H} \quad (2.3)$$

where a and b are empirical coefficients, H and K are building height and non-dimensional concentration. Since vehicle-emitted pollution can be perceived as line pollutant source, Rafailidis and Schatzmann (1997) used the non-dimensional form

$$K = \frac{CUHL}{Q_e} \quad (2.4)$$

to represent pollutant distribution in street canyons. Here, C represents the measured vol./vol. ethane trace concentration (in the range of [0,1]); U represents reference velocity at reference height; L is the length of the line source; Q_e is the volumetric flow rate of the gas source.

Studies have explored the mechanisms of pollutant transportation in street canyons. Concentrations of canyon volumes are mainly affected by three factors (Wedding et al., 1977; Hoydysh and Dabberdt, 1988; Lee and Park, 1994; Meroney et al., 1997; Kastner-Klein et al., 2000): canyon aspect ratio of height to width $AR =$

H/B , Reynold number at roof level $Re_r = \frac{Hu}{\nu}$, and Peclet number defined by $Pe_r = Re_r Pr_r$, where Pr_r represents Prandtl number at roof level. Roof-level Reynolds number Re_r is usually related to local turbulence intensity, and Peclet number Pe_r is related to local thermal effect. Three transfer mechanisms were proposed to characterize wind-induced pollutant transfer (Liu and Barch, 2001; Salizzoni et al., 2009): turbulence diffusion within the street canyon (\tilde{u}_d), advection due to mean recirculation flow (\tilde{u}_c), and turbulence dispersion across shear layer at roof level (\tilde{u}_t). There are shown in Figure 2.4.

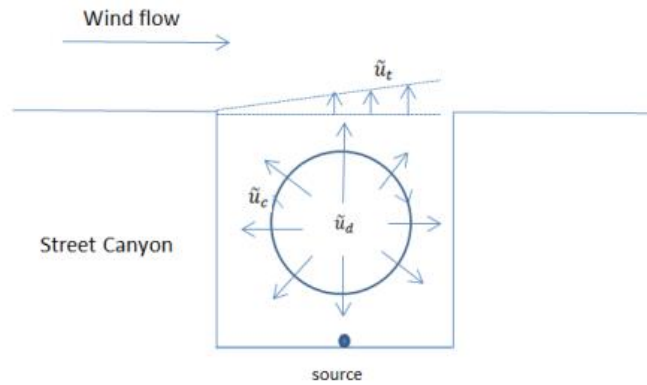


Figure 2.4. Simplified illustration of vehicle-emitted pollutant transfer mechanisms within the street canyons

2.5. The influence of geometry of street canyons

As mentioned previously, street canyon geometry is represented by aspect ratio (AR). Flow characteristics and regimes inside street canyons also directly depend on AR and the corresponding number of circulations. These flow regimes, and circulations inside street canyons, have a great effect on pollutant dispersion. The pollutant removal process is a combination of advection transport and turbulence diffusion. As street canyon width increases (decreasing AR), the pollutant dispersion depends more on advection transport (Lee and Park, 1994; Sini and Anquetin, 1995). Results also showed with SF, multi-vortex pollutant dispersion

will be dominated by turbulence diffusion, while convective effects are negligible. In such cases, vehicle-emitted pollution at canyon bottom is mainly dominant by diffusion from bottom vortex to upper vortex, and pollution is difficult to transfer out of the street canyon. For one-vortex SF, WIF, and IRF wind flows, pollutant dispersion has a weak connection with turbulence diffusion (Ellen et al., 2005) and will have low pollutant concentration inside street canyons. Pollutant concentrations on windward side of street canyons are normally lower than on leeward side.

Hoydysh and Dabberdt (1988) carried out a field test to study the effect of asymmetric street canyons with flat roofs on kinetic and dispersion characteristics. Wind-tunnel experiments (Rafailidis and Schatzmann, 1995; Kastner-Klein and Plate, 1999) were also conducted to investigate effect of roof shapes on pollutant distribution inside street canyons. Results showed that concentrations in the step-up notch are lower than for the other two notches, since high mean circulation velocity is generated inside street canyons. Pollutant concentration at the windward surface is higher than at the leeward surface for even and step-up notches. For step-down notches, the concentration distribution reversed. Kastner-Klein et al. (2004) explained the increased pollution level for pitch roofs at upwind buildings. The increase was attributed to a recirculation zone formed at the upwind building ridge and spanning across the downwind building. At the recirculation zone, low wind velocity hampered formation of street-canyon vortices. As a consequence, flow became almost stagnant and pollution was trapped.

Chan et al. (2001) investigated effects of relative height, from 0.5 to 2.0, on pollutant concentration of isolated roughness flow for a two-dimensional street canyon. There is maximum value of pollutant concentration when relative height increases from 0.5 to 2.0. As the blockage effect from the leeward building side increases, the pollutant concentration will tend to increase with relative height. From the viewpoint of efficient dispersion, the street canyons should not be uniform. Variations in roof height provide better ventilation.

Xie et al. (2005) studied roof shapes and building geometry effects on pollutant dispersion inside street canyons. Huang (2007) studied the impact of wedge-shaped roofs on the pollution dispersion, including 17 case studies. Yassin (2011) studied pollution dispersion by comparing different roof shape and heights.

Results showed that, the even and step-up configurations generally have the same pollutant concentration in street canyons, and that concentration on the leeward is greater than on the windward side. The main reason for the variation is attributed to circulation wind speed and number of vortices generated within the canyon. For step-down configuration, ability of pollutant dispersion is smaller than with the even and step-up. Double-eddy or so called counter-vortex appeared in the street canyon. Pollutant concentration on the leeward side was smaller than on the windward side. Vortices at canyon bottoms bring the pollutants from the leeward to the windward side. Furthermore, shear zone at roof level also changes, depending on roof shape.

2.6. Schmidt number

The most widely-applied approach for simulating turbulent flows is that based on the Reynolds-Averaged Navier-Stokes (RANS) equations, where the turbulent scalar fluxes are mostly estimated by assuming the Standard Gradient Diffusion Hypothesis (SGDH) (Rossi, 2012)

$$-\overline{u_i c'} = D_t \frac{\partial c}{\partial x_i} \quad (2.5)$$

where D_t is the turbulent mass diffusivity and $\frac{\partial c}{\partial x_i}$ the mean mass gradient.

To represent the ratio of the turbulent momentum diffusivity (eddy viscosity) ν_t and the turbulent mass diffusivity D_t , the turbulent Schmidt number, Sc_t , is defined as follows:

$$Sc_t = \frac{\nu_t}{D_t} \quad (2.6)$$

This approach is a natural extension of the Fickian formulation for laminar fluxes; thus, the same name is used in the context of turbulent flows. The turbulent Schmidt number is driven by the turbulent flow and has no universal value. Therefore, it needs to be calibrated to select an appropriate value for the pollutant transport in urban street canyons as mentioned by Tominaga and Stathopoulos (2007).

As shown in Table 3.5 at the Section 3.3.1 below, the value of the turbulent Schmidt number is varied in a wide range from 0.1 to 2.5; therefore, it causes difficulties to define an appropriate value for pollutant dispersion in urban street canyons.

2.7. Three-dimensional modelling

Street-canyon flow is essentially a 3D problem because of the high Reynolds number characteristics. But there are still many studies (e.g., [Ca et al., 1995](#); [Sini et al., 1996](#); [Chan et al., 2002](#)) adopting 2D approach to study this problem. The main rationale for 2D simulations is that a 2D case represents street canyons with infinite length in span-wise direction. In fact, this approach has many limitations in flow and air pollution research. On one hand, some phenomena, such as the double-eddy circulation described in [Baik and Kim \(1999\)](#), are observed only in 3D situations and play an important role in distributing pollutants around the building. [Hunter et al. \(1992\)](#) and [Leitl and Meroney \(1997\)](#) investigated 3D lateral and secondary flows, which are absent in 2D simulations but strongly influence the vertical mixing of pollutant concentrations. On the other hand, pollutants escape from street canyons mainly by turbulence processes ([Baik and Kim, 2002](#)). These transient processes should be recognized to be essentially 3D. Without vortex stretching in the span-wise direction, it is unable to understand strengthening of a vortex through this process. Also, instabilities in the span-wise direction could lead to stretching

and pulling of vortical structures. The 2D simulations (and also those RANS models) evidently neglect these important features.

In order to validate the proposed numerical model, simulations of dispersion sources release, which are expected to reproduce the wind tunnel experiments, have been carried out. Three datasets from the Compilation of Experimental Data for Validation of Microscale Dispersion Models (CEDVAL) provided by the Environmental Wind Tunnel Laboratory in University Hamburg are used in this study. The datasets are chosen because all the experiments were well organized and clearly documented, and the datasets are fully accessible at <http://www.mi.uni-hamburg.de/Data-Sets.432.0.html>. These wind tunnel experiments were carried out at a scale of 1:200 in the BLASIUS wind tunnel at the Meteorological Institute of the University of Hamburg. The first two corresponded to detailed measurements of the flow and dispersion characteristics around an isolated rectangular obstacle, respectively, and the third one corresponded to array of obstacles. Dynamic similarity was maintained between simulations and wind tunnel experiments.

2.8. CFD modelling of street canyon flow

Computational Fluid Dynamics (CFD) has been widely used as research and design tool since last century. This section first summarizes the general advantages of CFD modelling over physical model and field measurement and points out its limitation. Then, this section reviews the application of CFD modelling in studying street canyon flow and discusses its performance and accuracy in association with a few modelling cases.

With the rapid development of computer technology, CFD is serving as an important tool for studying fluid dynamics. It possesses a few attractive advantages

over experimental and theoretical fluid dynamics. Fletcher (1991) summarized five main advantages of CFD over experimental fluid dynamics as follows:

- Lead time in design and development is significantly reduced.
- CFD can simulate flow conditions not reproducible in experimental model tests (e.g., full-scale geometry).
- CFD provides more detailed and comprehensive information.
- CFD is increasingly more cost-effective than wind-tunnel testing
- CFD produces lower energy consumption.

The uppermost advantage of CFD modelling is good cost-effectiveness. A typical CFD model takes a few hours to set up and another few hours or days to run. In contrast, a field measurement typically takes days or months, and requires much more manual effort (Glover, 2015). An experimental model usually does not take such long time in the measuring stage, but it requires much time and effort in preparing and testing stages (Karra, 2012).

CFD modelling is able to simulate many flow conditions which are unable or difficult to realize in wind tunnels or water channels. For example, the full-scale geometry of an urban area, which is unable to be constructed in lab environment, can be easily reproduced and modelled by CFD software (Glover, 2015). Another good example is that making systematic changes of model geometry are straightforward in CFD modelling (Gu et al., 2011); whereas in experimental model, a small change of model geometries means additional efforts for repositioning measuring device and further tests and calibration (Kastner-Klein, 1999).

Another outstanding advantage of CFD modelling is that high-resolution data are available in whole computational domain. In contrast, many field measurements have issues of low spatial and temporal resolutions, and high-resolution experimental measurements are usually limited to a few measuring positions (Meroney, 1996). Owing to the availability of high-resolution data, many

secondary quantities, such as drag coefficient over a surface and mass flux through an area, can be directly calculated in the post-process stage of CFD modelling, while making further assumption and analyzing measuring error are usually required to obtain such quantities from experimental measurements (Tao, 2001).

On the other hand, CFD modelling has certain limitations. The most concern is about modelling itself. It is always considered that CFD modelling has lower accuracy than experimental measurements, and that is why experiments are used to validate CFD models (Solazzo et al., 2009). Although computer technology has been rapidly developed, CFD modelling is still not an economic means for research at current stage. The license for CFD software and strong knowledge of fluid dynamics are essential for conducting modelling work. Moreover, performing accurate and reliable CFD modelling further requires not only high performance hardware but also plenty of computing time (Le et al., 1997).

Recent advances in numerical modelling and computer capability lead to an increasing number of investigations on numerical simulation of urban area dispersion in a variety of controlled configurations, with some excellent reviews (e.g., Li et al., 2006) of atmospheric dispersion modelling. The flow, turbulence, and dispersion fields on the urban city block (1 km) to building scales (10 m) are directly influenced by the fine scale geometric features of the city. As a result, the models that accurately predict large scale dispersion based on simplified mathematic models,

such as box models, Gaussian plume models, and Lagrangian puff models, are unable to predict accurately in urban areas. More sophisticated approaches, such as Computational Fluid Dynamics (CFD), capable of modelling the flow and the response of buildings to winds, are developed to simulate the urban area dispersion problems. There are a bunch of investigations about Reynolds-Averaged Navier-Stokes (RANS) based CFD (Krus et al., 2003; Riddle et al., 2004; Coirier et al., 2005; Di Sabatino et al., 2007; Mavroidis et al., 2007; Santos et al., 2009; Tewari et al., 2010; Solazzo et al., 2011) as well as Large Eddy Simulation (LES) based

CFD (Nozawa and Tamura, 2002; Cheng et al., 2003; Gousseau et al., 2011). Some studies even involved real complex urban-type geometries (Kr̄us et al., 2003; Hanna et al., 2006; Tewari et al., 2010). Clearly, the LES approach is better in prediction (Cheng et al., 2003; Gousseau et al., 2011), because it addresses many deficiencies brought about by the RANS models (namely, scale resolution). However, the LES simulations are computationally expensive, noted as “about 640 times greater than the k - ϵ model applied with wall functions and 26 times greater than the two-layer k - ϵ model” in Cheng et al. (2003). In view of this, the steady RANS based models appear to be a good compromise between solution accuracy and amount of computation.

3. METHODOLOGY

Computational Fluid Dynamics (CFD) refers to using computational techniques to solve the governing equations for fluid flows (Versteeg and Malalasekera, 2007). It provides an alternative to theoretical and experimental fluid dynamics to study fluid flows. With the development of computer technology in recent years, CFD has been used as powerful research and design tools in many disciplines (Versteeg and Malalasekera, 2007). In particular, it has been successfully applied to model airflow in urban areas.

This thesis uses CFD modelling as research methodology, considering the advantages of CFD discussed in Section 2.6.1. Thus, the primary goal of this chapter is to introduce the fundamental of CFD. Section 3.1 introduces the Navier-Stokes equations as the governing equations for fluid flows. Section 3.2 introduces the concept of turbulence model, since the direct solving of Navier-Stokes equations are not feasible for high Reynolds number turbulent flow at present. Section 3.3 introduces the scalar transport equation. This modelling method is also used in this thesis.

3.1. Reynolds-Averaged Navier-Stokes Equation (RANS)

Since the complexity of flow patterns and pollutant dispersion characteristics impacted by buildings, numerical model is introduced to analyze flow and scalar-transportation phenomenon in surface sub-layer. The coordinate system of the numerical model is defined as follows. The positive longitudinal direction is given by flow direction. The vertical direction is given upward from the surface, originating at buildings' ground floor of buildings. Lateral direction is given as a right-hand orthogonal coordinate system. The wind velocities in the coordinate system at longitudinal, lateral, and vertical directions are labeled as u , v , w , respectively. In order to easily represent novel velocity quantities, $u_i = U_i + u'_i$ is

given in the model, and x_i represents the coordinate axis in the different directions. Time-averaged mean velocities are referred to as U_i , and instantaneous turbulent quantities are represented as u'_i .

The term fluid flow problems refer to the solution of series of differential equations of Navier-Stokes and continuity equations, with appropriate boundary conditions. These equations are derived from Newton's Second Law and describe with the conservation of momentum, combined with the continuity equation, which are used to solve flow variables issues. The typical Navier-Stokes equation is expressed as:

$$\frac{\partial u_i}{\partial t} + u_j \frac{\partial u_i}{\partial x_j} = -\frac{1}{\rho} \frac{\partial p}{\partial x_i} + \frac{1}{\rho} \frac{\partial}{\partial x_i} \left(\mu \frac{\partial u_i}{\partial x_j} \right) \quad (3.1)$$

In the model, body force, such as Coriolis force, is ignored because they are very small at ground level. Other body forces, such as gravity force, are also ignored in the current research. Non-dimensional Navier-stokes equations are introduced to give insight into all terms in the equation. Based on reference length scale L_{ref} and reference velocity scale U_{ref} , the time scale is referred as L_{ref}/U_{ref} . Pressure term scale is referred to as ρU_{ref}^2 . All dimensional variables transform into non-dimensional form as:

$$U_i^* = \frac{u_i}{U_{ref}}; x_j^* = \frac{x_j}{L_{ref}}; t^* = \frac{t}{\left(\frac{L_{ref}}{U_{ref}}\right)}; p^* = p/(\rho U_{ref}^2) \quad (3.2)$$

Therefore, non-dimensional Navier-Stokes equation is

$$\frac{\partial U_i^*}{\partial t^*} + U_j^* \frac{\partial U_i^*}{\partial x_j^*} = -\frac{1}{\rho} \frac{\partial p^*}{\partial x_i^*} + \frac{1}{Re_{ref}} \frac{\partial}{\partial x_j^*} \left(\frac{\partial U_i^*}{\partial x_j^*} \right) \quad (3.3)$$

where Re_{ref} defined as

$$Re_{ref} = \frac{\rho L_{ref} U_{ref}}{\mu} \quad (3.4)$$

As seen in Equation 3.3, background flow field is dominated by Re_{ref} . Only at the same Reynolds number Re_{ref} , can flow fields be similar to each other. This allows

the experiments to be conducted at a smaller scale, based on the assumption that excluded physical effect in non-dimensional equations are not important for the flow field. However, this presents a problem particularly for reproducing atmospheric boundary layer in wind-tunnels. At smaller scales of prototype, higher velocity is needed to ensure Reynolds number independent.

In a real environment wind field is a time-variable. It is impossible to directly solve wind field. In order to solve the equations, Reynolds averaged method is introduced and an assumption is made that time-averaged turbulent velocity quantities $\overline{u'_i}$ are equal to zero

$$\overline{u'_i} = 0$$

Therefore, the general form of the three-dimensional, incompressible Reynolds-averaged Navier-Stokes (RANS) Equation is transformed as follows:

$$\frac{\partial U_i}{\partial t} + U_j \frac{\partial U_i}{\partial x_j} = -\frac{1}{\rho} \frac{\partial p}{\partial x_i} + \frac{1}{\rho} \frac{\partial}{\partial x_j} \left(\mu \left(\frac{\partial U_i}{\partial x_j} \right) - \overline{u'_i u'_j} \right) \quad (3.5)$$

The continuity equation is also transformed into time-averaged form as

$$\frac{\partial U_i}{\partial x_i} = 0 \quad (3.6)$$

The five terms from left to right denote the time change rate of velocity, convection, internal source due to pressure, diffusion due to viscosity and Reynolds stress.

3.2. Turbulence models and validation

For wind flow calculation, the RANS equations were modeled by various two-equation turbulence closure models, such as various k- ϵ models (standard, RNG, realizable), and k- ω models (k- ω , k- ω SST). However, the simulation of turbulent flow and pollutant dispersion in urban street canyon has to deal with a wide range

of spatial and temporal scales and complex geometry configurations, a robust and efficient turbulence model needs to be selected.

Here, five specific RANS models, the (standard, RNG, realizable) k - ε models and the (k - ω , k - ω SST) k - ω models, are introduced and discussed, as they have been frequently used in modelling street canyon flow. They will be tested in the section 3.2.6, and the RNG k - ε model will be used after in the following chapters.

3.2.1. The standard k - ε model

The standard k - ε model is a widely-used and validated turbulence model in many fields, for its robustness, economy and reasonable accuracy (Versteeg and Malalasekera, 2007). After reviewing relevant literature, it is found that the standard k - ε model is the most frequently used turbulence model for modelling street canyon flow.

The mass conservation (continuity) equation

$$\frac{\partial U_i}{\partial x_i} = 0 \quad (3.7)$$

The momentum conservation (RANS) equations

$$\frac{\partial U_i}{\partial t} + U_j \frac{\partial U_i}{\partial x_j} = -\frac{1}{\rho} \frac{\partial p}{\partial x_i} + \frac{1}{\rho} \frac{\partial}{\partial x_j} \left(\mu \left(\frac{\partial U_i}{\partial x_j} \right) - \overline{u'_i u'_j} \right) \quad (3.8)$$

Turbulent viscosity assumption

$$-\overline{u'_i u'_j} = \nu_t \left(\frac{\partial U_i}{\partial x_j} + \frac{\partial U_j}{\partial x_i} \right) - \frac{2}{3} k \delta_{ij} \quad (3.9)$$

which $k = \frac{1}{2} \overline{u'_i u'_i}$ is the turbulent kinetic energy.

$$\nu_t = C_\mu \frac{k^2}{\varepsilon} \quad (3.10)$$

Turbulent kinetic energy equation

$$\frac{\partial k}{\partial t} + U_j \frac{\partial k}{\partial x_j} = \frac{\partial}{\partial x_j} \left[\left(\nu + \frac{\nu_t}{\sigma_k} \right) \frac{\partial k}{\partial x_j} \right] + G - \varepsilon \quad (3.11)$$

Dissipation equation

$$\frac{\partial \varepsilon}{\partial t} + U_j \frac{\partial \varepsilon}{\partial x_j} = \frac{\partial}{\partial x_j} \left[\left(\nu + \frac{\nu_t}{\sigma_\varepsilon} \right) \frac{\partial \varepsilon}{\partial x_j} \right] + C_{1\varepsilon} \frac{\varepsilon}{k} G - C_{2\varepsilon} \frac{\varepsilon^2}{k} \quad (3.12)$$

$$G = -\overline{u'_i u'_j} \frac{\partial u_i}{\partial x_j} = \nu_t \left(\frac{\partial u_i}{\partial x_j} + \frac{\partial u_j}{\partial x_i} \right) \frac{\partial u_i}{\partial x_j}$$

Based on the assumptions of Boussinesq approximation and isotropic eddy viscosity, Reynolds stress is linked to the mean rate of strain velocity $S_{ij} = \frac{\partial \bar{u}_i}{\partial x_j} + \frac{\partial \bar{u}_j}{\partial x_i}$ with a positive scalar coefficient ν_t (Pope, 2000). This coefficient is named as turbulent viscosity or eddy viscosity, since it has the same unit as kinematic viscosity. It is specified by Equation 3.10 in which ν_t is proportional to k^2/ε , where k is turbulent kinetic energy, ε is the turbulent dissipation (here simply called dissipation) and C_μ is one of the model constants for the standard $k - \varepsilon$ model (Launder and Spalding, 1974).

The turbulent viscosity assumption has introduced two additional unknown quantities k and ε . To close the model equations, the transport equations for k and ε are added (Equations 3.11 and 3.12), which explains that the standard $k - \varepsilon$ model is a two-equation model (Tu et al., 2008). These equations are not mathematically derived from the Navier-Stokes equations, but they are derived according to phenomenological considerations and empiricism (Launder and Spalding, 1974). In Equation 3.11 from left to right, TKE k is balanced between the advection of TKE, the diffusion of TKE, the production of TKE due to mean velocity gradients, the dissipation of TKE, and additional source of TKE (Versteeg and Malalasekera, 2007). In Equation 3.12 from left to right, dissipation ε is balanced by the advection of dissipation, the diffusion of dissipation, the production of dissipation

due to mean velocity gradients, the destruction of dissipation, and additional source of dissipation (Versteeg and Malalasekera, 2007). The last two terms in Equation 3.12 are assumed to be proportional to the last two terms in Equation 3.11 respectively (Versteeg and Malalasekera, 2007).

There are five model constants in the standard k- ϵ model given in Table 3.1

Table 3.1. The model constants for the standard k- ϵ model, proposed by Launder and Sharma (1974).

Model constant	C_μ	$C_{1\epsilon}$	$C_{2\epsilon}$	σ_k	σ_ϵ
Value	0.09	1.44	1.92	1.0	1.314

The standard k- ϵ model has an obvious defect in terms of model accuracy. It performs poorly for complex flows which involve severe pressure gradient, separation and strong streamline curvature. Pope (2000) attributes the poor performance to the turbulent viscosity assumption and the dissipation (ϵ) equation. Violating the turbulent viscosity assumption and introducing new modelling approach, such as what have been done in Reynolds Stress Model (RSM), are rather complicated and are not economical. On the other hand, modifying the ϵ equation is a more economical solution. The RNG k- ϵ model, which will be discussed in the following section, is a good example that improves model accuracy by modifying the existing terms and introducing a new term in the ϵ equation.

3.2.2. The RNG $k - \epsilon$ model

The RNG k- ϵ model is proposed using a statistical technique “Re-Normalization (RNG) method” by Yakhot and Orszag (1986). In contrast, the model equations of

the standard k- ε model are not derived from the Navier-Stokes equations in any systematic fashion (Yakhot and Orszag, 1986).

The RNG k- ε model has similar model equations to the standard k- ε model, except for different model constants given in Table 3.2 below and a new dissipation (ε) equation given as Equation 3.13. These model constants are derived by statistical approaches, compared to the model constants empirically determined in the standard k- ε model. The dissipation equation contains an additional term (the highlighted term in Equation 3.13) that accounts for the effects of small-scale motions (Yakhot and Orszag, 1986). This term is specified by mean rate of strain S , TKE k and dissipation ε , and η_0 and β are two model constants for the RNG k- ε mode.

Dissipation equation

$$U_j \frac{\partial \varepsilon}{\partial x_j} = \frac{\partial}{\partial x_j} \left[\left(\nu + \frac{\nu_t}{\sigma_\varepsilon} \right) \frac{\partial \varepsilon}{\partial x_j} \right] + C_{1\varepsilon} \frac{\varepsilon}{k} \overline{u'_i u'_j} \frac{\partial U_i}{\partial x_j} - C_{2\varepsilon} \frac{\varepsilon^2}{k} - \frac{C_\mu \eta^3 (1 - \eta/\eta_0)}{1 + \beta \eta^3} \frac{\varepsilon^2}{k} \quad (3.13)$$

where $\eta = S \frac{k}{\varepsilon}$, $S = \sqrt{\frac{1}{2} \left(\frac{\partial U_i}{\partial x_j} + \frac{\partial U_j}{\partial x_i} \right)^2}$, $\eta_0 = 4.38$, and $\beta = 0.012$.

Table 3.2. The model constants of the RNG k- ε model, proposed by Yakhot et al. (1992).

Model constant	C_μ	$C_{1\varepsilon}$	$C_{2\varepsilon}$	σ_k	σ_ε
Value	0.0845	1.42	1.68	0.7194	0.7194

3.2.3. The realizable k- ε model

Turbulent kinetic energy equation

$$\frac{\partial k}{\partial t} + U_j \frac{\partial k}{\partial x_j} = \frac{\partial}{\partial x_j} \left[\left(\nu + \frac{\nu_t}{\sigma_k} \right) \frac{\partial k}{\partial x_j} \right] + P_k - \varepsilon \quad (3.14)$$

Dissipation equation

$$\frac{\partial \varepsilon}{\partial t} + U_j \frac{\partial \varepsilon}{\partial x_j} = \frac{\partial}{\partial x_j} \left[\left(\nu + \frac{\nu_t}{\sigma_\varepsilon} \right) \frac{\partial \varepsilon}{\partial x_j} \right] + C_1 S \varepsilon - C_2 \frac{\varepsilon^2}{k + \sqrt{\nu \varepsilon}} \quad (3.15)$$

$$C_1 = \max \left\{ 0.43, \frac{\eta}{\eta + 5} \right\}, \eta = S \frac{k}{\varepsilon}, S = \sqrt{\frac{1}{2} \left(\frac{\partial U_i}{\partial x_j} + \frac{\partial U_j}{\partial x_i} \right)^2}$$

$$\sigma_k = 1.0, \sigma_\varepsilon = 1.2, C_2 = 1.9$$

3.2.4. The k- ω model

The $k - \omega$ model is proposed by Wilcox (1988), which uses the turbulence frequency $\omega = \varepsilon/k$ (dimensions s^{-1}) as the second variable.

Turbulent kinetic energy

$$\frac{\partial k}{\partial t} + U_j \frac{\partial k}{\partial x_j} = \frac{\partial}{\partial x_j} \left[\left(\nu + \frac{\nu_t}{\sigma_k} \right) \frac{\partial k}{\partial x_j} \right] + P_k - \beta^* k \omega \quad (3.16)$$

The specific rate of dissipation equation

$$\frac{\partial \omega}{\partial t} + U_j \frac{\partial \omega}{\partial x_j} = \frac{\partial}{\partial x_j} \left[\left(\nu + \frac{\nu_t}{\sigma_\omega} \right) \frac{\partial \omega}{\partial x_j} \right] + \gamma_1 \left(2S_{ij} \cdot S_{ij} - \frac{2}{3} \omega \frac{\partial U_i}{\partial x_j} \delta_{ij} \right) - \beta_1 \omega^2 \quad (3.17)$$

$$\nu_t = \frac{k}{\omega}$$

Table 3.3. The model constants of the k- ω model proposed by Wilcox (1988)

Model constant	β^*	γ_1	β_1	σ_k	σ_ω
Value	0.09	0.553	0.075	2.0	2.0

3.2.5. The SST k- ω model

Menter (1992) noted that the results of the k- ε model are much less sensitive to the (arbitrary) assumed values in the free stream, but its near-wall performance is unsatisfactory for boundary layers with adverse pressure gradients. The Reynolds

stress computation and the k-equation are the same as in Wilcox's original k- ω model, but the ε -equation is transformed into an ω -equation by substituting $\varepsilon = k\omega$.

The specific rate of dissipation equation

$$\frac{\partial \omega}{\partial t} + U_j \frac{\partial \omega}{\partial x_j} = \frac{\partial}{\partial x_j} \left[\left(\nu + \frac{\nu_t}{\sigma_\omega} \right) \frac{\partial \omega}{\partial x_j} \right] + \alpha S^2 - \beta \omega^2 + 2(1 - F_1) \sigma_{\omega 2} \frac{1}{\omega} \frac{\partial k}{\partial x_j} \frac{\partial \omega}{\partial x_j} \quad (3.18)$$

$$\nu_t = \frac{\alpha_1 k}{\max\{\alpha_1 \omega, SF_2\}}, \quad F_2 = \tanh \left[\left[\max \left(\frac{2\sqrt{k}}{\beta^* \omega y}, \frac{500\nu}{y^2 \omega} \right) \right]^2 \right]$$

$$F_1 = \tanh \left\{ \left\{ \min \left[\max \left(\frac{2\sqrt{k}}{\beta^* \omega y}, \frac{500\nu}{y^2 \omega} \right), \frac{4\sigma_{\omega 2} k}{CD_{k\omega} y^2} \right] \right\}^4 \right\},$$

$$CD_{k\omega} = \max \left\{ 2\rho \sigma_{\omega 2} \frac{1}{\omega} \frac{\partial k}{\partial x_i} \right\}$$

$$P_k = \min \left\{ \overline{-u'_i u'_j \frac{\partial U_i}{\partial x_j}}, 10\beta^* k\omega \right\}$$

Table 3.4. The model constants of the SST k- ω model proposed by Menter (2003)

Model constant	β^*	α	α_1	γ_1	β_1	β	σ_k	$\sigma_{\omega 1}$	$\sigma_{\omega 2}$
Value	0.09	0.44	5/9	0.553	0.075	0.0828	1.18	2.0	0.856

3.2.6. Validation of RANS models

We have tried to validate the results obtained from different turbulence models against different experimental measurements of Li et al. (2008) and Brown et al. (2000). Figure 3.1 shows a validation of vertical velocity profiles obtained from different turbulence closure models against the measurements of Li et al. (2008). Figure 3.2 shows the comparisons of velocity profiles and turbulence kinetic energy between numerical results obtained from different turbulence models (standard, realizable, RNG, k- ω and k- ω SST) and the measurements of Brown et

al. (2000) for flat roofs. From Figures 3.1, 3.2 and 3.3, it shows that the results obtained from various k - ε and k - ω models are not noticeable differences in comparison with experimental data. However, the standard and RNG k - ε models are in favor of practical applications for large scale simulations due to their robustness and efficiency. Furthermore, it is well-known that the standard k - ε model under-predicts reattachment length (Demirdzic, 1982; Thangam and Speziale, 1991), and the velocity close to wall boundaries within the cavity (Sahm et al., 2002); it also has some deficiencies when the standard k - ε model is applied to simulate flow impingement and separation (Apsley and Castro, 1997). The flow in urban street canyons, by its nature, is inherent the characteristics of the flow over backward-facing step, and the flows including reattachment, separation, and recirculation zone. A modification of the strain-dependent correction term in the ε -equation of RNG k - ε model, has overcome the limitation of the standard k - ε turbulence. Yakhot et al. (1992) reported that RNG k - ε model showed very good predictions of the flow over backward-facing step. Particularly, Rotach (1995), Chan et al. (2003), Li et al. (2005), Memon and Leung (2011), and Koutsourakis et al. (2012) have recommended that RNG k - ε turbulence closure model has best overall performance among k - ε model variants for the simulation of turbulent flow and pollutant dispersion in urban street canyons. In fact, the difference is not significant as shown in Table 3.5; however, it is well-known that RNG k - ε model and k - ε model are more robust and inexpensive than other turbulence models in term of computational costs. In addition, RNG k - ε model is performed better than k - ε in the application for urban street canyon dominated by strong separation flow (as in cavity flow); therefore, the selection of RNG k - ε is based the economic aspect for the simulation of large scale areas as an entire big city.

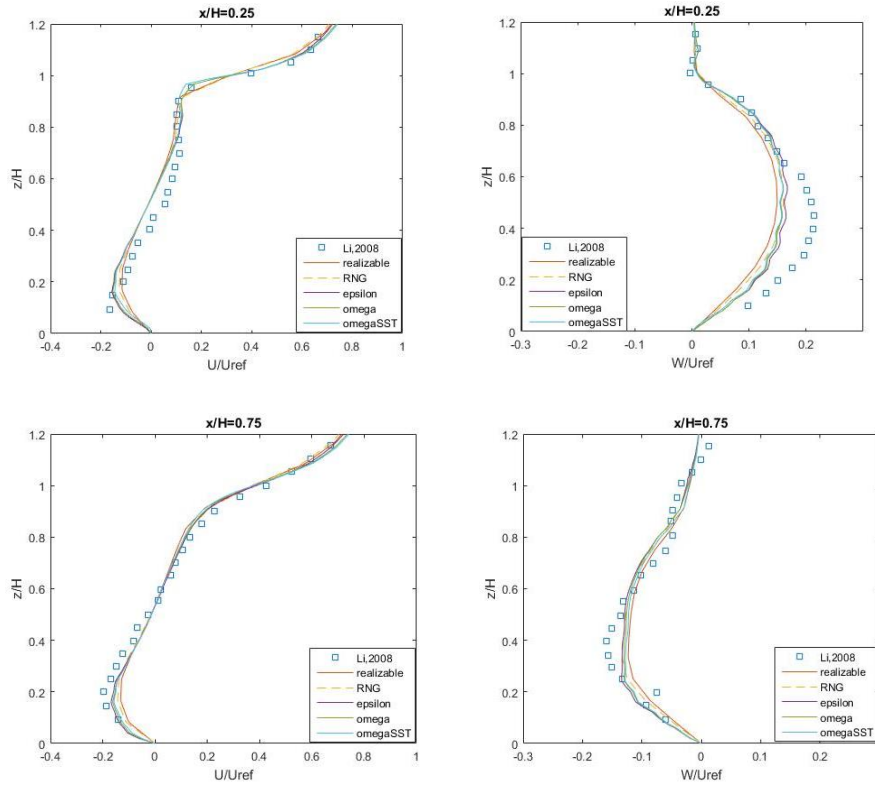


Figure 3.1. A comparison of vertical velocity profiles (U/U_{ref} and W/U_{ref}) between numerical results obtained from different turbulence models and experimental data (Li et al., 2008).

Table 3.5. The RMSE of Figure 3.1

	$x/H = 0.25$		$x/H = 0.75$	
	U/U_{ref}	W/U_{ref}	U/U_{ref}	W/U_{ref}
Realizable	0.0396	0.0285	0.0311	0.0206
RNG	0.0395	0.0283	0.0203	0.0172
Epsilon	0.0397	0.0372	0.0310	0.0213
Omega	0.0459	0.0415	0.0354	0.0185
OmegaSST	0.0462	0.0421	0.0246	0.0262

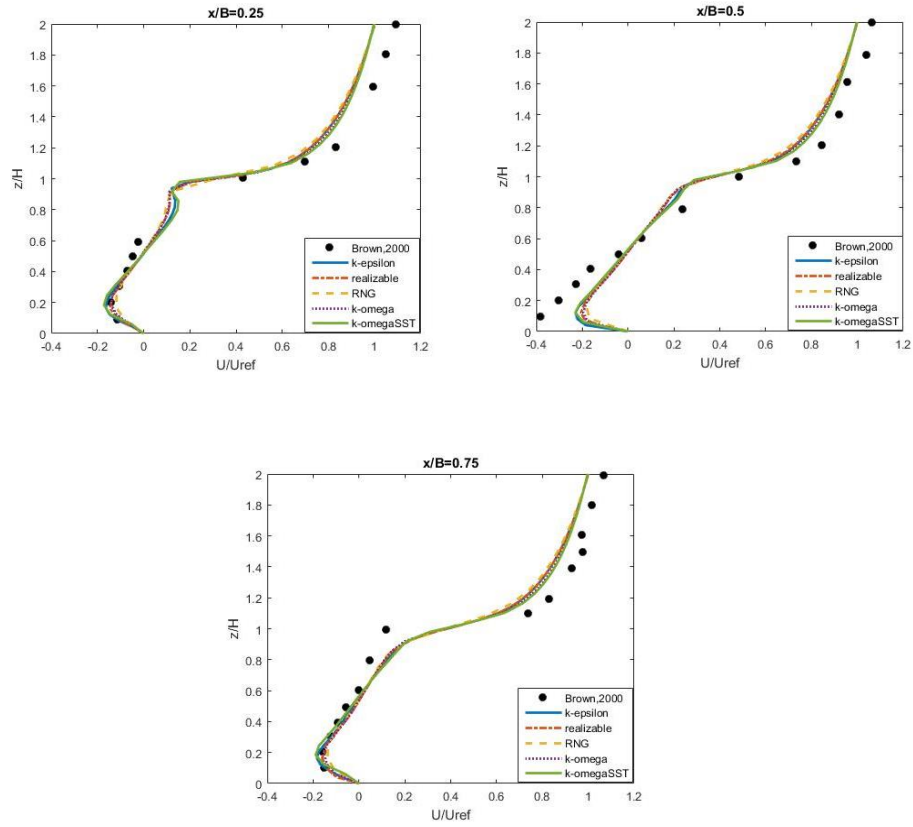


Figure 3.2. A comparison of vertical velocity profiles (U/U_{ref}) between numerical results obtained from different turbulence models and experimental data (Brown et al., 2000).

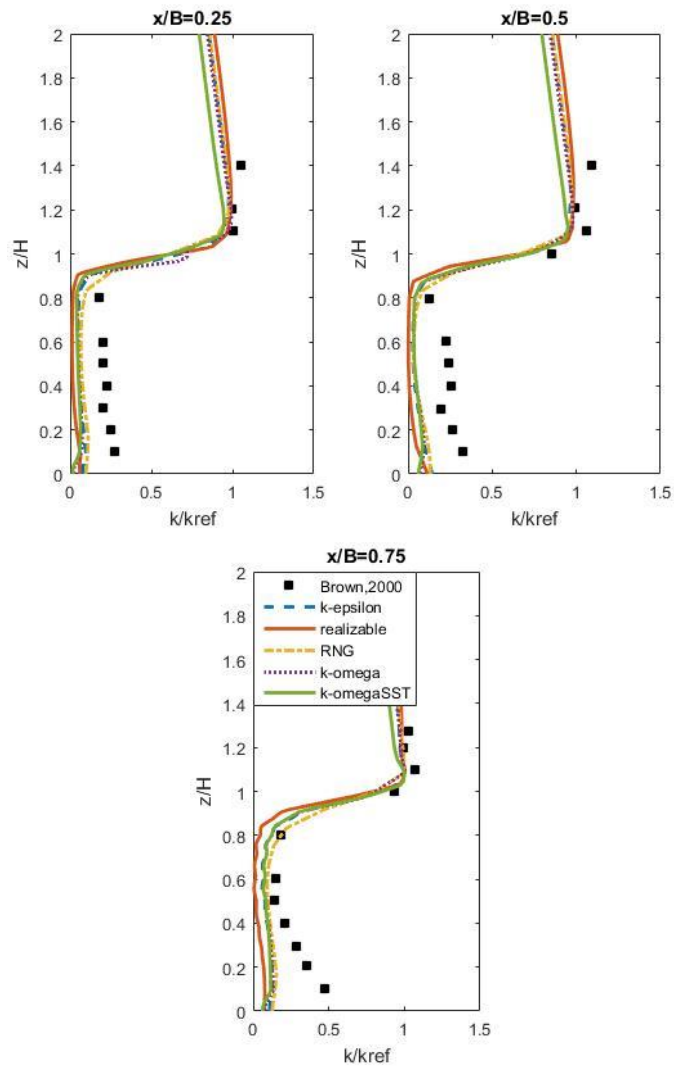


Figure 3.3. A comparison of turbulence kinetic energy (TKE) between numerical results obtained from different turbulence models and experimental data (Brown et al., 2000).

3.3. Scalar transport equation and the implementation of code

3.3.1. Standard Gradient Diffusion Hypothesis (SGDH)

Similarly, as the same manner to obtain RANS equations, the time-averaged transport equation for a scalar C is obtained:

$$\frac{\partial C}{\partial t} + U_j \frac{\partial C}{\partial x_j} = \frac{\partial}{\partial x_j} \left(D \frac{\partial C}{\partial x_j} \right) - \frac{\partial}{\partial x_j} (\overline{u'_j c'}) + S \quad (3.19)$$

where the prime denotes a fluctuating value, D is molecular diffusion coefficient, S is a pollutant source.

The simplest model for turbulent scalar flux follows from the standard gradient diffusion hypothesis (SGDH), where the turbulent scalar flux is assumed proportional to mean scalar gradient as follows:

$$\overline{u'_j c'} = -D_t \frac{\partial C}{\partial x_j} \quad (3.20)$$

So we can rewrite the equation (3.19) as

$$\frac{\partial C}{\partial t} + U_j \frac{\partial C}{\partial x_j} = \frac{\partial}{\partial x_j} \left((D + D_t) \frac{\partial C}{\partial x_j} \right) + S \quad (3.21)$$

where D_t is turbulent diffusion coefficient which is assumed to be isotropic and homogeneous.

The turbulent diffusion coefficient D_t is modeled by the relationship eddy-viscosity and the turbulent Schmidt number, $Sc_t = \frac{\nu_t}{D_t}$.

As shown in Table 3.6, the values for Sc_t were widely distributed in the range of 0.1 – 2.5. Since the optimum values of Sc_t largely depended on the local flow characteristics, they recommended that Sc_t should be determined by considering the dominant effect in the turbulent mass transport and local effects (anisotropic

effects) in each case; therefore, it causes difficulties to define an appropriate value for pollutant dispersion in urban street canyons.

The SGDH relates the scalar Reynolds fluxes to the spatial gradient of the time-averaged concentration through the turbulent diffusivity. The SGDH model adopts a scalar, the eddy-diffusivity, assuming an alignment of the scalar flux vector with the mean scalar gradient; the possibility of having different diffusivities in each direction is explored with the use of a diffusivity tensor, which is both diagonal and anisotropic. However, in many cases, this assumption is not verified. Alternatively, other tensorial eddy-diffusivity approaches could be introduced to achieve more accurate predictions of scalar transport and dispersion in complex flows. Such a type of model is given by the so-called Generalized-Gradient-Diffusion Hypothesis (GGDH) (Daly, 1970) and also the High-Order extension of the GGDH model (HO-GGDH) (Abe, 2001). More generally, it has been recognized for a long time now that the width of a dispersing patch in a turbulent environment grows proportionally with time, rather than the square root of time, if not a little faster (Fischer, 1974, p.484). Recently, a new approach using a non-local quantity, which may be interpreted in terms of the probability density distribution of the turbulent velocity, has been proposed (Cushman-Roisin, 2008). This approach assumes that the diffusivity grows with the patch size and that eddies of the scale most comparable to the size of the patch are the most effective at distorting and dispersing it, letting the smaller eddies to smear details and the larger eddies to transport the patch. In addition, there is recently important literature on fully-non-Fickian approaches, aimed at providing prediction for the “heavy-tail” behaviour of the mass-transport of some substances.

Table 3.6. Values used in previous studies on building and urban diffusion simulation

Year	Author	Turbulent Schmidt number
2007	Tominaga and Stathopoulos	Review paper. $Exp/Num - Sc_t = 0.2 - 1.3$
2007	Di Sabatino and Buccolieri	$Exp/Num - Sc_t = 0.4 - 0.7$
2008	Blocken et al.	$Exp/Num - Sc_t = 0.3 - 1$
2011	Yassin	$Num - Sc_t = 0.9$
2012	Mokhtarzadeh-Dehghan et al.	$Exp/Num - Sc_t = 0.4 - 2.5$, as a function of Richard number
2013	Ebrahimi and Jahangirian	$Exp/Num - Sc_t = 0.7$
2014	Chen et al.	$Exp/Num - Sc_t = 1$
2017	Gualtieri et al.	Review paper

3.3.2. Generalized Gradient Diffusion Hypothesis (GGDH)

To overcome the limitation of SGDH as mentioned above, another model for turbulent scalar flux is given by the so-called Generalized Gradient Diffusion Hypothesis (GGDH) proposed by Daly and Hallow (1970), and Ince and Launder (1989). The approach was developed and applied in the heat transfer problem by (Kenjeres, 1998), (Thielen, 2005), (Vieira, 2013), (Kumar, 2014). Their studies showed that the GGDH approach can take into account the scalar dispersion driven by turbulence better than the SGDH approach.

In this approach, the turbulent scalar flux is derived as

$$\overline{u'_j c'} = -C_c \tau_c \frac{\overline{u'_i u'_j}}{k} \frac{\partial c}{\partial x_i}, \quad (3.22)$$

which $C_c = 0.3$, $\tau_c = k/\varepsilon$.

Applying to the equation (3.19), we obtain

$$\frac{\partial c}{\partial t} + u_i \frac{\partial c}{\partial x_i} = \frac{\partial}{\partial x_i} \left(\left(D + C_c \frac{k}{\varepsilon} \overline{u'_i u'_j} \right) \frac{\partial c}{\partial x_i} \right) + S \quad (3.23)$$

In the formula (3.22), the turbulent scalar flux depend on Reynold stress tensor, turbulent kinetic energy k and the turbulent dissipation ε . These variables describe the local flow characteristics well, particularly the Reynolds stress $\overline{u'_i u'_j}$, is taken into the near wall anisotropic effects.

3.3.3. Implementation of the scalar transport equation in OpenFOAM

OpenFOAM (Open source Field Operation And Manipulation) is a free and open source finite volume CFD toolbox originally developed at the Imperial College by (Jasak, 1996) and (Rusche, 2002). It is a cell-centred finite volume framework for computational fluid dynamics supporting unstructured polyhedral meshes. OpenFOAM consists in a bundle of libraries and codes to solve complex problems such as turbulence, fluid flows, electromagnetics, chemical reactions, combustion... It also features applications to pre- and post- process, including mesh generation tools (e.g. blockMesh, snappyHexMesh), setting and modifying field values, mesh decomposition and sampling data (Fig. 3.4). It is prepared to run cases in parallel, allowing an easy set-up and a straightforward calculation method.

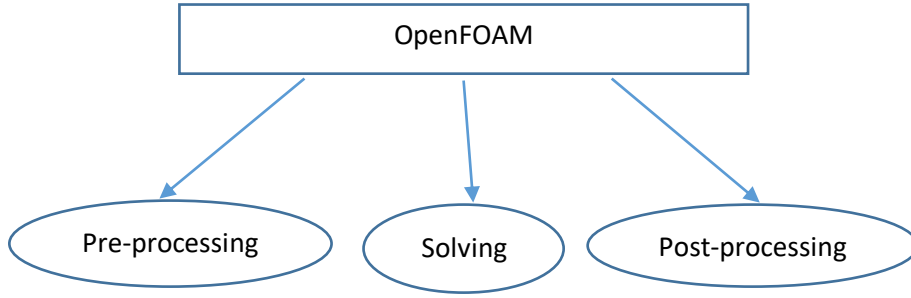


Figure 3.4. OpenFOAM structure

The applications in OpenFOAM consist of two groups, i.e. solvers and utilities. The solvers are developed to solve particular problems, which are different from case to case and the utilities are normally associated with the data manipulation and visualization in either pre-processing or post-processing.

There exists a solver (scalarTransportFoam), which resolve a transport equation for a passive scalar in OpenFOAM library. Its governing equation is

$$\frac{\partial C}{\partial t} + U_i \frac{\partial C}{\partial x_i} = \frac{\partial}{\partial x_i} \left(D \frac{\partial C}{\partial x_i} \right)$$

where C is concentration of passive scalar, U_i are velocity components and D is the diffusion coefficient. The current solver in OpenFOAM can solve only the concentration field on a given stationary velocity field (i.e. $U_i = \text{constant}$). So, it uses only constant diffusion coefficient, and cannot take account for turbulent flow. The modification of original solver is required to resolve the concentration field driven by the turbulent flow.

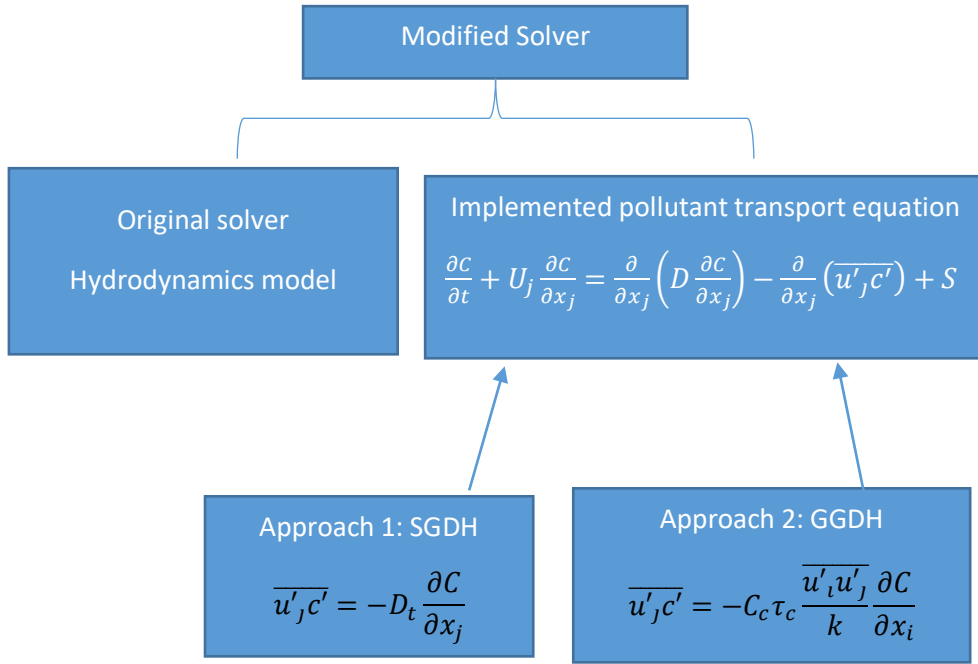


Figure 3.5. Schematic of the modified solver.

The solver employed in this study to solve the hydrodynamics model is the `pimpleFoam` solver. The turbulence properties, velocity field and pressure field, which are calculated by PIMPLE algorithm, can be obtained. The solver is implemented the advection-diffusion equation to calculate the concentration of the pollutant. As mentioned above, there are two modified solvers corresponding to two approaches to approximate the turbulent scalar flux term (Fig. 3.5). The information of velocity field in unsteady-state and turbulent diffusion coefficient in every time step. The implemented code is showed in detail in the Appendix.

The computations of model are carried on High Performance Computing (HPC) cluster of CFD Laboratory at SNU (<https://cfdlabsnu.com/>). In this research, each case is run with 24-36 cores. The time consuming is about 1-3 days for each simulation case.

3.3.4. Validation of the SGDH approach

A range of turbulent Schmidt number (i.e. $Sc_t=0.3, 0.5, 0.7, 0.9$ and 1.1) has been tested before the benchmarking study, as different values of this number would strongly affect the turbulent diffusion of pollutant and therefore affect overall concentration in street canyon. It is found that the values 0.7 and 0.9 provide the closet prediction of concentration to the measurements for benchmark cases 1 and 2 which are modelled by 2D geometries. This finding is consistent with many experimental results (not the experiments for this study) that the turbulent Schmidt number is typically in the range of 0.7 – 0.9 for various types of flow. Therefore, it has been determined to use $Sc_t=0.9$ for benchmark cases before making other tests, and all the modelled concentrations for these two cases are based on $Sc_t=0.9$ (Fig. 3.6).

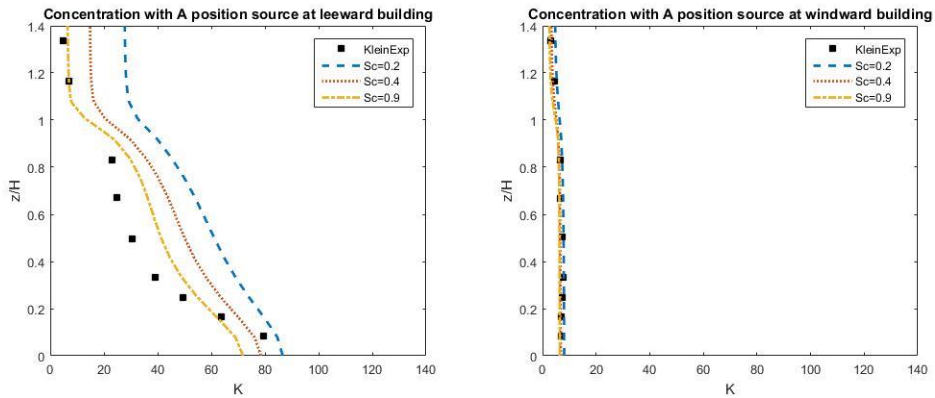


Figure 3.6. The comparison of Schmidt numbers (0.2, 0.4, 0.9) with the reference case of Klein at the leeward building (left) and windward building (right)

3.3.5. Validation of the GGDH approach

Fig. (3.7, 3.8) show the comparison between SGDH (for the best shot of $Sc_t=0.9$) and GGDH methods. All four cases show that GGDH method provide the results better than SGDH, whereby we don't need to calibrate the Sc_t .

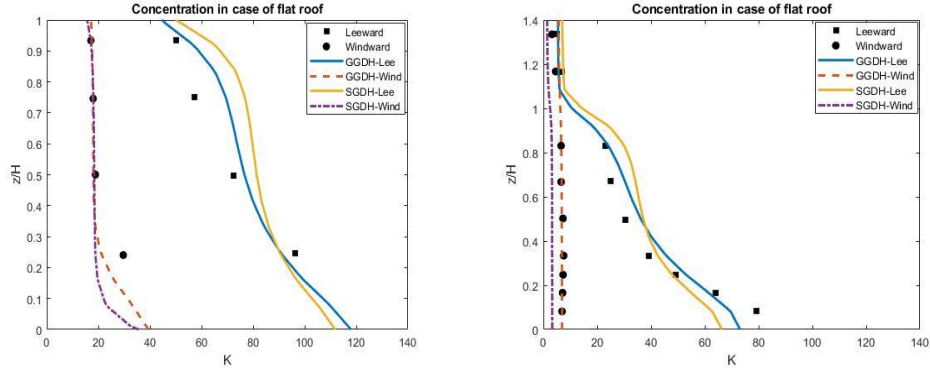


Figure 3.7. The comparison of concentration distribution at leeward and windward building in the case of flat roof of Rafailidis's experiment (left) and Klein's experiment (right)

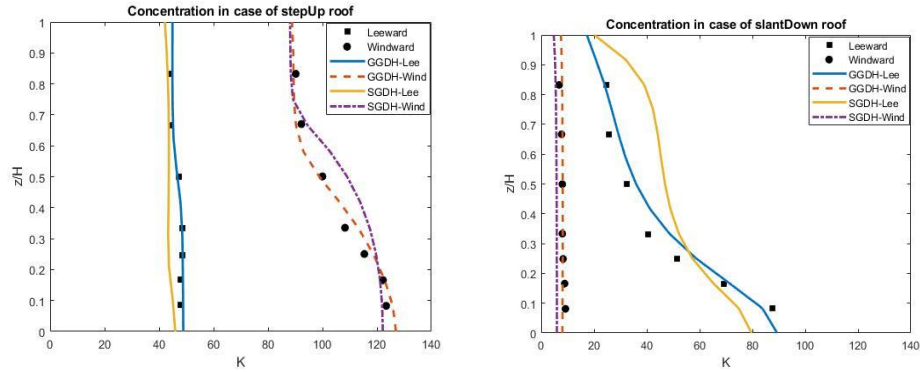


Figure 3.8. The comparison of concentration distribution at leeward and windward building in the case of stepUp roof shape (left) and slantDown roof shape (right) of Klein's experiment.

3.4. Initial and boundary condition

Boundary conditions for CFD are a set of additional constraints for the Navier-Stokes equations or the governing equations of turbulence model. For CFD models that use the same turbulence model, the governing equations are the same, so the different boundary conditions are the reason for the different solutions. Thus, setting appropriate boundary conditions is a key point for CFD modelling. A boundary condition is specified by its type, its position and some parameters on it, which are discussed separately in Sections 3.4.2 and 3.4.3. In these sections, the boundary conditions used in the literature are reviewed to determine the boundary conditions to be used in this thesis.

3.4.1. Boundary type

A typical street canyon model is created by a rectangular domain which encloses all geometries. Boundary conditions are defined on six surfaces of the rectangular domain, on building surfaces and on emission sources. After reviewing the boundary types used in the literature, the boundary types for this thesis are determined and given in Table 3.7 below. It should be mentioned that an emission source is usually specified as a velocity inlet with extremely small velocity (set as 0.001m/s in this thesis) and zero turbulence, for the purpose of not intruding the original flow in the street canyon. Pollutant concentration is defined as zero flux on all the boundaries except on the emission source that concentration is defined to have a fixed value (set as 0.04 in this thesis). The detailed value will not affect the normalized concentration in the computational domain, due to the similarity law.

Table 3.7. Typical boundary conditions for a CFD model that simulates flow around street canyon.

Name	Boundary type and essential parameters
Inlet boundary	Velocity inlet with appropriate velocity, TKE and dissipation profiles
Outlet boundary	Outflow or pressure outlet with 0 Pa (i.e. equal to the reference pressure defined in CFD model)
Bottom boundary	No-slip wall with no roughness or no-slip wall with appropriate roughness parameters
Top boundary	Symmetry boundary (for full-scale real street canyons) or no-slip wall (for scaled-down experimental models)
Side boundary	Symmetry boundary (for full-scale real street canyons) or no-slip wall (for scale-down experimental models)
Building surface	No-slip wall with no roughness
Emission source	Velocity inlet with a very small normal velocity and 0% turbulence intensity

3.4.2. Boundary position

To perform CFD modelling of street canyon flow, sufficient distances should be placed between street canyon geometries and the boundaries of the computational domain, in order to generate sensible flow fields around the street canyons. The COST best practice guideline (Franke et al., 2007) and the AIJ guidelines (Tominaga et al., 2008) have recommended the minimum distance for each boundary measured by characteristic building height (H), as summarized in Table 3.8 below. These requirements are observed in most CFD modelling.

It should be noted that providing longer distances after and alongside street canyon geometries does not affect the flow in the streets. However, pointed out that

providing a too long distance between inlet boundary and the first building could cause less accurate approaching flow. The reason was that the atmospheric boundary layer could not be sustained without setting an appropriate shear stress at top boundary, but estimating accurate shear stress was difficult. Therefore, the distance between inlet boundary and the first building should be specified neither too long nor too short, just around 5H.

Table 3.8. Minimum distances between the boundaries and the buildings for modelling street canyon flow. Recommended by the COST best practice guideline (Franke et al., 2007) and the AIJ guidelines (Tominaga et al., 2008).

Boundary	Minimum distance
Inlet boundary	5H before the first building
Outlet boundary	15H after the last building
Side boundaries	5H from the flank of the buildings
Top boundary	10H above the ground

3.4.3. Inlet boundary profile

Amongst all the boundaries of a CFD model, inlet boundary has the uppermost importance on the flow in computational domain. In one aspect, it is the only type of boundary on which additional parameters need to be defined, contrasting to outflow, symmetry and wall boundaries on which only boundary type need to be specified. In another aspect, it is apparent that the approaching flow condition will affect the downstream flow.

For k- ϵ type of turbulence models, mean velocity, TKE and dissipation need to be defined on the inlet boundary. They are usually specified in the forms of empirical profiles. These specifications are more precise than specifying velocity, TKE and dissipation as constants, and are more robust and convenient than importing measured data. Discussions of these empirical profiles are made below.

In modelling street canyon flow, the velocity of inlet boundary is usually defined by either a logarithmic law profile or a power law profile. The logarithmic law profile (Equation 3.24), which accounts for surface roughness and atmospheric stability, describe the wind velocity profile of the atmospheric boundary layer (ABL) more accurately. It is a preferred choice in modelling experimental flow, since the roughness can be accurately estimated from high-resolution experimental measurements and the stability can be controlled. On the other hand, when the roughness and stability information is not available, the wind velocity profile of the ABL is more reliably approximated by the power law profile (Equation 3.25). It is a preferred choice in modelling full-scale real cases, since friction velocity and roughness height are usually unable to be accurately estimated due to limited measurements at different heights.

The logarithmic law is usually specified by

$$U = \frac{U_\tau}{\kappa} \ln \frac{z+z_0}{z_0} \quad \text{or} \quad U = \frac{U_\tau}{\kappa} \ln \frac{z}{z_0} \quad (3.24)$$

where U_τ is the friction velocity, κ is the von Karman constant and has a value of 0.41, and z_0 is the roughness height.

The power law is usually specified by

$$U = U_{ref} \left(\frac{z}{z_{ref}} \right)^\alpha \quad (3.25)$$

where z_{ref} is the reference height, U_{ref} is the velocity at the reference height, and α is the power law index.

The TKE and dissipation profiles of inlet boundary are specified by several forms in the literature. Three typical forms are provided below. Depending on the available information for the ABL, each of them might be a suitable choice to describe the turbulence information on the inlet boundary.

Richards and Hoxey (1993) proposed mathematically consistent turbulent kinetic energy and dissipation profiles for two-dimensional flows (Equations 3.26 and 3.27). These profiles are based on two assumptions that the ABL has a logarithm velocity profile and shear stress is constant in the ABL. The second assumption implies that TKE (k) remains constant in the ABL, dissipation (ε) decreases inversely with height.

These profiles have been applied in many CFD models which study atmospheric flow or street canyon flow (Blocken et al., 2007; Hargreaves and Wright, 2007; Xie et al., 2005a). These profiles are also recommended by the COST best practice guideline (Franke et al., 2007) and the AIJ guidelines (Tominaga et al., 2008) as preferred inlet boundary settings for street canyon models.

$$k = \frac{U_\tau^2}{\sqrt{c_\mu}} \quad (3.26)$$

$$\varepsilon = \frac{U_\tau^3}{\kappa(z+z_0)} \quad \text{or} \quad \varepsilon = \frac{c_\mu^{3/4} k^{3/2}}{\kappa(z+z_0)} \quad (3.27)$$

The profile proposed by Richards and Hoxey (1993), however, are not suitable to describe modelled ABL in scaled-down experiment. This is because in experimental models, shear stress and TKE are not constant but decreases with height. Solazzo et al. (2009) suggested that a suitable modification was to multiply both TKE and dissipation profiles by a factor of $(1 - z/\delta)$ (Equations 3.28 and 3.29), while Castro and Apsley (1997) suggested a different multiplier $(1 - z/\delta)^2$ only for TKE profile. Both modified profiles results in negative k and ε above the boundary layer height δ . Castro and Apsley (1997) provided a solution to this issue, by specifying constant k and ε above 0.9δ .

$$k = \frac{U_\tau^2}{\sqrt{c_\mu}} \left(1 - \frac{z}{\delta}\right) \quad (3.28)$$

$$\varepsilon = \frac{U_\tau^3}{\kappa(z+z_0)} \left(1 - \frac{z}{\delta}\right) \quad (3.29)$$

The AIJ guidelines (Tominaga et al., 2008) recommended TKE and dissipation profiles which was dependent on the model constant C_μ , the power-law index α and the boundary layer height δ (Equations 3.30 and 3.31). These profiles are used together with power law velocity profile, as power law index and boundary layer height are available in power law profile, while friction velocity and roughness height are not available or difficult to be estimated accurately.

$$k = 0.1U \left(\frac{z}{\delta} \right)^{-0.05-\alpha} \quad (3.30)$$

$$\varepsilon = C_\mu^{1/2} k \frac{U_{ref}}{z_{ref}} \alpha \left(\frac{z}{z_{ref}} \right)^{\alpha-1} \quad (3.31)$$

4. VALIDATION OF CFD MODELS

Benchmark studies are reported in this chapter, in order to assess the accuracy of CFD modelling. The structure of this chapter is given as follows. A CFD model is validated against Li (2008)'s water channel experiments to assess flow characteristics inside urban street canyon. A CFD model is validated against Kastner-Klein (1999)'s experimental measurements to assess concentration distribution in urban street canyon. A CFD model is validated against Llaguno-Munitxa (2017)'s experiment to study the flow characteristics in case of round-shaped roofs. A CFD model is validated against CEDVAL data to study the flow characteristics for 3-D isolated building.

4.1. Studying the flow characteristics in street canyon with different aspect ratios by comparison to Li (2008)'s experiment

4.1.1. Description of experiment setup

The experiments were carried out in a 10-m-long, 0.3-m-wide, and 0.5-m-high laboratory flume located at the Croucher Laboratory of Environmental Hydraulics, at The University of Hong Kong. The schematic diagram of the laboratory flume is shown in Fig. 1a. Recirculating water flow could be maintained in the flume at a flow rate up to 28 L s^{-1} . The working test section was located in the middle of the flume and all experiments were performed there for the best flow uniformity. The sidewalls of the test section were made of toughened transparent glass. The ambient flow speed inside the test section was adjusted by varying the flow rate and the water depth through an adjustable overflow weir at the downstream end of

the test section. The two-component flow velocities and turbulent intensities (in the stream-wise and vertical directions) were measured with a two-color LDA. The LDA was a fiber-optic system (model 55X, supplied by Dantec Dynamics). It used a 4-W argon ion laser for the laser source and a correlation-based processor for the computation of flow velocities from the Doppler bursts. The LDA worked in the backscatter mode with a frequency shift to measure the reverse velocities. It is a nonintrusive measurement method, except for the presence of seeding particles; hence, the original flow field will not be disturbed by the measurement devices. In this study, the flow was seeded with the polycrystalline powders of nominal diameter of 30 μm (supplied by Optimage). This type of seeding particle was selected because of its advantage of having neutral buoyancy, extra-fine grain, and good light-scattering properties. No density stratification was considered in this study. Six to 10 identical model buildings (29.8 cm x 10 cm x 10 cm in size) were aligned perpendicular to the prevailing flow direction in the working test section to form the street canyons, with the target canyon located at the center (Fig. 4.1a). The upstream canyons can serve to make the inflow turbulence fully developed before it reaches the target canyon. The enlarged view of the target canyon is shown in Fig. 4.1b.

The dimensions of the computational domain are $L \times W \times H = 30H \times 3H \times 4H$ (with H being the height of building) and replicate the geometry of the experiment setup. The height of the buildings was fixed at $H = 10$ cm and the width of the canyon B could be varied according to the characteristic aspect ratio (street height/canyon width, H/B). The minimum grid resolution is set to $0.1H$ and is expanded towards the horizontal and vertical directions. This follows the practice guidelines for the use of CFD in wind engineering (Tominaga, 2008). The grid independence is tested and the result does not change significantly with different grid systems.

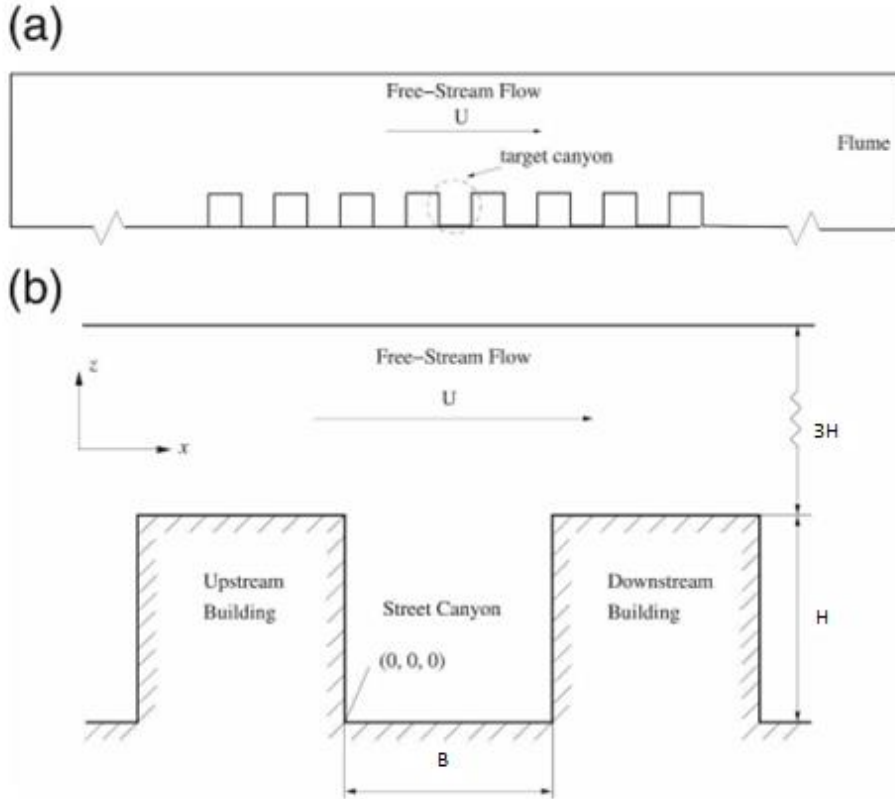


Figure 4.1. Schematic diagrams of street canyon arrangement: (a) whole view and (b) enlarged view of target street canyon.

4.1.2. Street canyon of $AR = 1$

This case is similar to the flat roof shape experiments of Rafailidis and Schatzmann (1995). As classified by Oke (1988), the flow regime in this configuration ($AR = 1$) is skimming whereby the bulk flow does not enter the canyon. It is characterized by a stable and isolated vortex at the street canyon center due to an ambient flow outside on top of the street canyon as shown in Figure 4.16a below.

Figure 4.2 shows the normalized vertical profiles of the stream-wise (left column) and vertical (right column) velocities along leeward ($x/B = 0.25$), center ($x/B = 0.5$), and windward ($x/B = 0.75$) locations in the street canyon with an aspect ratio

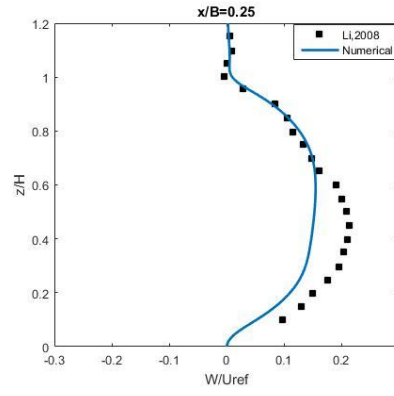
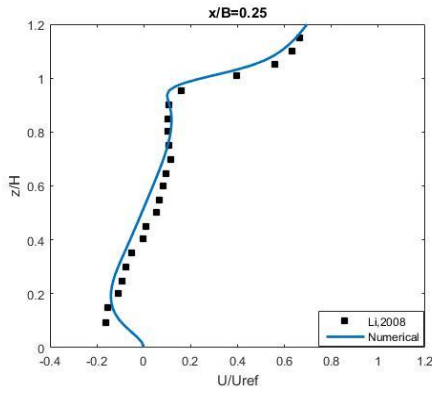
AR=1. The numerical results of stream-wise velocity (U/U_{ref}) show a very good agreement with experimental data as shown on left column. While the numerical results of vertical velocity (W/U_{ref}) are well captured the observation data at $x/B = 0.25$ and 0.75 , similar to the numerical results obtained from the simulation of Rafailidis and Schatzmann's experiment, the result in this case does not capture well the vertical velocity profile (W/U_{ref}) at $x/B = 0.5$. However, our results are overall very similar to the results obtained from Li et al. (2005) using k- ϵ model, and better than the results obtained from Liu et al. (2004) using LES model. Actually, they also have failed to reproduce the vertical velocity at the center of street canyon ($x/B = 0.5$).

The vertical velocity profiles clearly show the flow moves up at upstream (near leeward) and moves down at downstream (near windward), producing a stable clockwise vortex at the center of street canyon. Due to the clockwise vortex at the street canyon center, the stream-wise velocity is negative below half-height roof level, and positive over half-height level. The vertical velocity approached to zero at the roof-top level ($z/H = 1$) because the ambient wind above the roof-top level plays a role as a driven-lid for the street canyon. Figure 4.3 shows the horizontal profiles of the normalized stream-wise and vertical velocities along a roof level and half-height line. The vertical velocity at roof level (Fig. 4.3a, downright) is very small due to the suppression of the upper motion by the ambient wind, which made the flow in the street canyon similar to the flow in a lid-driven cavity. The vertical velocity at the half-height level (Fig. 4.3b, upright) changes direction at about the center of canyon width; i.e. it takes positive value on the upstream half-width of the canyon, and negative value on downstream half-width of the canyon. The stream-wise velocity at the half-height level (Fig.4.3b, up-left) is almost negative. All of these features demonstrate the characteristics of an isolated circulation at the center of street canyon as a cavity center.

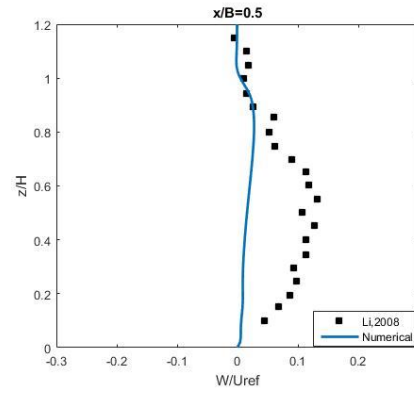
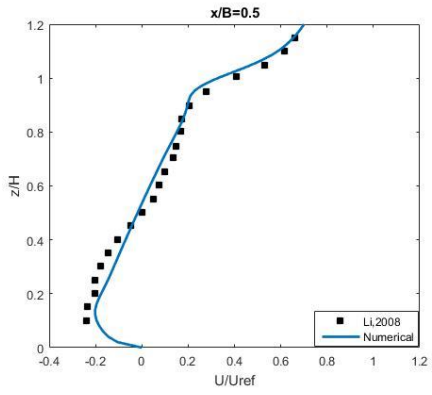
Figure 4.4 shows the normalized turbulence kinetic energy (k/U_{ref}^2) at three vertical lines; leeward ($x/B = 0.25$), center ($x/B = 0.5$) and windward ($x/B = 0.75$)

locations, in street canyon. Similar to the case of $AR=2$, it shows our model can pick up the turbulent kinetic energy inside the street canyon (below the roof height); particularly the numerical results are matching well with experimental data at on upstream and center of street canyon, but it was not in good agreement beyond the roof level, where it occurs the interaction of the ambient flow and the flow from inside the canyon.

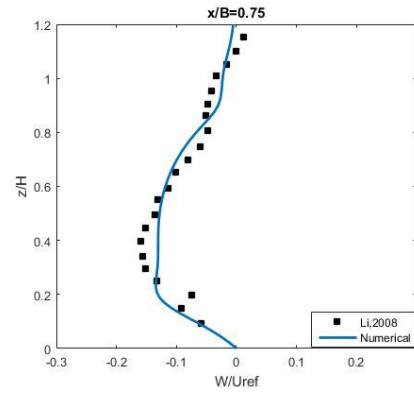
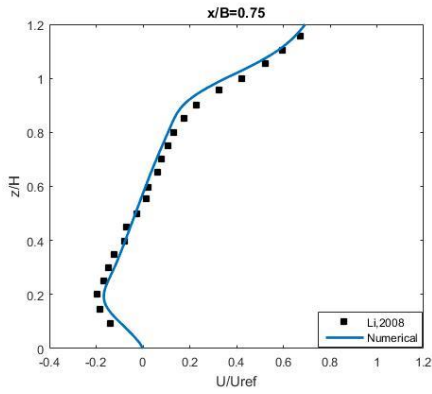
However, our numerical results of turbulence kinetic energy are still closer to the experimental data than the numerical results obtained from Li et al. (2005) and Liu et al. (2004).



a. At leeward location $x/B = 0.25$

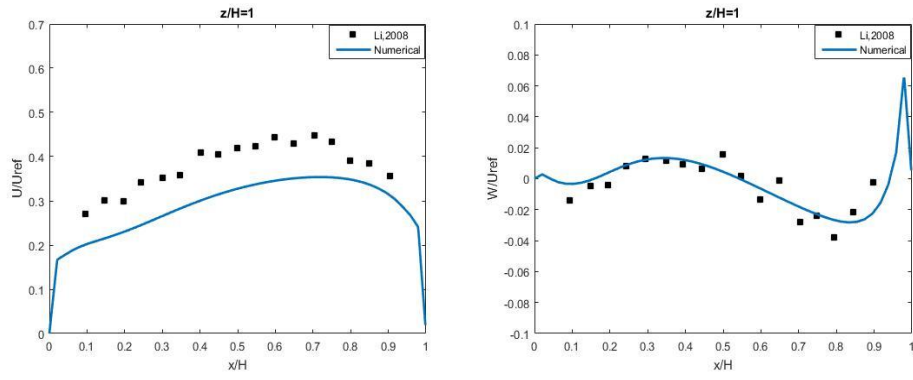


b. At center location $x/B = 0.50$

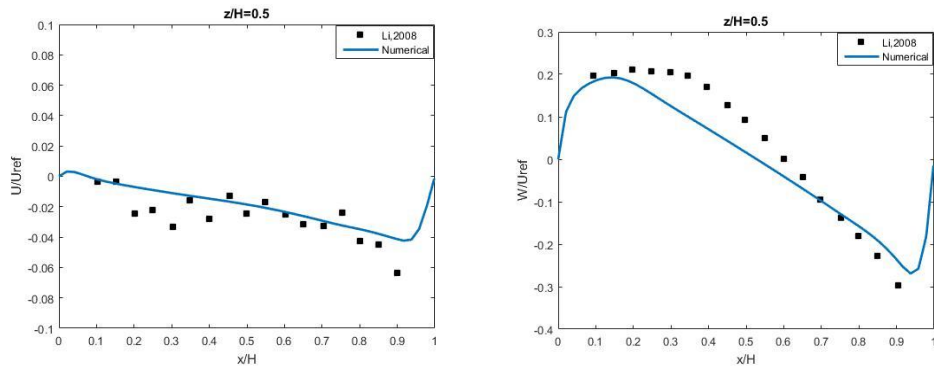


c. At windward location $x/B = 0.75$

Figure 4.2. The vertical profile of normalized stream-wise U/U_{ref} (left column) and vertical W/U_{ref} (right column) velocities with $AR = 1$.



a. At $z/H = 1.0$



b. At $z/H = 0.5$

Figure 4.3. The vertical profile of normalized stream-wise U/U_{ref} (left column) and vertical W/U_{ref} (right column) velocities at roof height (a) and center height (b) with $AR = 1$.

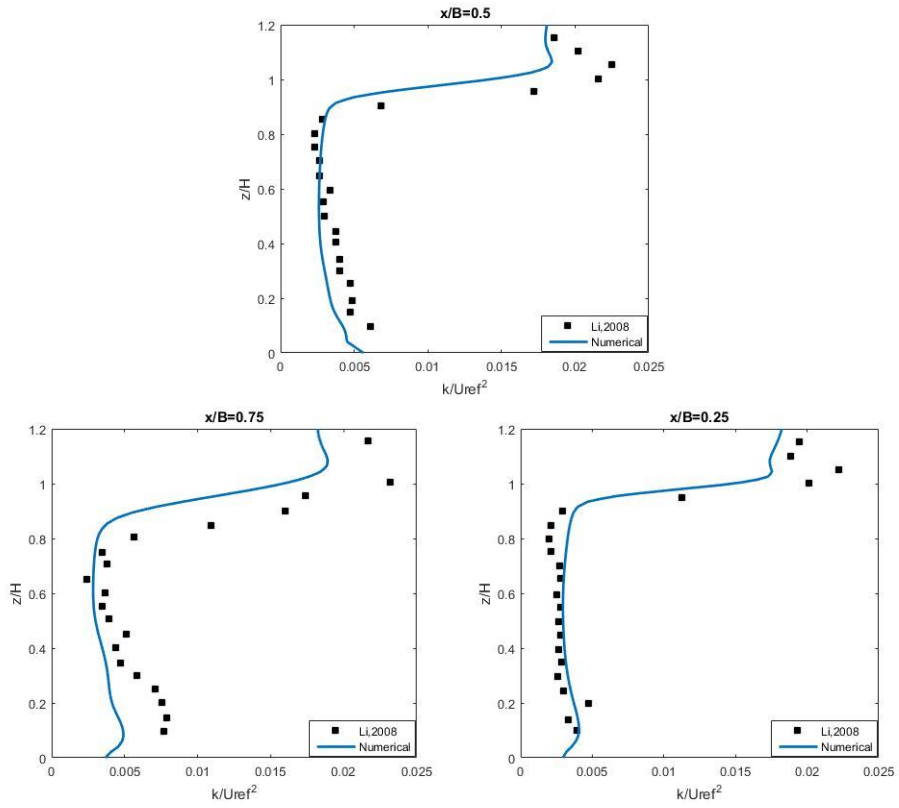


Figure 4.4. Turbulence kinetic energy at $x/B = 0.25$ (left), $x/B = 0.5$ (center) and $x/B = 0.75$ (right) with $AR = 1$.

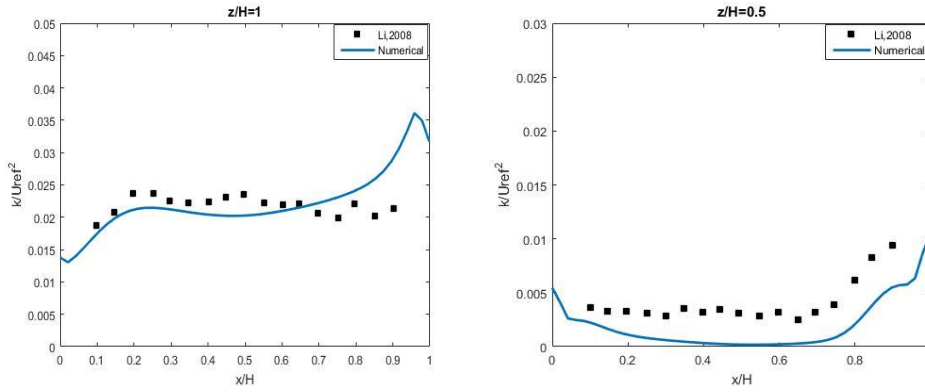
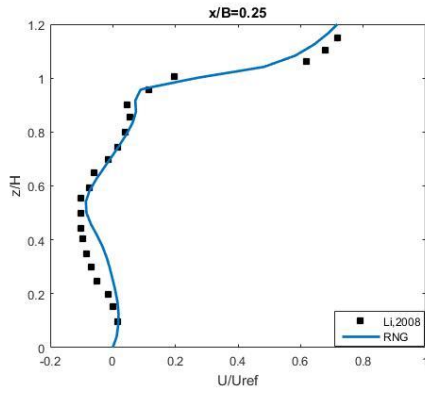


Figure 4.5. Turbulence kinetic energy at roof height $z/H = 1$ (left), and at center height $z/H = 0.5$ (right) with $AR = 1$.

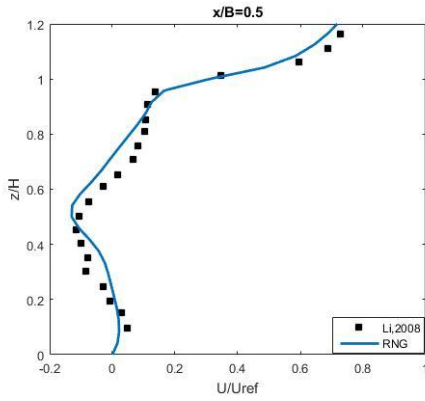
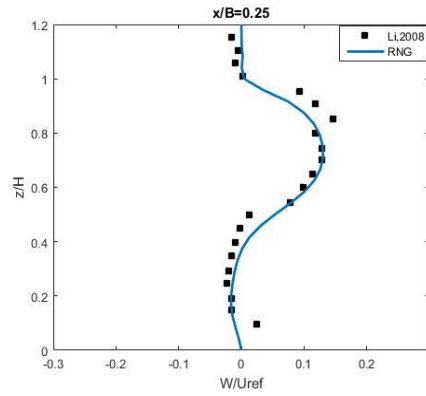
4.1.3. Street canyon of $AR = 2$

According to Oke's classification (1988), the flow in this configuration is in a skimming flow regime; its flow pattern is more complex than the flow of the aspect ratio $AR=1.0$. Similar to the results obtained from Liu et al. (2004), the flow generates two main vortices in the street canyon, which are in opposite directions; an anticlockwise vortex below the half building height, and another clockwise vortex above the half building height as shown in Figure 4.10. This is a phenomenon to explain why the stream-wise velocities changed direction twice from bottom to the roof level as shown in Figure 4.6 (left column). Figure 4.6 shows a comparison between numerical results and measurements of the normalized stream-wise (U/U_{ref} - left column) and vertical (W/U_{ref} - right column) velocity profiles along leeward ($x/B = 0.25$), center ($x/B = 0.5$), and windward ($x/B = 0.75$) lines in the street canyon. It shows a very good agreement between our numerical results and Li et al.'s measurements. Within the street canyon, our results are similar to the results of Li et al. (2005) using $k-\epsilon$ turbulent closure model, and the results of Liu et al. (2004) using LES model, whereas our results show a bit better agreement with the experimental data than Li et al.'s and Liu et al.'s results beyond the roof level. Figure 4.7 shows well-matched comparisons between our

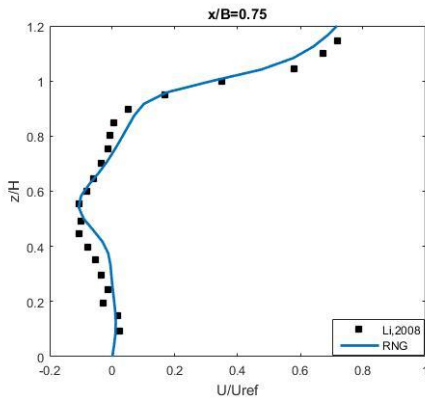
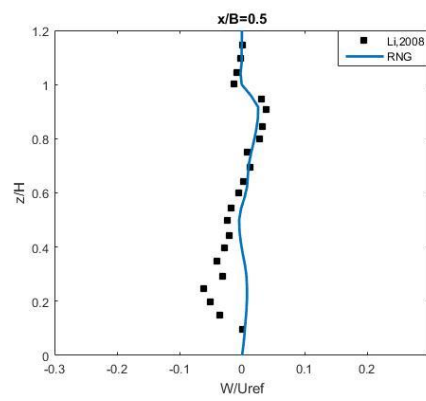
results and experimental data (Li et al.) of the horizontal velocity profiles at the roof level ($z/H = 1.0$) and at half building height ($z/H = 0.5$). In general, our results are closer to the experimental data than the results obtained from Li et al. (2005) and Liu et al. (2004). Figure 4.8 shows the comparisons of turbulence kinetic energy (TKE) between our numerical and experimental results.



a. At leeward location $x/B = 0.25$



b. At center location $x/B = 0.5$



c. At windward location $x/B = 0.75$

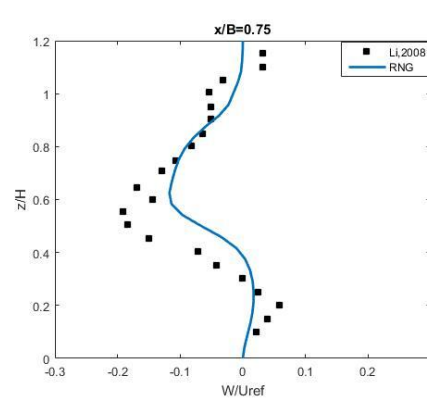
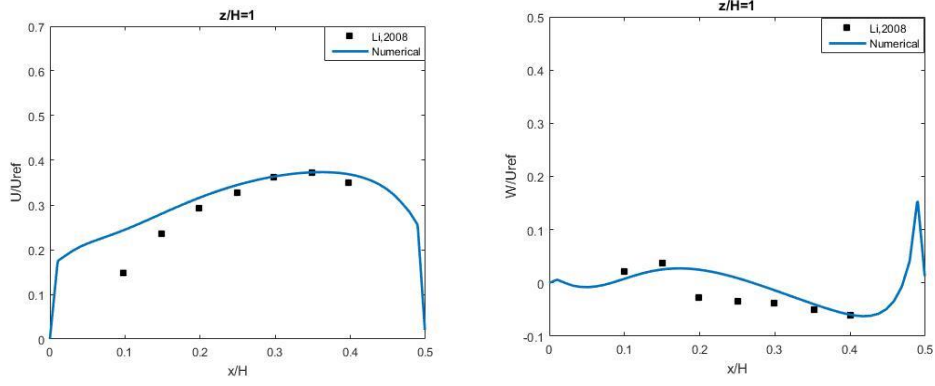
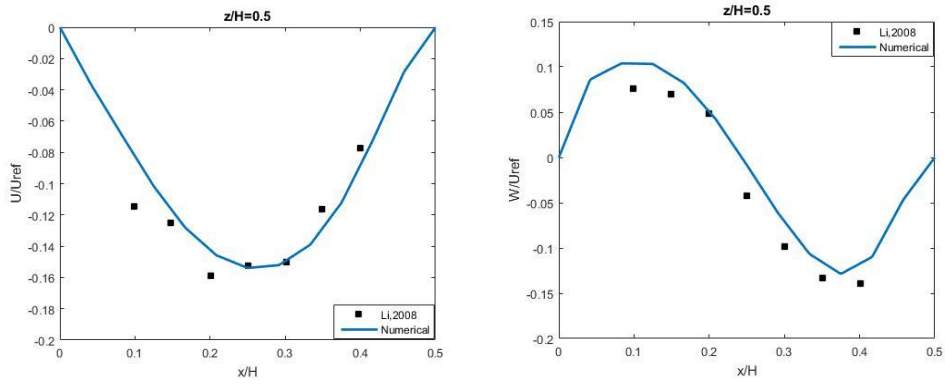


Figure 4.6. The vertical profile of normalized stream-wise U/U_{ref} (left column) and vertical W/U_{ref} (right column) velocities with $AR = 2$.

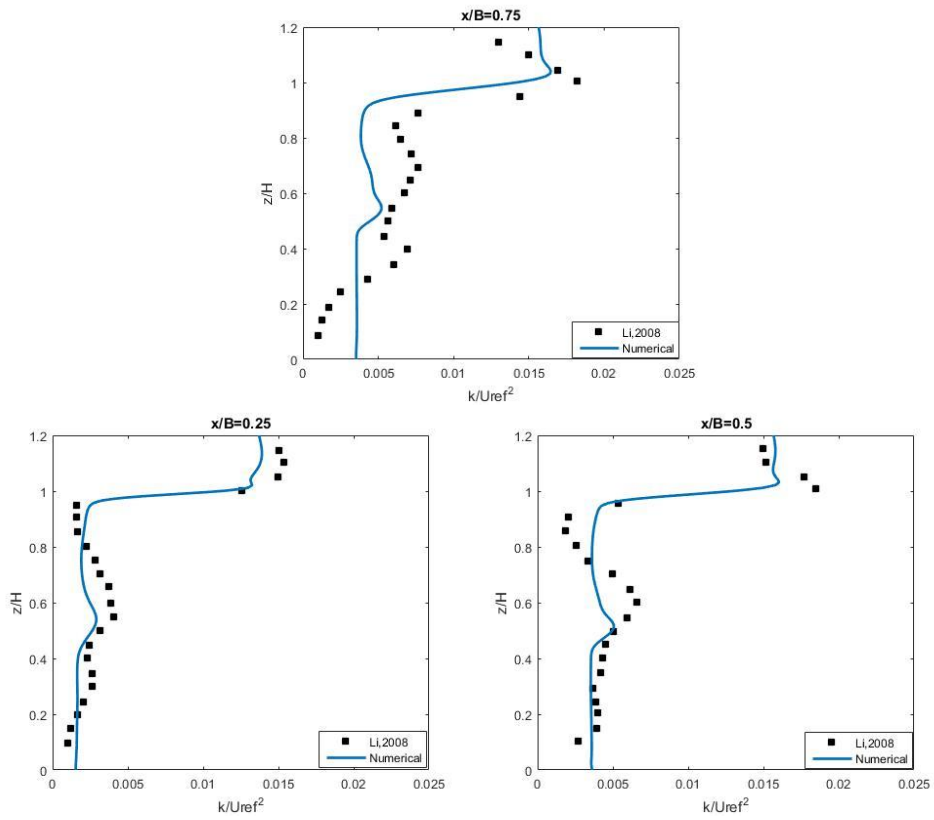


a. At roof height location $z/H = 1$



b. At center height $z/H = 0.5$

Figure 4.7. The vertical profile of normalized stream-wise U/U_{ref} (left column) and vertical W/U_{ref} (right column) velocities at roof height (a) and center height (b) with $AR = 2$.



c. At windward location $x/B = 0.75$

Figure 4.8. Turbulence kinetic energy at $x/B = 0.25$ (left), $x/B = 0.5$ (center) and $x/B = 0.75$ (right) with $AR = 2$.

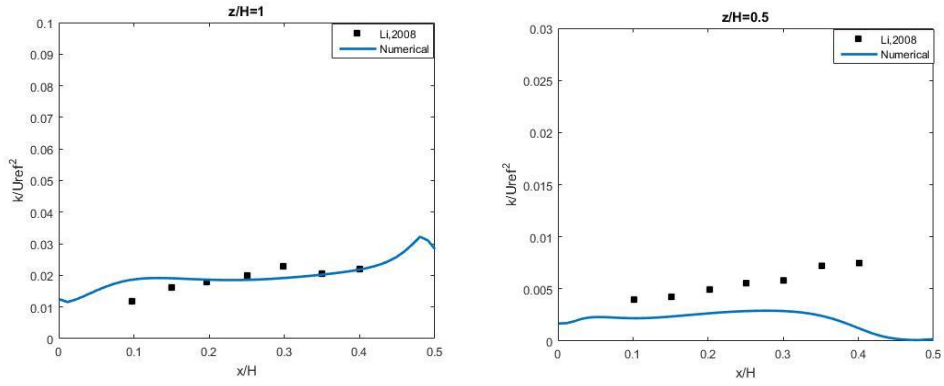


Figure 4.9. Turbulence kinetic energy at roof height $z/H = 1$ (left), and at center height $z/H = 0.5$ (right) with $AR = 2$.

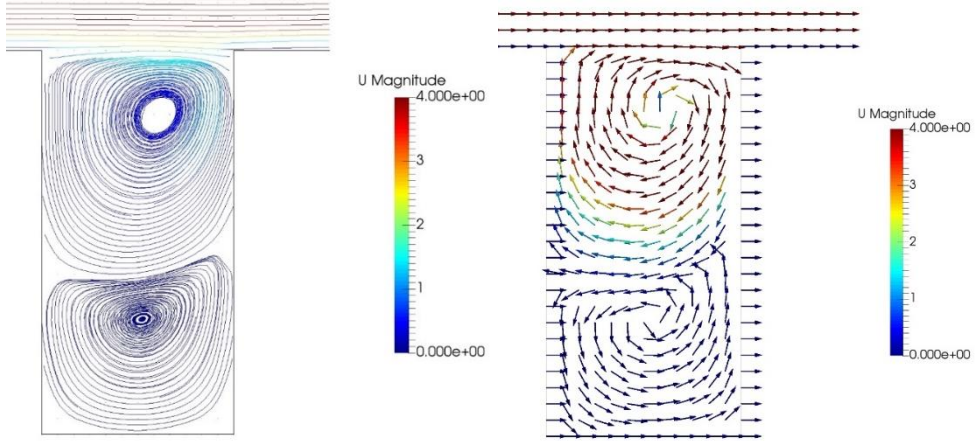
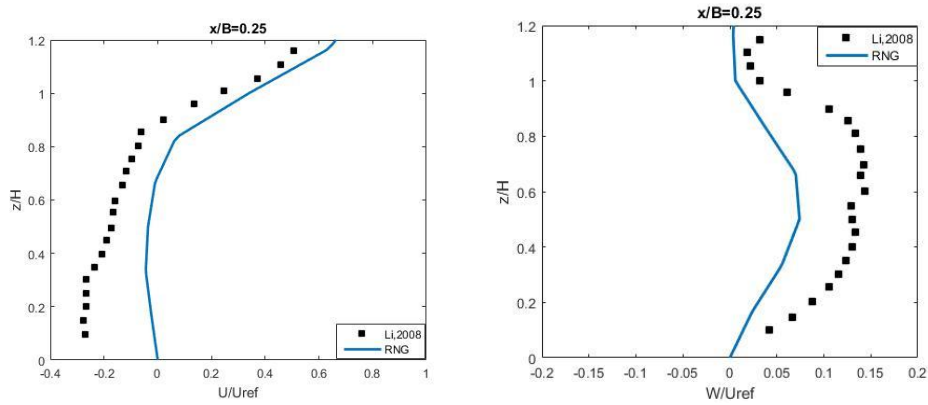


Figure 4.10. Streamlines and velocity vector⁽¹⁾ of wind flow inside the street canyons with $AR=2$. (¹ Due to the velocity inside the canyons is too small in comparison with the ambient velocity, the magnitude of velocity vector presented in the graphs (from now on in the manuscript) is scaled by the color bar rather than by the length of the vector.)

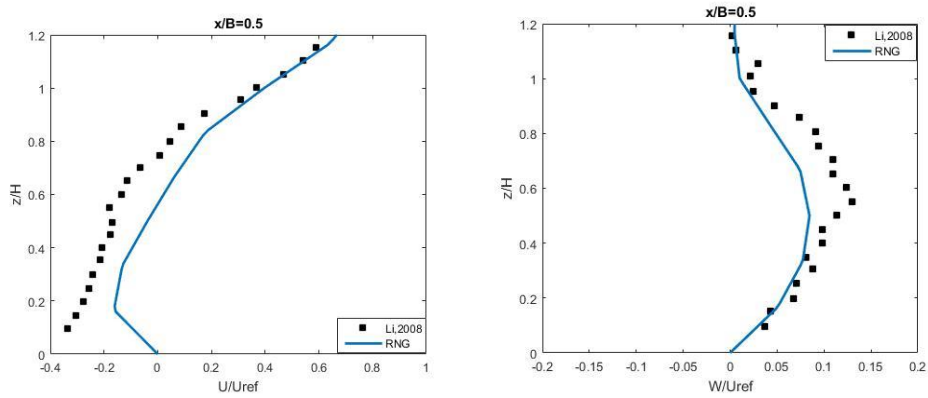
4.1.4. Street canyon of $AR = 0.5$

Due to the aspect ratio of 0.5, the flow in this geometry configuration belongs to the wake interference flow regime in which there are two horizontal interacting

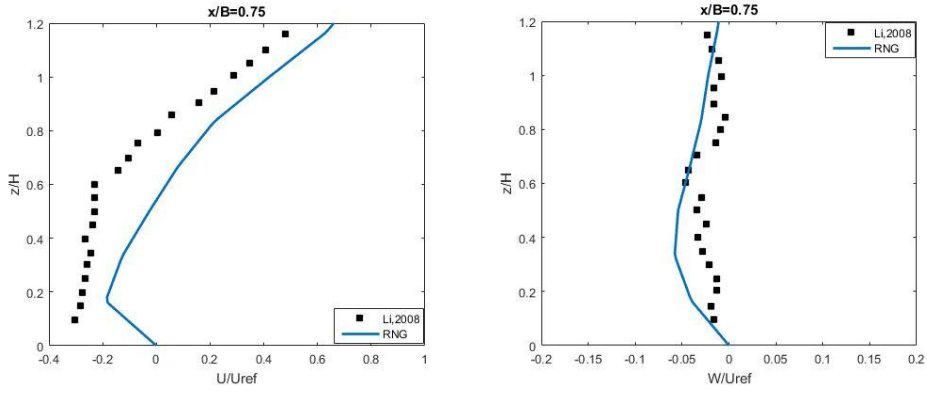
vortices, the downwind building disturbs the recirculation vortex before readjustment can occur. Similar to the results obtained from Liu et al. (2004), the flow forms three vortices inside the street canyon; the largest one occupied about 2/3 area of the street canyon, and located on windward side; the second large one is located on upstream near to the lower corner on leeward; the little third vortex is located at the right lower corner of the canyon as shown in Figure 4.13.



a. At leeward location $x/B = 0.25$



b. At center location $x/B = 0.5$



c. At wind ward location $x/B = 0.75$

Figure 4.11. The vertical profile of normalized stream-wise U/U_{ref} (left column) and vertical W/U_{ref} (right column) velocities with $AR = 0.5$.

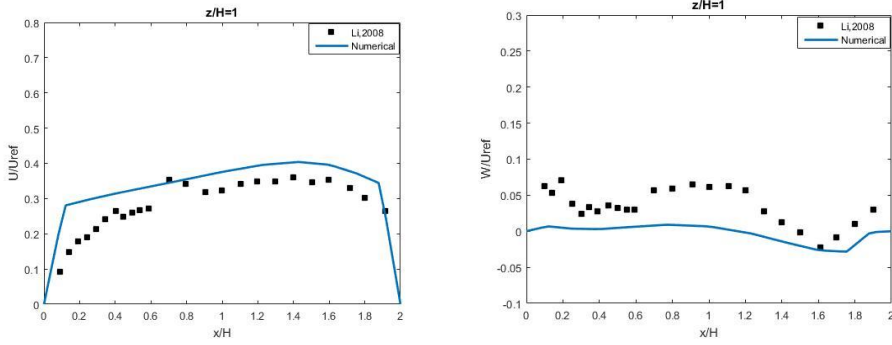


Figure 4.12. The vertical profile of normalized stream-wise U/U_{ref} (left column) and vertical W/U_{ref} (right column) velocities at roof height $z/H = 1$ with $AR = 0.5$.

Figures 4.11-4.12 show the comparisons between the numerical results and the experimental measurements of the vertical profiles of the normalized stream-wise and vertical velocities along the vertical lines at $x/B = 0.25$, 0.5 and 0.75 , and horizontal lines at the roof level ($z/H = 1$) in the street canyon. Although there are some discrepancies from the experiment data, the figures show that the numerical model can capture the form of the velocity profiles.

Figure 4.14 shows the normalized turbulence kinetic energy (k/U_{ref}^2) at three vertical lines; leeward ($x/B = 0.25$), center ($x/B = 0.5$) and windward ($x/B = 0.75$)

locations inside the street canyon. It shows the numerical results are reasonable agree with experimental data at leeward and center locations, but windward location. This trend is similar to the cases of $AR = 1$ and 2 . Table 4.1 shows the evaluation of RMSE of velocity and turbulence kinetic energy between the numerical results and experimental data of all cases, $AR = 0.5$, 1.0 and 2.0 ; it shows a very good agreement between the numerical results and the measurements.

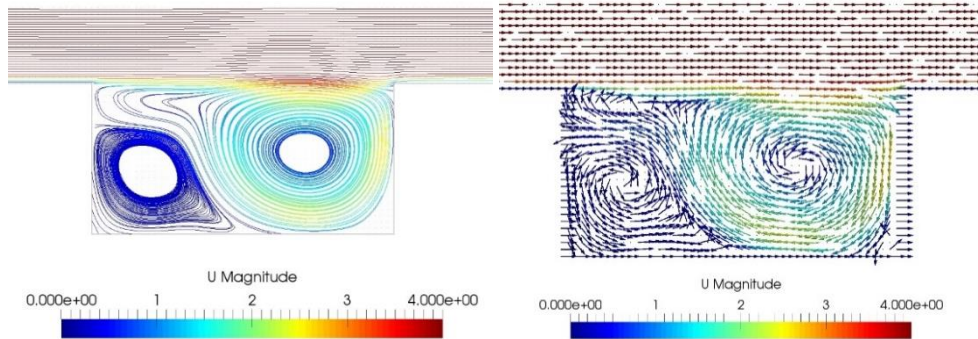


Figure 4.13. Streamline and velocity vector of wind flow inside the street canyons with $AR=0.5$.

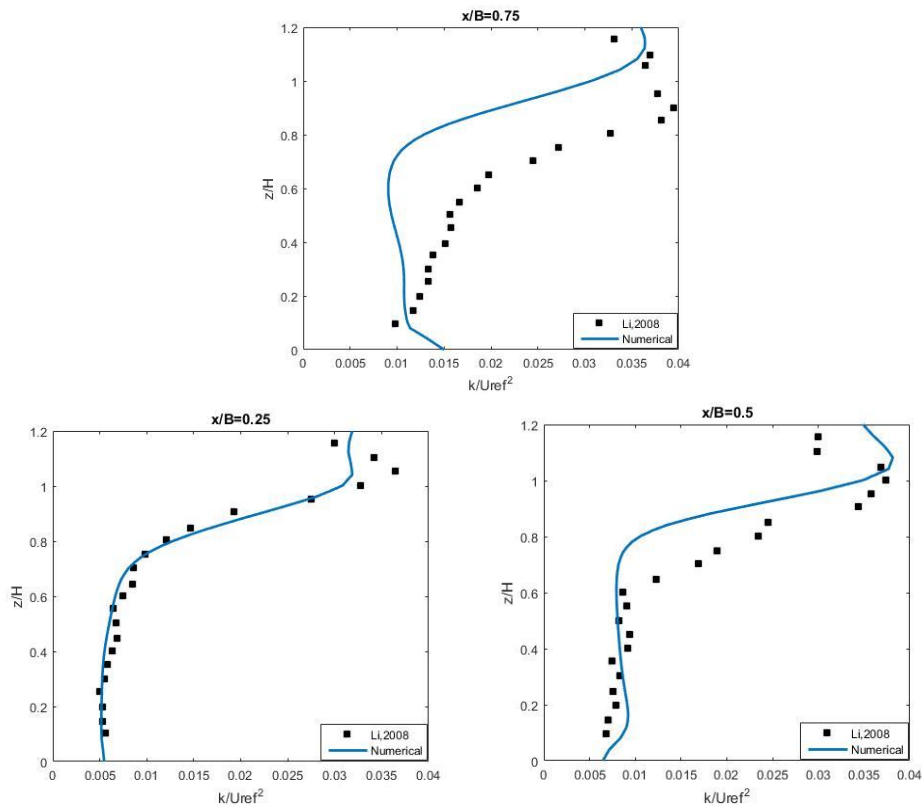


Figure 4.14. Turbulence kinetic energy at $x/B = 0.25$ (left), $x/B = 0.5$ (center) and $x/B = 0.75$ (right) with $AR = 0.5$.

Table 4.1. Evaluation of RMSE between the numerical results and experimental data.

RSME			
AR & Locations	U/U_{ref}	W/U_{ref}	k/U_{ref}^2
AR=1, leeward x/B =0.25	0.047494	0.037244	0.0019757
AR=1, center x/B =0.5	0.039275	0.069596	0.0029624
AR=1, windward x/B =0.75	0.034884	0.019541	0.0043557
AR=1, horizontal z/H =1	0.081349	0.0082272	0.0030251
AR=1, horizontal z/H =0.5	0.010711	0.056035	0.0029356
AR=2, leeward x/B =0.25	0.040991	0.023321	0.0010755
AR=2, center x/B =0.5	0.040424	0.027107	0.0015106
AR=2, windward x/B =0.75	0.038628	0.046439	0.0026547
AR=2, horizontal z/H =1	0.041743	0.028641	0.0032026
AR=2, horizontal z/H =0.5	0.015691	0.023619	0.0035876
AR=0.5, leeward x/B =0.25	0.16607	0.060783	0.0016257
AR=0.5, center x/B =0.5	0.12213	0.02524	0.0059935
AR=0.5, windward x/B =0.75	0.17427	0.021158	0.010245
AR=0.5, horizontal z/H =1	0.0817	0.039397	0.010373

4.2. Studying the air dispersion in various roof shapes by validating against Kastner-Klein and Plate (1999)'s experiment

4.2.1. Description of the experiment setup

The experiments were performed in the boundary layer wind tunnel of the Institute of Hydrology and Water Resources (IHW), University of Karlsruhe. The full experiment report can be found in Kastner-Klein (1999). The test section of the wind tunnel was 10.5 m long, 2 m wide and 1 m high. Two buildings were placed in the wind tunnel, constructing an ideal street canyon with an aspect ratio one. The modeled building height is of $H = 12$ cm, which is a typical average building height $H_n = 20$ m in urban areas. There are six geometry configuration of building roof shapes shown in Figure 4.15.

The approaching flow was directed perpendicular to the axis of the street. The vertical velocity profile of the wind is described by the power law as follows:

$$\frac{u}{u_r} = \left(\frac{z}{z_r} \right)^\alpha$$

where $z_r = 100m$ (similar to the nature), $u_r = u_{100} = 7.7$ m/s, and $\alpha = 0.23$.

Line sources is designed following Meroney et al. (1996), and located at position A distancing 3.5 cm from building I as shown in Figure 4.15. The pollutant source was mixture of air and a tracer gas (SF_6), which were released at located A, to model traffic emission. The use of SF_6 is thought to be owing to four reasons: (1) it is not reactive with the composition of air and the building surface, (2) its concentration can be measured with a satisfactory accuracy at very low

concentrations, (3) its concentration in the atmosphere is negligible (Hogan, 2011), and (4) it has low settling velocity in the air.

Concentration values are normalized as $cu_{100}HL_q/Q$, where c is the tracer-gas concentration measured in the wind tunnel, u_{100} is the reference wind velocity, H is the building height, Q the source strength and, L_q is the source length, which was 144 cm in all street-canyon experiments. More technical details of experiments with street-canyon configurations are given in Kastner-Klein and Plate (1996).

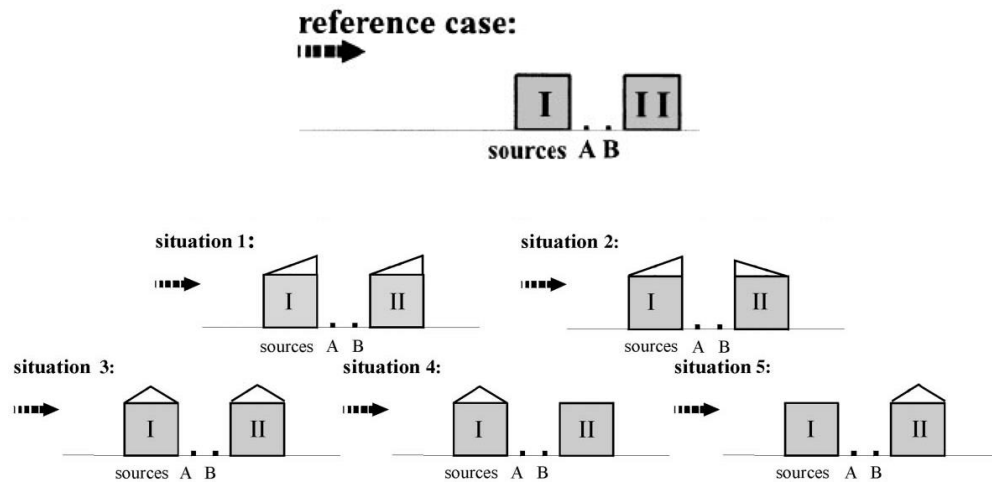


Figure 4.15. Schematic diagrams of the street canyon arrangement.

Reference case: flat roof shapes; Situation 1: one-side pitched roof shapes (step-up); Situation 2: step-up and step down roof shapes; Situation 3: slanted roof shapes; Situation 4: street canyon between slanted and flat roof shapes; Situation 5: street canyon between flat and slanted roof shapes. A & B are source positions.

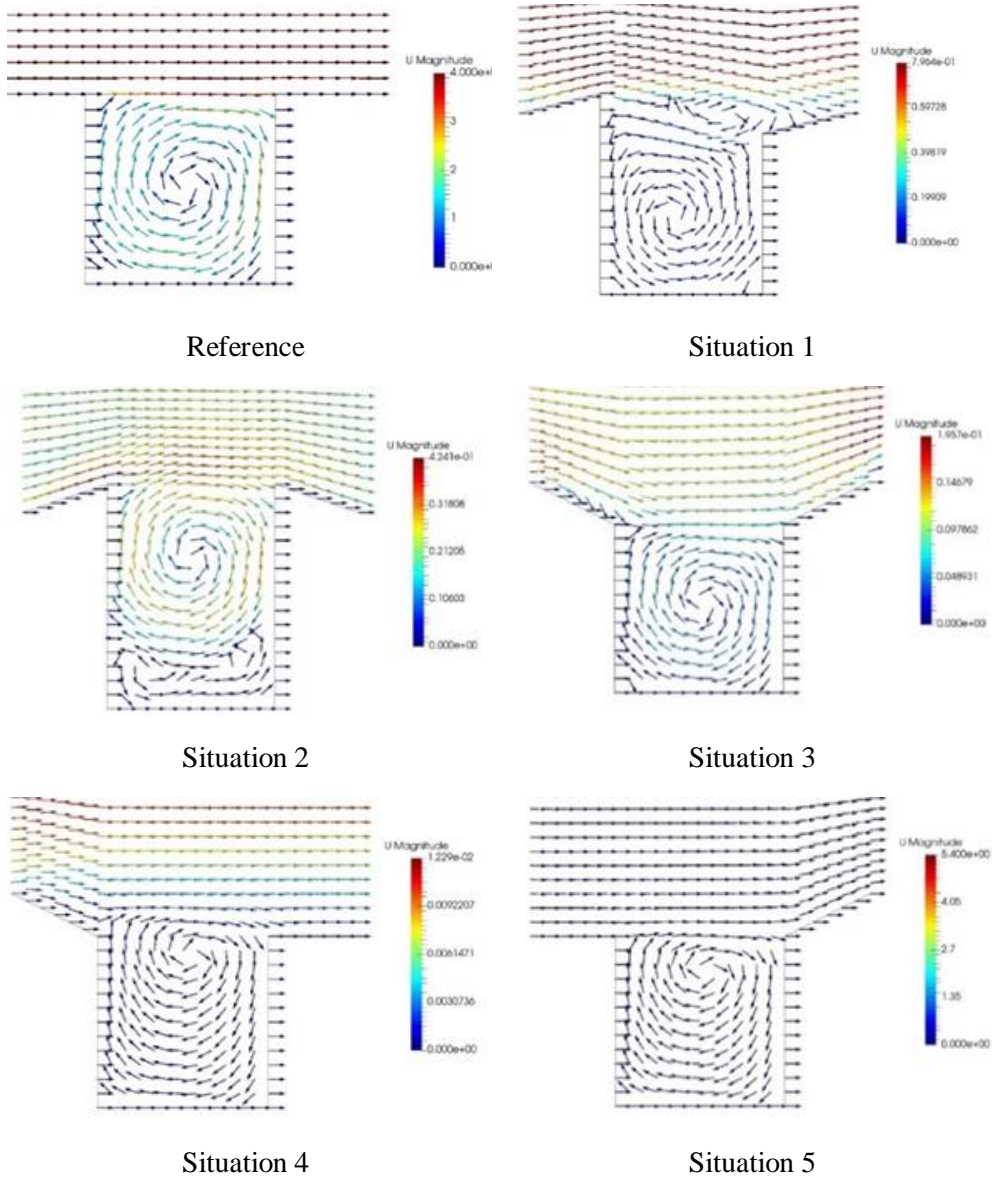


Figure 4.16. Velocity vector of wind flow inside the street canyons with different roof shape configurations.

As shown in Figure 4.16, in comparison to the reference case (flat roof), the flow patterns inside the urban street canyons of the situations described in Figure 4.15 are very distinguished from each others. Only the flow in the situation 3 (stepdown-stepup) is quite similar to the flow in the reference case. Moreover, the

flow in the reference case, the situations 3, 4 and 5 forms only one main vortex, whose direction is clockwise except the flow in the situation 1 (stepup-stepup). The flow in the situations 4 and 5 is quite similar, the location of the vortex center is quite the same, and located close to building roof level and depressed by outer ambient air flows. In the situations 1 and 2, the flow formed 2 vortices in the street canyon; one main largest and one small; however the order of two vortices is different in these situations. While the largest vortex is a bit downward to the street surface, and the small vortex is located at building roof level near windward side in the situation 1; the largest vortex is a bit upward to the building height level, and the small vortex is located near leeward close to street surface in the situation 2.

4.2.2. Validation and discussion

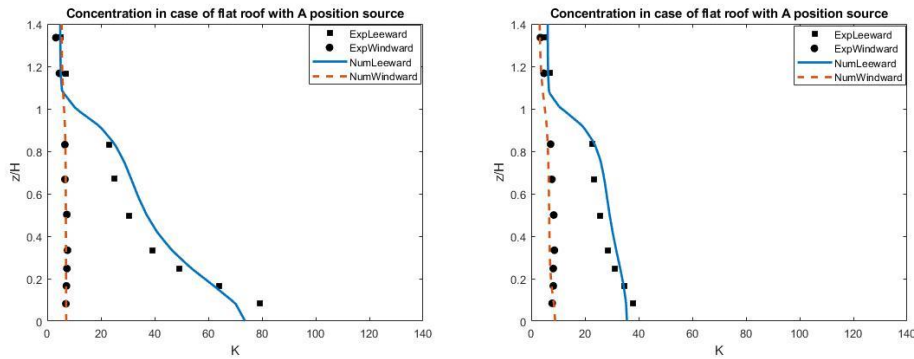
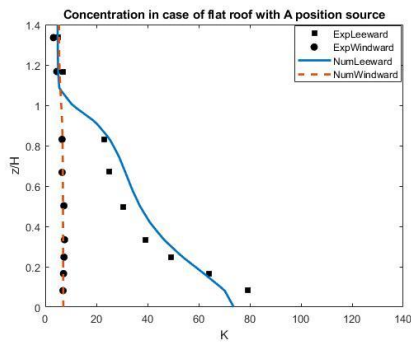


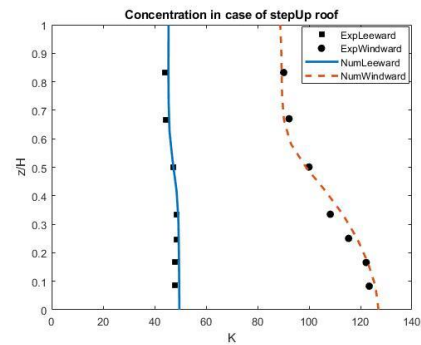
Figure 4.17. The dimensionless concentration K along the leeward and windward sites in the reference case (flat roof) corresponding to position sources located at A (left) and B (right).

Figures 4.17 and 4.18 show a good agreement between the numerical results and experimental measurements of the dimensionless concentration K along the leeward and windward lines. In case of flat roof (reference case), similar to the results obtained from Rafailidis' experiments, it again shows that the concentration

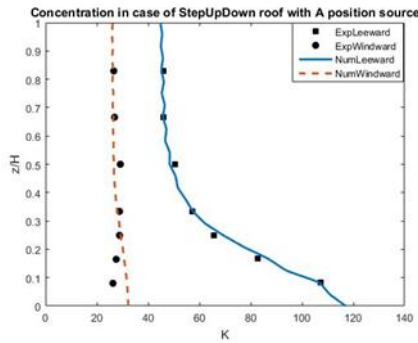
at the windward is smaller than at the leeward side. At the leeward, the largest concentration is found near to street surface, and it dropped off significantly upward. In addition, below the half building height ($z/H < 0.5$) the pollutant concentration at leeward site is almost twice larger when the source location changed from location A to position B. While the pollutant concentration was not changed and kept almost steady from the road surface to the roof level at leeward and windward sites when the source location changed from A to B, as shown in Figure 4.16.



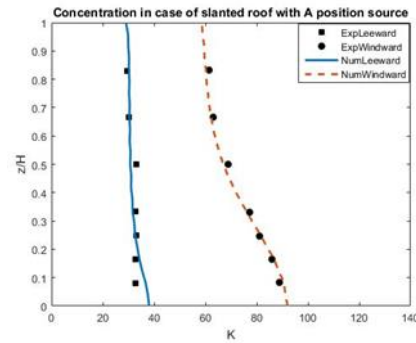
a. Reference case



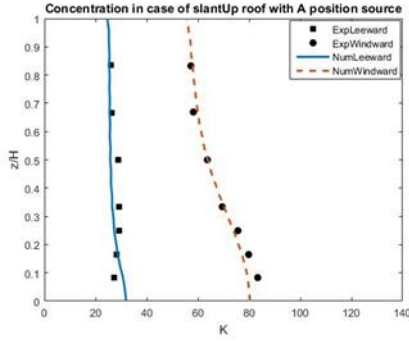
b. Situation 1



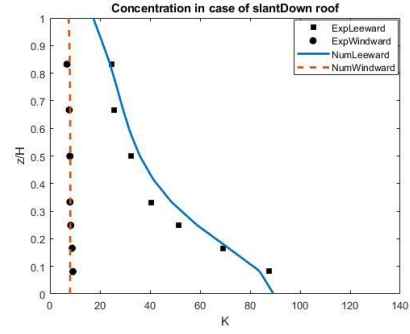
c. Situation 2



d. Situation 3



e. Situation 4



f. Situation 5

Figure 4.18. The dimensionless concentration K along the leeward and windward sites in the case of flat roof corresponding to position sources located at A.

Figure 4.18 shows the comparisons of pollutant concentrations released from position source A with different building roof configurations. In the reference case, situations 2 and 5, as shown in Figure 4.18 (a, c, and f), the concentration at leeward side is much larger than the concentration at windward side; moreover the concentration is significantly upward dropped at leeward site, while it keeps steady at windward site. Whereas, in the situations 1, 3 and 4 as shown in Figure 4.18 (b, d, and e), it shows an opposite trend to the results obtained from the reference case, situations 2 and 4; i.e. the concentration at windward side is much larger than the concentration at leeward side; and the concentration is significantly upward dropped at windward site, while it keeps steady at leeward site.

4.3. Validation of round-shaped roof against the measurement data from Llaguno-Munitxa et al.'s experiment (2017)

In this section, we have applied the numerical model to study the flow over buildings with round roof shapes. The numerical results have been validated against the data obtained from the experiment of Llaguno-Munitxa et al. (2017). The experiments have been carried in the wind tunnel to observe the flow over 7

building models by the box size (0.07 m x 0.07 m), and the canyon width $B=0.07$ m as shown in Figure 4.18. Llaguno-Munitxa et al. have carried out the experiments with three different inlet boundary conditions, however we validated only for the case with uniform inlet velocity $U=10$ m/s in this study. Figure 4.20 shows the comparison of the velocity profile of normalized stream-wise (left) and the turbulence kinetic energy (right) at the center of canyon ($x/B=0.5$), between numerical results obtained from our model and the results obtained from the experiment and simulation (using LES by Fluent software) of Llaguno-Munitxa et al. (2017). It shows that the simulation by LES method captures the stream-wise velocity profile better than our model, whereas our model can capture the turbulence kinetic energy better than LES method by Llaguno-Munitxa et al. (2017). Figure 4.21 shows a comparison of the pressure distribution and velocity vector field (background) inside the street canyon and ambient flow over tops of round roofs, which are obtained from our model (top) and LES simulation of Llaguno-Munitxa et al. (bottom). It shows a similar trend obtained from both models.



Figure 4.19. Geometry configuration of Llaguno-Munitxa et al.'s experiment (2017).

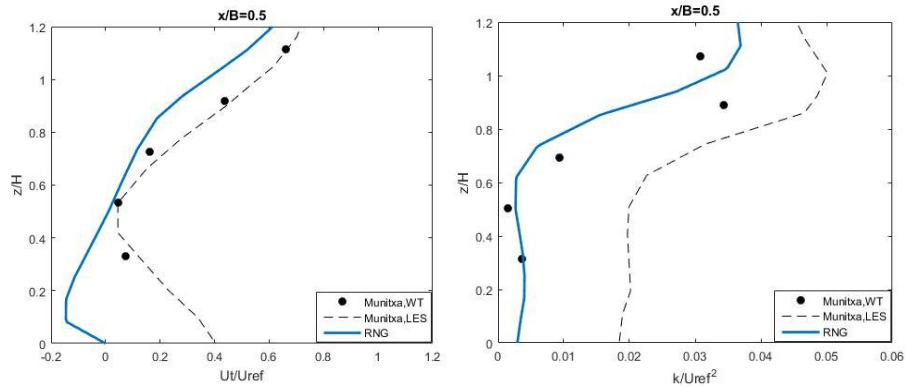


Figure 4.20. The velocity profile of normalized stream-wise (left) and turbulence kinetic energy (right) at the center of canyon.

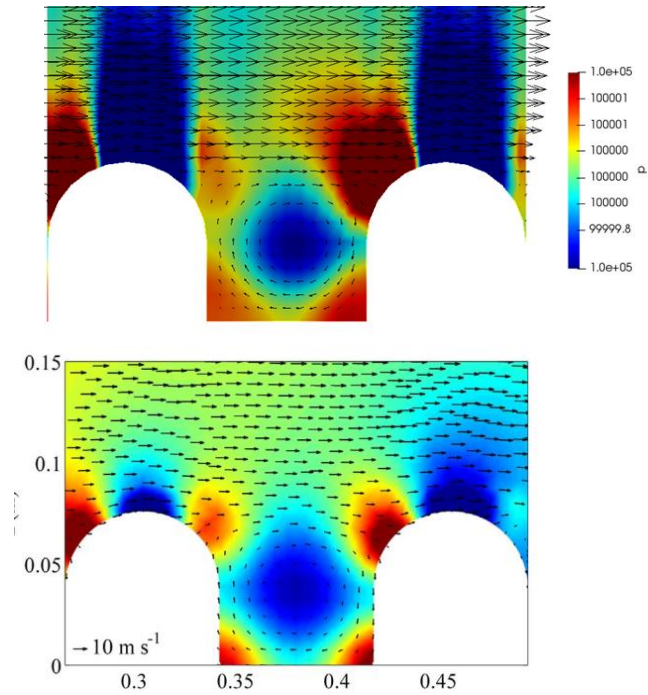


Figure 4.21. A comparison of the pressure distribution between numerical results obtained from our model (top) and Llaguno-Munitxa et al. (bottom).

4.4. Validation against CEDVAL data to study the flow characteristics for 3-D isolated building

Two datasets (A1-1 and A1-5) from the Compilation of Experimental Data for Validation of Microscale Dispersion Models (CEDVAL) provided by the Environmental Wind Tunnel Laboratory in University Hamburg are used in this study. The datasets are chosen because all the experiments were well organized and clearly documented, and the datasets are fully accessible at <https://mi-pub.cen.uni-hamburg.de/index.php?id=432>. These wind tunnel experiments were carried out at a scale of 1:200 in the BLASIUS wind tunnel at the Meteorological Institute of the University of Hamburg.

4.4.1. Simulation setup

Two datasets (A1-1 and A1-5) of CEDVAL were selected to validate the simulations of isolated building. Although the A1-1 and A1-5 data belong to different experiments, they share the same experimental parameters, including roughness length ($= 7 \times 10^{-4}$ m), friction velocity ($= 0.377 \text{ m s}^{-1}$), and so forth. The difference between these two datasets is the type of measured data: A1-1 dataset contains the measured data of flow characteristics and A1-5 dataset contains the measured data of dispersion.

In this case, two simulations were set up to correspond to A1-1 and A1-5 data, respectively. The simulation applied the real scale ($H=25$ m). Table 4.2 and Figure 4.23 shows detailed parameters a schematic representation of the computational domain and mesh used. The setup sketch of the single obstacle and sources is showed in Figure 4.22. The sources were released continuously and constantly.

Because the concentration in this study is defined in a dimensionless form, the source strength can be prescribed as any value and is omitted in this study.

The domain was extended up to a large distance in three directional axes to ensure that zero gradient assumption is rational along the lateral, outlet, and top boundaries. At the inlet boundary, velocity components \bar{V} (y-direction) and \bar{W} (z-direction) are considered to be equal to zero and the wind velocity and TKE profiles are provided according to the measured data (approximating a power law velocity profile with an exponent of around 0.27).

Table 4.2. Numerical grids for the simulation conducted in this study

Parameter (unit)	Symbol	Isolated obstacle simulation
Grid points	$N_x \times N_y \times N_z$	92x84x47
Length scale (m)	H	25
Domain size (H)	$L \times W \times Z$	18.4 x 19.1 x 7.4
Obstacle size (H)	$l \times w \times z$	0.8 x 1.2 x 1.0
Time step	Δt	0.05

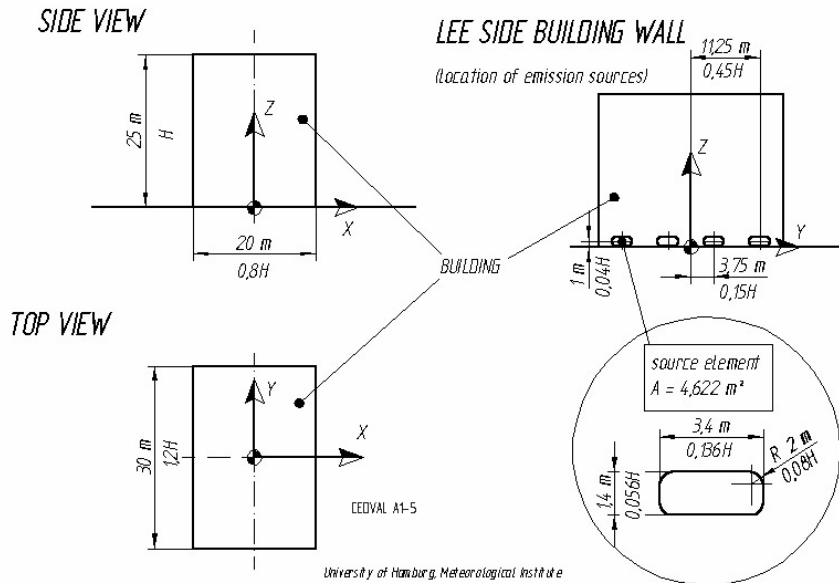


Figure 4.22. The setup sketch of the single building and sources.

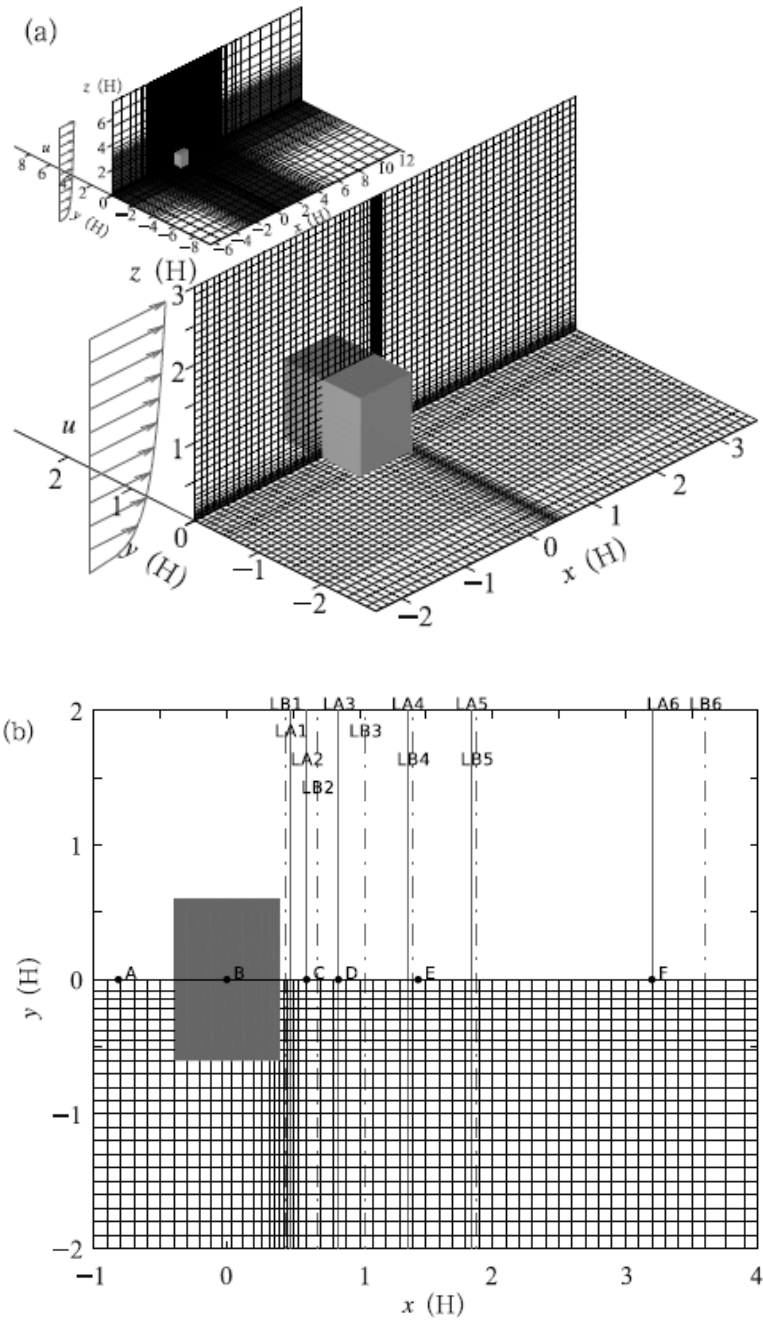


Figure 4.23. Schematic representation of isolated rectangular building simulation domain: (a) mesh used for the computational simulations (the whole area is shown in the insert) and (b) positions of comparisons between simulation results and

measured data. The points and lines indicate the positions for the validation in Section 4.4.2.

4.4.2. Validation of the isolated rectangular building simulation

Figure 4.24 shows the velocity field around the isolated building. It is found that the mean flow impinging the windward face of the building is decelerated rapidly and part of the momentum in the main direction is transferred to the span-wise and vertical momentum. The wind flow deflects and separates from the horizontal plane (Fig. 4.24), and the flow is driven into vertical downward and upward. The downward part creates a reverse flow extending to about $0.4H$ in front of the lower half height of the building (Fig. 4.24), reattaches on its front face, and generates the horseshoe vortex (Fig. 4.24). The upward part flow separates at the sharp leading edge and then reattaches to the roof of the building, and separates again at the downwind edge (Fig. 4.24). Similar behaviour is also found at the sides of the building (Fig. 4.25). The separated flow passes over the building, and reattaches on the ground further downwind at about $1.4H$ after the leeward side of the building (Fig. 4.24). The flow comes from the flow adjacent to the roof and lateral side of the building travels upstream at the reattaching point and results in the formation of a recirculation region behind the building (Figs. 4.24 and 4.25).

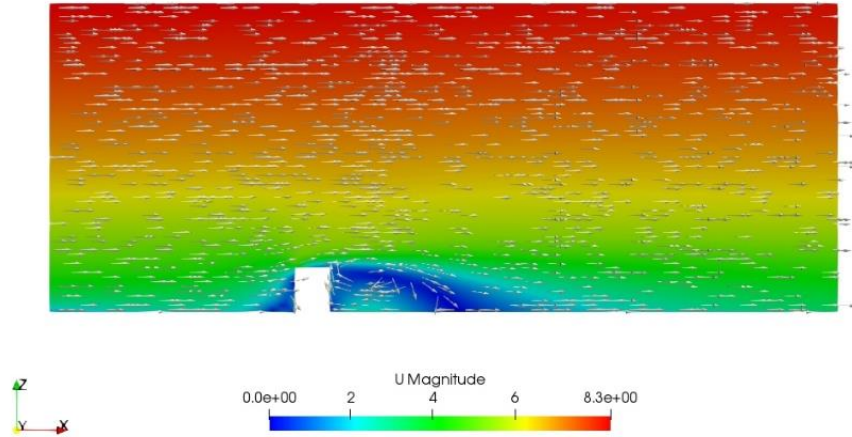


Figure 4.24. The velocity field in side view

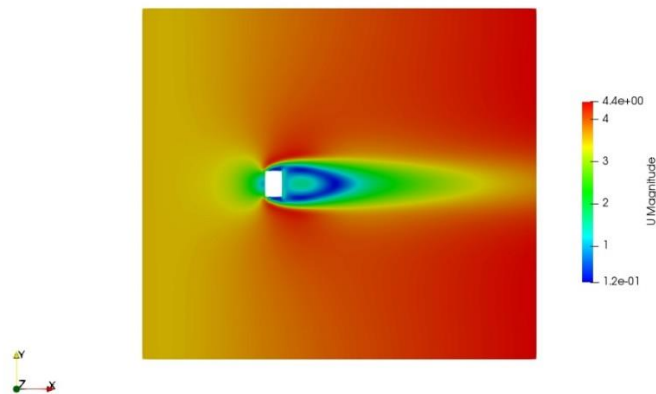
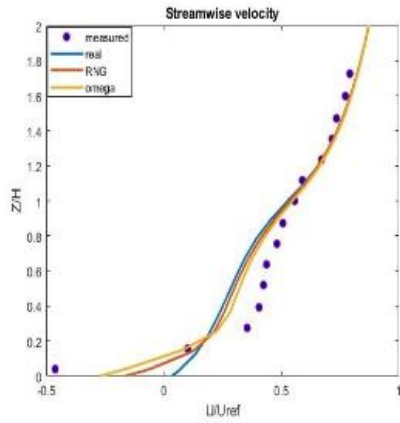


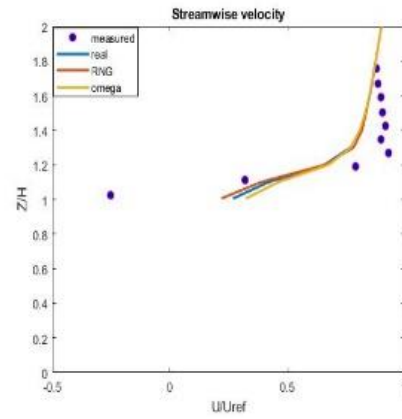
Figure 4.25. The velocity field at the height of 10m in the top view

Comparison of the computed and measured velocity is shown in Fig. 4.26. The velocities are non-dimensionalized by the reference velocity at the height of $4H$. The velocity profiles appear to be predicted reasonably well, especially in Figs. 4.26a and 4.26c-f. In Fig. 4.26b, the measured velocity adjacent to the roof is

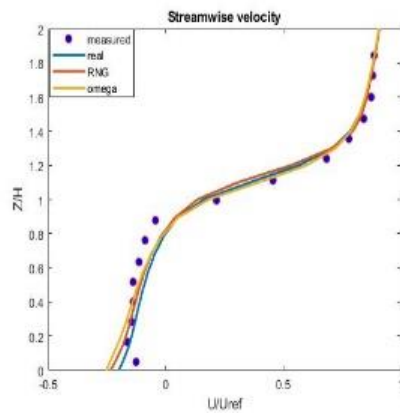
negative, while the computational velocity is not, which indicates that the model under-predicts the separation intensity of the flow on the roof.



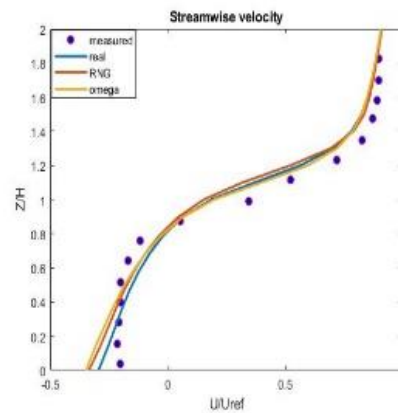
A



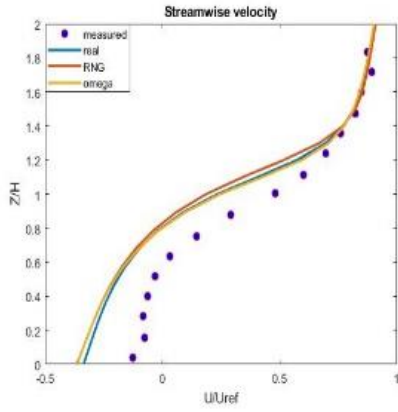
B



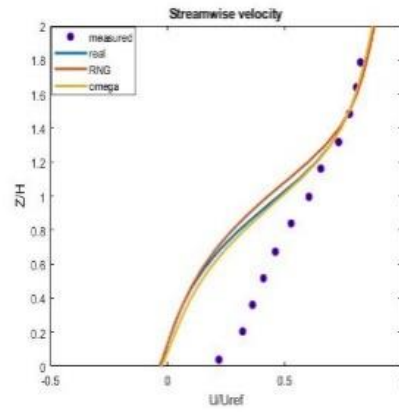
C



D



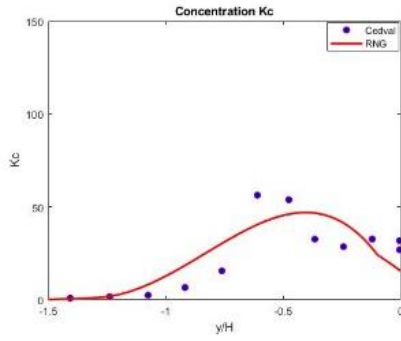
E



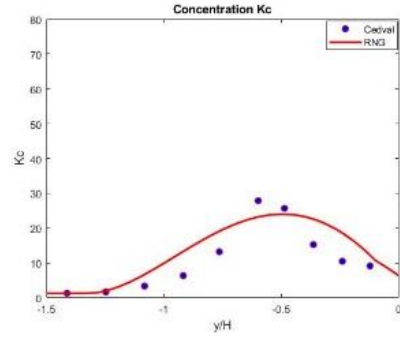
F

Figure 4.26. The vertical profile of stream-wise velocity at A, B, C, D, E, F points (see Fig. 4.22b).

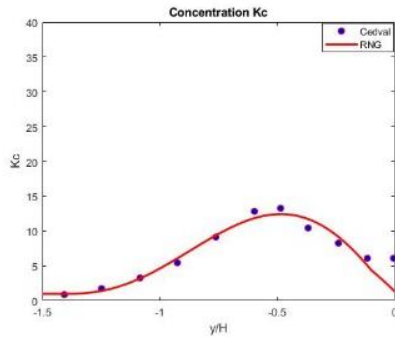
The concentration has been dimensionless. The concentration field after the time when it reaches equilibrium is chosen to validate. Comparison of the computed and measured concentration is shown in Fig. 4.27. The shape and peak locations are well predicted.



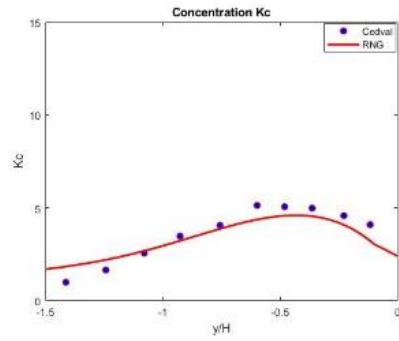
LA1



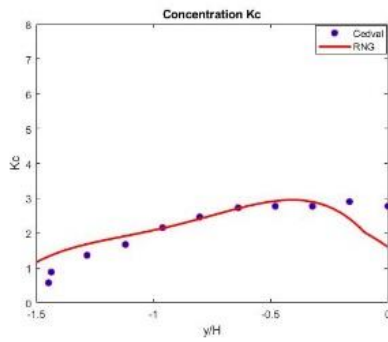
LA2



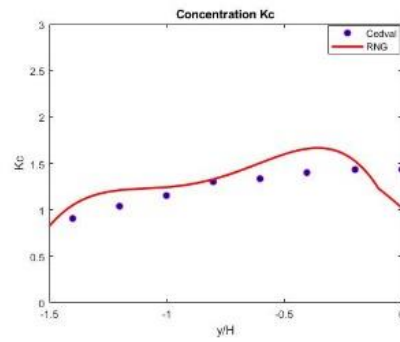
LA3



LA4



LA5



LA6

Figure 4.27. The dimensionless concentration at the lines LA1, LA2, LA3, LA4, LA5, LA6 line (see Fig. 4.23b).

5. APPLICATION – A CASE STUDY OF AIRFLOW AND POLLUTANT DISPERSION IN SHINJUKU URBAN AREA IN TOKYO

The Shinjuku special ward of Tokyo contains a large number of skyscrapers which pose several interesting wind engineering problems including how the wind shed will affect pedestrians nearby and the microclimate of the surrounding region. With each additional skyscraper, pedestrians walking in the area encountered great difficulties in walking on gusty windy days, and, in the worst cases, people were injured from falls caused by gusty wind and umbrellas were damaged on rainy windy days.



Figure 5.1. Shinjuku sub-central area, Tokyo in 1977 (Google Earth)

Wind tunnel experiments and field measurements had been carried out in cooperation with many research organizations during construction (Yoshida, 1978; Asami, 1978). Using these data, the validity of the prediction accuracy of CFD was assessed.

- (1) Wind tunnel experiment: a number of wind tunnel experiments had been performed on the Shinjuku sub-central area. Here, the CFD simulations were carried out based on the condition of the 1977 experiment.
- (2) Field measurement: field measurements were carried out from December 1975 to November 1983. The present CFD simulation were performed for conditions in 1977 when the situation of field measurements was similar to those of the wind tunnel experiment model. In the field measurements, three-cup anemometers were used. The measurement heights differed according to the measuring point, being 3-9 m above the ground surface. The reproduced urban area and the measuring point distribution are shown in Fig. 5.3. Measured wind speeds at encircled points (Nos. 6, 7, 13, 15) were compared with the calculated ones.

The computational domain is firstly defined by CAD data representing 1000 x 1000m of the Shinjuku sub-central area (Fig. 5.2). This building geometry data extends for approximately one block beyond the central region containing the measurement points (the exception being point 11 close to the south border) and this follows the AIJ guidance (Yoshie, 2007).

This case study has geometric complexity representative of urban environments of practical interest and represents a challenge in terms of mesh generation. The OpenFOAM snappyHexMesh tool has proved able to mesh the case study geometry with a high degree of automation and good parallel efficiency. The tool generates hex-dominant meshes with a topology whereby a background cubic mesh is subdivided a number of times as the ground and building surfaces are approached. At the building surfaces the cells are modified to snap to the underlying CAD geometry (triangulated stereo-lithography format in this case).

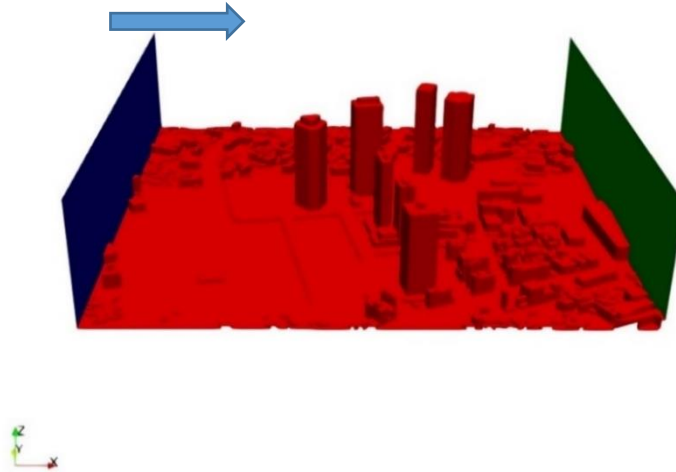


Figure 5.2. The computational domain simulated in OpenFoam.



Figure 5.3. Shinjuku urban area and observation points.

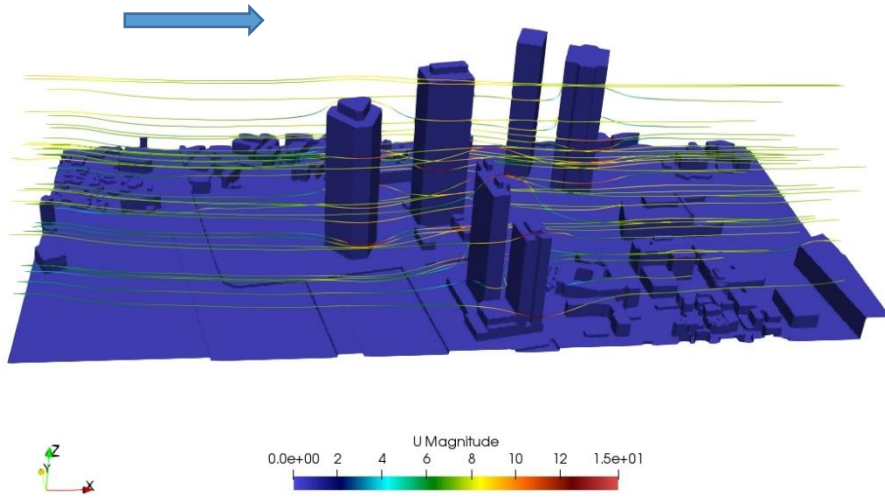


Figure 5.4. The streamline colored by the velocity magnitude

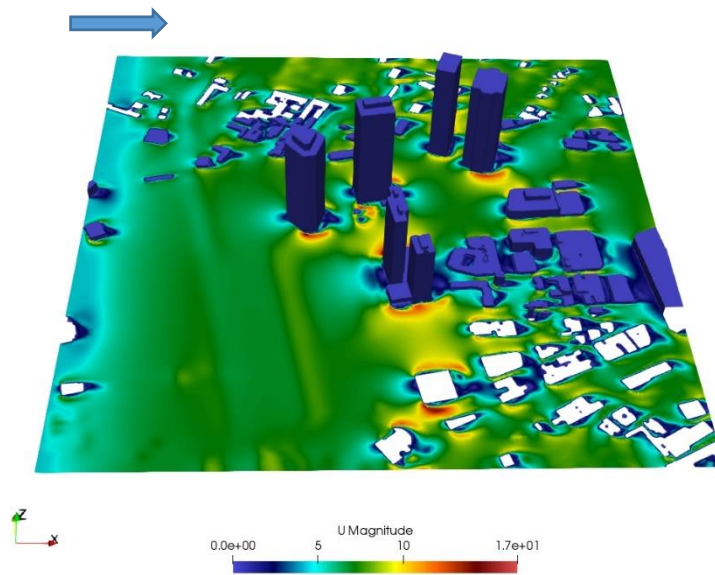


Figure 5.5. The velocity field at the height of 20m in the top view.

The simulated wind fields are shown in Fig 5.4 and 5.5. Fig. 5.4 shows the streamline of velocity in the whole domain. Streamlines deflects when impinging the windward face of the buildings. The separated flows pass over the buildings, and reattach after the leeward side of the buildings. The flows coming from the flow adjacent to the roof and lateral side of the buildings travel upstream at the reattaching point and result in the formation of a recirculation region behind the buildings. Fig. 5.5 and 5.6 show the speed of the wind flows increases at lateral side of the buildings or above the roof of the buildings. It is also found that the speed of wind flows decrease in front of the buildings (in the horseshoe vortex region) and behind the buildings (in the recirculation region).

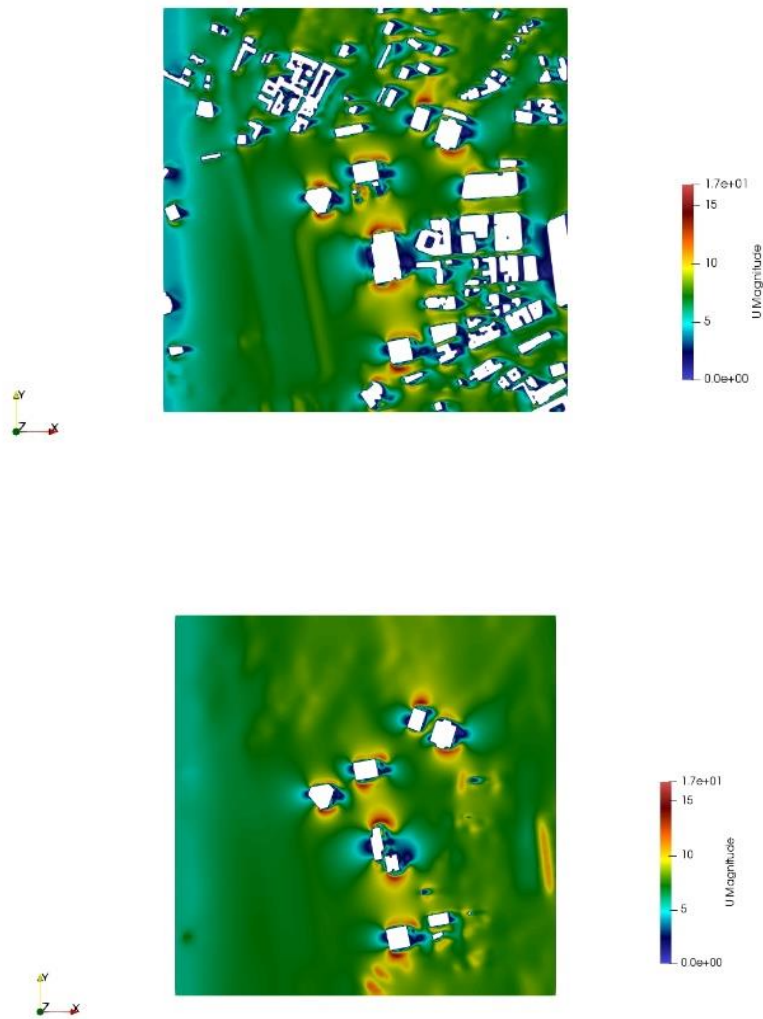


Figure 5.6. The velocity field at the height of 20m (top) and 50m (down)

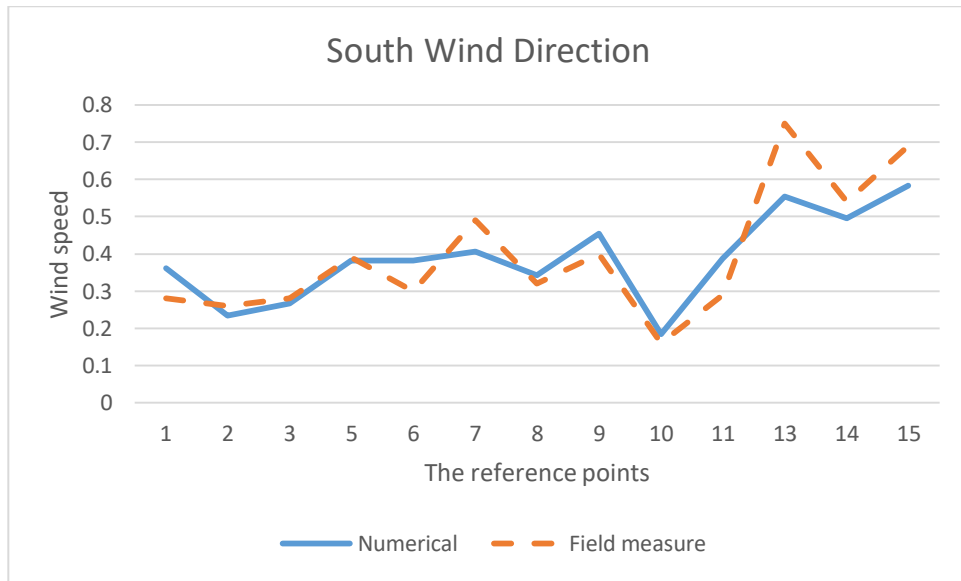


Figure 5.7. The dimensionless wind speed at the first thirteen reference points (see Fig. 5.3).

Fig. 5.7 presents the numerical wind speed ratios alongside the field measurement at the measuring points for the South wind directions. The result shows the good agreement between the numerical and the field measurement. The numerical wind speed is lower than the field measurement at the point 13 due to the complexity in the recirculation region.

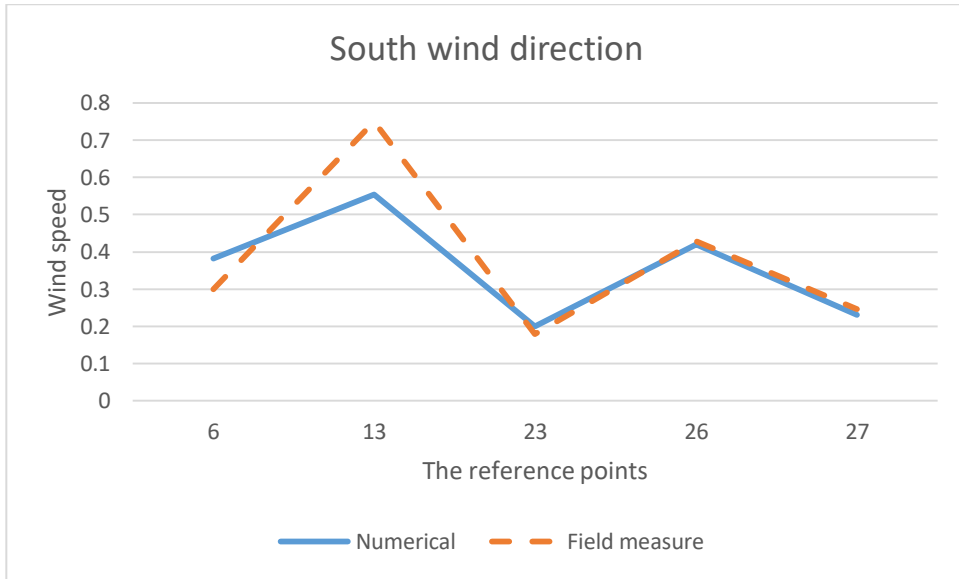


Figure 5.8. The dimensionless wind speed at the reference points along the center street (see Fig. 5.3).

Fig. 5.8 presents the numerical result and field measurement at the reference point along the center street. In general, the difference between the numerical result and field measure is small except the point No.13 due to the interaction of the reattachment region.

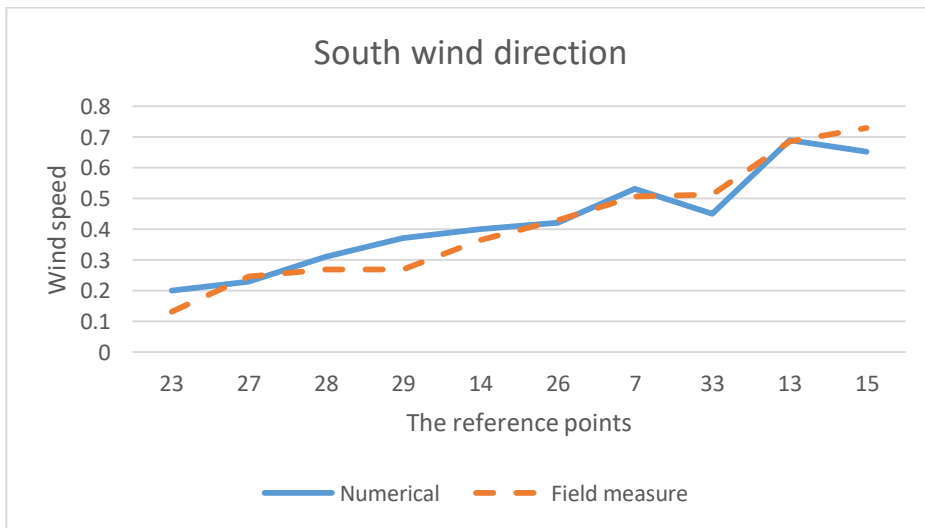


Figure 5.9. The dimensionless wind speed at the measure points in simulation (blue) and field measure (orange dash-line) (see Fig. 5.3)

Fig. 5.9 compares the wind speed at the measuring points with South wind direction. The numerical results show good matching with the field measurements.

6. CONCLUSIONS AND FUTURE WORK

6.1. To develop a reliable and economic tool to study flow in urban street canyon

The implemented solvers in OpenFoam is accomplished by carrying out a benchmark study. The benchmark study validates 5 RANS models against Kastner-Klein's experiments. All the models give reasonable predictions of flow pattern, flow properties and pollutant concentration.

From the validation of the numerical model against various experimental data obtained from various experiments, such as Li et al.'s experiment (2008) for different aspect ratios ($H/B = 1.0, 2.0, \text{ and } 0.5$); and Rafailidis and Schatzmann's (1995), Kastner-Klein's (1999) and Llaguno-Munitxa et al.'s (2017) experiments for various roof shape combinations, it shows that the flow pattern and pollutant distribution are strongly depended on the roof geometries and their configurations of the urban street canyons.

6.2. To study the impact of various roof shapes and different aspect ratios on air flow and pollutant dispersion in street canyons.

6.2.1. Effect of aspect ratios on flow patterns

The numerical simulations for different aspect ratios (AR) following Li et al.'s experiment (2008) are shown at Section 4.2. The flows over the street canyons with the aspect ratios of 2.0 and 1.0 are belonged to the skimming regime following the

classification by Oke (1988); whereby the flow inside the canyons is characterized by the lid-driven cavity flow because the ambient wind above the roof-top level plays as a driven-lid for the street canyon. In the case of $AR=2$, the flow generates two vortices in the street canyon, which are opposite directions; an anticlockwise vortex below the half building height, and a clockwise vortex above the half building height. While the flow formed a stable clockwise vortex at the center of street canyon in the case of $AR=1$, and the vortex circulation is strongest in this case as mentioned by Oke (1988) as well. The number of the vortices generated inside the canyon are corresponding to the number of times when the direction of vertical profile of stream-wise velocity is changed from negative to positive and vice versa.; e.g. the stream-wise velocity is negative below half-height roof level, and positive over half-height level in the reference case $AR=1$; while the stream-wise velocities changed direction twice from bottom to the roof level in the case of $AR=2$. In the case of $AR=0.5$, the flow belongs to the wake interference flow regime, in which two main interacting vortices and a small vortex were formed inside the canyon; the downwind building disturbs the recirculation vortex before readjustment can be occurred; the largest vortex was taking place on the windward side, and occupied about $2/3$ area of the street canyon; the second large vortex was taking place on the leeward ward side near to the lower corner; and the little third vortex is located at the right lower corner of the canyon (Figure 4.23, right).

Table 6.1. The effect of aspect ratio on the number of vortices in the street canyon.

Regime	Wake interference flow	Skimming flow	
$AR=H/B$	0.5	1.0	2.0
Vortices	2	1	2

Moreover, the value of turbulence kinetic energy is generally small below about $4/5$ roof-level height, while it was significantly increased upward from there to

near the roof level. This trend is also found the same in the round roofs in Llaguno-Munitxa et al.'s experiment, whereby the AR (H/B) is also of 1.

6.2.2. Effect of roof shapes on the flow patterns and pollutant distribution

In this study, the flat roof with the aspect ratio $AR=1.0$ was used as a reference case to compare the results. From the simulations following Rafailidis and Schatzmann's (1995), Kastner-Klein's (1999) and Llaguno-Munitxa et al.'s (2017) experiments, it shows that the flow patterns inside the urban street canyons under the effects of roof geometries are very distinguished from each others. Only the flow over a street canyon formed by the slanted roof with the slanted slope $Z_H/H = 0.17$ (of Rafailidis and Schatzmann's experiment) or stepdown-stepup in the situation 3 (of Kastner-Klein's experiment) or round roofs (of Llaguno-Munitxa et al.'s experiments) is quite similar to the flow in the reference case, i.e. the flow formed a stable clockwise vortex at the center of street canyon. However, when the slope of slanted roof (Z_H/H) is increased over 0.33 (as shown in the Rafailidis and Schatzmann's experiment) or the roof shapes changed from flat roofs (reference case) to stepdown-flat (situation 4) or to flat-stepup (situation 5) configurations (in Kastner-Klein's experiment), the center of vortex is lifted upward to the roof level.

Table 6.2. The effect of roof shape on the number of vortices in the street canyon

Case	Number of vortices
Flat (reference case), Slanted (situation 3), Slanted-Flat (situation 4), Flat-Slanted (situation 5)	1
Stepup-Stepup (situation 1), Stepup-Stepdown (situation 2)	2

In the stepup-stepup configuration (situations 1), the flow inside canyon interfered by the outside ambient flow forms 2 vortices; a main largest one below and a small one located at building roof level. In the stepup-stepdown configuration (situation 2), this geometry increases the aspect ratio, consequently the flow formed 2 vortices in the street canyon; the largest vortex is a bit upward above mid-roof level, and the small vortex is located close to street surface.

Table 6.3. The effect of the roof shape on the pollutant distribution

Roof shape	Concentration accumulated at
Flat, stepup-stepdown(sit.2), flat and slanted (sit.5)	windward wall greater than leeward wall
Stepup-stepup (sit.1), slanted (sit.3), slanted and flat (sit.4)	leeward wall greater than leeward wall

In comparison to the reference case, the vertical distributions of pollutant concentration at leeward side in the situations 2 (stepup-stepdown) and 5 (flat-slanted) are the same as in the reference case; i.e. the pollutant concentrations at leeward is much larger than those at windward side, particularly below mid-height roof level. In addition, the vertical pollutant concentration is significantly decreased upward at leeward site, while it keeps quite steady at windward site. Whereas, in the situations 1 (stepup-stepup), 3 (slanted) and 4 (slanted-flat), it shows an opposite trend to the results obtained from the reference case, situations 2 and 5; i.e. the vertical concentrations at windward side is much larger than those at leeward site; and the concentration is significantly dropped upward at windward site, while it keeps steady at leeward site. Moreover, the vertical pollutant concentration is gradually decreased upward at windward site, and kept steady at leeward site in those cases (situations 1, 3 and 4).

Flow patterns and vehicle pollutant dispersion inside two-dimensional street canyons are systematically investigated in this thesis. A morphometric model, numerical turbulent RANS models and non-chemical reaction vehicle line pollutants were combined for mathematical modeling to predict airflow and pollutant concentration inside street canyons. The morphometric method was based on wind-tunnel experiments and a homogeneous assumption. Different morphometric methods demonstrated deviation predictions of aerodynamic parameters, especially for medium-spaced buildings. In real urban environments, wind speed and turbulence structure were significantly influenced by inhomogeneous of ground roughness elements. Variations in wind direction had a large influence on aerodynamic parameters. The uncertainty of wind speed and turbulence structure was enlarged by inhomogeneous elements and wind direction at the vicinity of roof level. In field measurements and wind-tunnel experiments, an intensified shear layer existed at roof level that cannot be illustrated by morphometric methods. However, the intensified shear layer strongly influenced pollutant dispersion inside street canyons. The morphometric method should be properly applied in densely spaced buildings to describe upcoming wind profiles. Thus, LES model will be applied in the future.

6.3. To develop a method to adjust accurately Schmidt number

The new method GGDH shows more accurate results than the method SGDH in some cases. With that method, the similar research on Prandtl number will be extended in the future, and this method should be intensively validated against different geometries and flow conditions.

6.4. Application to a real urban area

The numerical simulation of the Shinjuku sub-central area in Tokyo is accomplished. The model runs well and describes the flow characteristics in the urban area reasonably, however, due to the lack of field observation on the pollutant concentration, the validation of the simulation result in this case study was not implemented. A further study of the pollutant dispersion in the complex city should be carried out in details.

6.5. Future work

This study has several limitations with respect to research methods and model assumptions. First, all the studies in this thesis are based on steady-state RANS models. Although RANS models are advantageous in computational cost, they are not as accurate as LES and are unable to predict turbulence structure. Second, only one type of background wind direction is modelled – perpendicular background wind condition, which is usually the worst condition for ventilation and pollutant removal. However, the impacts of various roof shapes found under this condition might not be similar under other wind conditions. Third, thermal effect is not considered in this thesis. Thermal effects produced by solar radiation and other sources are universally existed in the real world and can have strong impacts on airflow and pollutant dispersion. Thus, ignoring thermal effect means reduced representativeness of the model. Fourth, due to the lack of data for the pollutant sources, the application to the real street urban area is still not fully.

In the future, the primary goal will be breaking through the above limitations, to achieve better accuracy and to model a variety of realistic situations.

REFERENCE

- Ahmad, K., Khare, M. and Chaudhry, K.K., 2005. Wind tunnel simulation studies on dispersion at urban street canyons and intersections – a review. *Journal of Wind Engineering and Industrial Aerodynamics*, 93(9), p. 697-717.
- Baik, J.J. and Kim, J.J., 2002. On the escape of pollutant from urban street canyons. *Atmospheric Environment*, 36(3), pp. 527-536.
- Baik, J.J. and Kim, J.J., 2003. Effects of inflow turbulence intensity on flow and pollutant dispersion in an urban street canyon. *Journal of Wind Engineering and Industrial Aerodynamics*, 91(3), p. 309–329.
- Berkowicz, R., Hertel, O., Larsen, S.E., Sorensen, N. N. and Nielsen, M., 1997. *Modelling traffic pollution in streets, Denmark: Ministry of Environment and Energy, National Environment Research Institute.*
- Blocken, B. and Carmeliet, J., 2004. A review of wind-driven rain research in building science. *Journal of Wind Engineering and Aerodynamics*, 92(13), pp. 1079-1130.
- Blocken, B., Carmeliet, J. and Stathopoulos, T., 2007. CFD evaluation of wind speed conditions in passages between parallel buildings—effect of wall-function roughness modifications for the atmospheric boundary layer flow. *Journal of Wind Engineering and Industrial Aerodynamics*, 95(9-11), pp. 941-962.
- Blocken, B., Carmeliet, J., 2006. The influence of the wind-blocking effect by a building on its wind-driven rain exposure. *Journal of Wind Engineering and Aerodynamics*, 94(2), pp. 101-127.

Blocken, B., Stathopoulos, T. and Carmeliet, J., 2007. CFD simulation of the atmospheric boundary layer: wall function problems. *Atmospheric Environment*, 41(2), p. 238–252.

Blocken, B., Stathopoulos, T., Saathoff, P. and Wang, X., 2008. Numerical evaluation of pollutant dispersion in the built environment: Comparisons between models and experiments. *Journal of Wind Engineering and Industrial Aerodynamics*, 96(10-11), pp. 1817-1831.

Bottema, M., 1995. Parameterisation of aerodynamic roughness parameters in relation to air pollution removal efficiency of streets. *Air Pollution Engineering and Management. Computational Mechanics*, pp. 235-242.

Bottema, M., 1997. Urban roughness modeling in relation to pollutant dispersion. *Atmospheric Environment*, 31(18), pp. 3059-3075.

Bredberg, J., 2001/8. On two-equation eddy-viscosity models, Chalmers: Internal report, Chalmers University of Technology.

Buccolieri, R., Mohamed, S. and Leo, L.S., 2011. Analysis of local tree – atmosphere interaction on pollutant concentration in idealized street canyons and application to a real urban junction. *Atmospheric Environment*, 45(9), p. 1702 – 1713.

Chan, A.T., So, E.S.P. and Samad, S.C., 2001. Strategic guidelines for street canyon geometry to achieve sustainable street air quality. *Atmospheric Environment*, 35(24), pp. 4089-4098.

Chan, T.L., Dong, G., Leung, C.W., Cheung, C.S. and Hung, W.T., 2002. Validation of a two-dimensional pollutant dispersion model in an isolated street canyon. *Atmospheric Environment*, 36(5), p. 861–872.

CODAS Database, 2008. Concentration data of street canyon internet database. Available at <https://www.windforschung.de/CODASC.htm>.

Counihan, J., 1975. Adiabatic atmospheric boundary layers: a review and analysis of data from the period 1880 – 1972. *Atmospheric Environment*, 9(10), pp. 871-905.

Dabberdt, W. G., 1988. Kinematics and dispersion characteristics of flows in asymmetric street canyons. *Atmospheric Environment*, 22(12), pp. 2677-2689.

Daly, B.J. and Harlow, F.H., 1970. Transport equations in turbulence. *Physics of Fluid*, 13.

DePaul, F.T. and Sieh, C.M., 1986. A tracer study of dispersion in an urban street canyon. *Atmospheric Environment*, 19(4), p. 555–559. Easong, G., 2000. Improved turbulence models for Computational Wind Engineering. Nottingham: Doctoral thesis in Nottingham University.

Ellen, S.P. So, Andy, Chan, T.Y. and Anton, Y.T. Wong, 2005. Large-eddy simulations of wind flow and pollutant dispersion in a street canyon. *Atmospheric Environment*, 39(4), pp. 3573-3582.

ESDU, 1985. Engineering Sciences Data Item 85020, Engineering Sciences Data Unit. London: Regent Street.

Feddersen, B., 2005. Wind tunnel modeling of turbulence and dispersion above tall and highly dense urban roughness. Switzerland: PhD thesis, Swiss Federal Institute of Technology.

Fenger, J., 1999. Urban air quality. *Atmospheric Environment*, 33(29), p. 4877–4900.

Fifield, A., 2017. Smog becomes a political issue in South Korean election. *Washingtonpost* Retrieved.

Fisher, B., Joffre, S., Kukkonen, J., et al., 2005. Meteorology applied to urban air pollution problems, Hamburg, Germany: Final Report Cost Action 715.

Franke, J., Hellsten, A., Schlunzen, H. and Carissmo, B., 2007. Best Practice Guideline for the CFD Simulation of Flows in the Urban Environment, Brussels: COST Action 732.

Franke, J., Hirsch, C., Jensen, A.G., Krus, H. W., Schatzmann, M., Westbury, P. S., Miles, S. D., Wisse, J.A., Wright, N. G., 2004. Recommendations on the use of CFD in wind engineering. Belgium, Proceedings of the International Conference on Urban Wind Engineering and Building Aerodynamics, Ed. Van Beeck, Japan, COST Action C, pp. 5-7.

Franke, J., 2006. Recommendations of the COST action C14 on the use of CFD in predicting pedestrian wind environment. Yokohama, Japan, The Fourth International Symposium on Computational Wind Engineering (CWE2006).

Gorle, C., Van Beeck, J., Rambaud, P., Van Tendeloo, G., 2009. CFD modeling of small particle dispersion: the influence of the turbulence kinetic energy in the atmospheric boundary layer. *Atmospheric Environment*, 43(3), pp. 673-681.

Gorle, C., Van Beeck, J., Rambaud, P., 2010. Dispersion in the wake of a rectangular building: validation of two RANS modeling approaches. *Boundary Layer Meteorology*, 137(1), pp. 115-133.

Grarrat, J. R., 1992. The atmospheric boundary layer. First edition red. UK: Cambridge University Press.

Grimmond, C. S. B. and Oke, T. R., 1998. Aerodynamic Properties of Urban Areas Derived from Analysis of Surface Form. *Journal of Applied Meteorology*, 38(9), pp. 1262-1292.

Gromke, C. and Ruck, B., 2009. On the impact of trees on dispersion processes of traffic emissions in street canyons. *Boundary-Layer Meteorology*, Volym 131, pp. 19-34.

Gromke, C., Denev, J. and Ruck, B., 2007. Dispersion of traffic exhausts in urban street canyons with tree plantings – Experimental and numerical investigations. Orleans, France, In: International workshop on physical modeling of flow and dispersion phenomena PHYSMOD.

Gromke, C., Ruck, B., 2007. Influence of trees on the dispersion of pollutants in an urban street canyon – Experimental investigation of the flow and concentration field. *Atmospheric Environment*, 41(16), pp. 3287-3302.

Hanna, S.R., Hansen, O.R., Dharmavaram, S., 2004. FLACS CFD air quality model performance evaluation with Kit fox, MUST, Prairie grass, and EMU observations. *Atmospheric Environment*, 38(28), p. 4675–4687.

Hargreaves, D. M. and Wright, N. G., 2007. On the use of the $k-\epsilon$ model in commercial CFD software to model the neutral atmospheric boundary layer. *Journal of Wind Engineering and Industrial Aerodynamics*, 95(5), p. 355–369.

Hogan, C. M., 2011. Air pollution line source. In: BEYCHOK, M. (ed.). *The encyclopedia of Earth*.

Hodysh, W. G. and Dabberdt, W. F., 1988. Kinematics and dispersion characteristics of flows in asymmetric street canyons. *Atmospheric Environment*, 22(12), pp. 2677-2689.

Huang, H., Akutsu, Y., Arai, M., Tamura, M., 2000. A two dimensional air quality model in an urban street canyon: evaluation and sensitivity analysis. *Atmospheric Environment*, 34(5), p. 689–698.

Huang, Y. D., Hu, X. N, and Zeng, N. B., 2009. Impact of wedge-shaped roofs on airflow and pollutant dispersion inside urban street canyons. *Building and Environment*, 44(12), pp. 2335-2347.

Hunter, L. J., Johnson, G. T. and Watson, I. D., 1992. An investigation of three-dimensional characteristics of flow regimes within the urban canyon. *Atmospheric environment*, Vol. 26B (4), pp. 425-432.

Husain, M. and Lee, B.E., 1980. Wind tunnel study of the mean pressure forces acting on large groups of low rise buildings. *Journal of Wind Engineering Industrial Aerodynamics*, 6(3-4), p. 207–225.

Ince, N. and Launder, B.E., 1989. On the computation of buoyancy-driven turbulent flows in rectangular enclosures. *International Journal of Heat and Fluid Flow*, 10.

Isyumov, N., 1999. *Wind tunnel studies of building and structures*. 2nd red. Virginia: ASCE.

Jasak, H., 1996. Error analysis and estimation for finite volume method with application to fluid flow.

Jeong, S.J. and Andrews, M.J., 2002. Application of the $k-\varepsilon$ turbulence model to the high Reynolds number skimming flow field of an urban street canyon. *Atmospheric Environment*, 36(7), p. 1137–1145.

Johnston, I., 2014. UK faces £300m fine over failure to meet air pollution targets by 2010. Independent.

Kastner-Klein, P. and Plate, E.J., 1999. Wind tunnel study of concentration fields in street canyons. *Atmospheric Environment*, 33(24-25), p. 3973–3979.

Kastner-Klein, P. and Rotach, M. W., 2004. Mean flow and turbulence characteristics in an urban roughness sub-layer. *Boundary-Layer Meteorology*, 111(1), pp. 55-84.

Kastner-Klein, P., Berkowics, R., and Plate, E.J., 2000. Modeling of vehicle induced turbulence in air pollution studies for streets. *International Journal of Environment Pollution*, Issue 14, pp. 496-507.

Kastner-Klein, P., Berkowicz, R. and Britter, R., 2004. The influence of street architecture on flow and dispersion in street canyons. *Meteorology Atmospheric Physics*, 87(1-3), pp. 121-131.

Kenjeres, S. and Hanjalic, K., 1995. Prediction of turbulent thermal convection in concentric and eccentric horizontal annuli, *International Journal of Heat and Fluid Flow*, 16.

Kenjeres, S., Gunarjo, S.B. and Hanjalic, K., 2005. Contribution to elliptic relaxation modeling of turbulent natural and mixed convection. *International Journal of Heat and Fluid Flow*, 26.

Kim, J.H., 2019 (a). Low-income group falls vulnerable to air pollution. *Korean Times* Retrieved 7 March 2019.

Kim, J. J. and Baik, J. J., 1999. A numerical study of thermal effects on flow and pollutant dispersion in urban street canyons. *Journal of Applied Meteorology*, 38(9), p. 1249–1261.

Kim, J. J. and Baik, J. J., 2001. Urban street-canyon flows with bottom heating. *Atmospheric Environment*, 35(20), p. 3395–3404.

Kim, M.J., 2019. The effects of transboundary air pollution from China on ambient air quality in South Korea. *Heliyon*. 5 (12).

Kovar-Panskus, A., Moulinneuf, L., Savory, E., etc, 2002. A wind tunnel investigation of the influence of solarinduced wall heating on the flow regime within a simulated urban street canyon. *Water, Air, and Soil Pollution, Issue Focus* 2, p. 555–571.

Kumar, R. and Dewan, A., 2014. URANS computations with buoyancy corrected turbulence models for turbulent thermal plume. *International Journal of Heat and Mass Transfer*, 72.

Launder, B. E. and Spalding, D. B., 1974. The numerical computation of turbulent flows. *Computational Methods Application Mechanics Engineering*, 3(2), pp. 269-289.

Lee, I. Y. and Park, H. M., 1994. Parameterization of the pollutant transport and dispersion in urban street canyons. *Atmospheric Environment*, 28(14), pp. 2343-2349.

Leitl, B. M. and Meroney, R. N., 1997. Car exhaust dispersion in a street canyon: Numerical critique of a wind tunnel experiment. *Journal of Wind Engineering and Industrial Aerodynamics*, Volume 67&68, pp. 293-304.

Li, X.X., Liu, C.H. and Leung, D., 2009. Numerical investigation of pollutant transport characteristics inside deep urban street canyons. *Atmospheric Environment*, 43(15), pp. 2410-2418.

Li, X.X., Liu, C.H., Leung, D.Y.C., K.M. L, 2006. Recent progress in CFD modeling of wind field and pollutant transport in street canyons. *Atmospheric Environment*, 40(29), pp. 5640-5658.

Li, X.X., Leung, D.Y.C, Liu C.H., Lam K.M., 2008. Physical modeling of flow field inside urban street canyons. *Journal of Applied Meteorology and Climatology*, 70, pp. 2058-2067.

Liu, C.H. and Barth, M.C., 2001. Large-Eddy Simulation of Flow and Scalar Transport in a Modeled Street Canyon. *Journal of Applied Meteorology*, 41(6), pp. 660-673.

Liu, C.H. and Barth, M.C., 2004. Large-Eddy Simulation of Flow and Pollutant Transport in Street Canyons of Different Building-Height-to-Street-Width Ratios. *Journal of Applied Meteorology*, 43(10), pp. 1410-1424.

Macdonald, R.W., Griffiths, R.F. and Hall, D.J., 1998. An improved method for the estimation of surface roughness of obstacle arrays. *Atmospheric Environment*, 32(11), pp. 1857-1864.

Llaguno-Munitxa, M., Bou-Zeid, E., Hultmark, M., 2017. The influence of building geometry on street canyon air flow: validation of large eddy simulations against wind tunnel experiments. *Journal of Wind Engineering & Industrial Aerodynamics* 165, pp. 115-130.

Martos A., Pacheco-Torres R., Ordonez J., Jadraque-Gago E., 2016. Towards successful environmental performance of sustainable cities: intervening sectors. A review. *Renew Sustain Energy Rev*; 57:479-495.

Menter, F. R, 1994. Two-equation eddy-viscosity turbulence models for engineering application. *AIAA Journal*, Volym 32, pp. 1598-1605.

Meroney, R.N., Pavageau, M., Rafailidis, S., Schatzmann, M., 1996. Study of line source characteristics for 2-D physical modeling of pollutant dispersion in street canyons. *Journal of Wind Engineering and Industrial Aerodynamics*, 62(1), p. 37–56.

Miles, S. and Westbury, P., 2003. Practical tools for wind engineering in the built environment. *QNET-CFD Network Newsletter*, 21(2), pp. 11-14.

Milliez, M. and Carissimo, B., 2007. Numerical simulations of pollutant dispersion in an idealized urban area, for different meteorological conditions. *Boundary-Layer Meteorology*, 122(2), p. 321–342.

Mochida, A., Tominaga, H., Iwata, T and Tabata, Y., 2006. Optimization of tree canopy model for CFD prediction of wind environment at pedestrian level.

Yokohama, Japan., The Fourth International Symposium on Computational Wind Engineering (CWE2006).

Nicholson, S.E., 1975. A pollution model for street-level air. *Atmospheric Environment*, 9(1), p. 19–31.

O’Sullivan, J.P., 2011. Consistent boundary conditions for flows within the atmospheric boundary layer. *Journal of Wind Engineering and Industrial Aerodynamics*, 99(1), pp. 65-77.

Oke, T.R., 1988. Street design and urban canopy layer climate. *Energy and Buildings*, 11(1-3), p. 103–113.

Panofsky, H. A. and Dutton, J. A., 1984. *Atmospheric turbulence, models and methods for engineering applications*. New York, USA.: John Wiley & Sons.

Parente, A., Gorle, C., Van Beeck, J., and Benocci, C., 2011. Improved k- ϵ model and wall function formulation for the RANS simulation of ABL flows. *Journal of Wind Engineering and Industrial Aerodynamics*, 99(4), pp. 267-278.

Park, J.O., 2015. The effects of air pollution on mortality in South Korea. *Procedia Environmental Sciences* 26.

Rafailidis, S. and Schatzmann, M., 1996. *Environmental Wind Tunnel Laboratory at Hamburg University*. Available at: http://www.mi.uni-hamburg.de/fileadmin/files/static_html/windtunnel/.

Rafailidis, S., 1997. Influence of building areal density and roof shape on the wind characteristics above a town. *Boundary-Layer Meteorology*, 85(2), pp. 255-271.

Raupach, M. R., Antonia, R. A. and Rajagopalan, S., 1991. Rough-wall turbulent boundary layers. *Applied Mechanics Review*, 44(1), pp. 1-25.

Raupach, M. R., 1994. Simplified expressions for vegetation roughness length and zero-plane displacement as functions of canopy height and area index. *Boundary Layer Meteorology*, 71(1-2), pp. 211-216.

Richards, P. J., 1993. Appropriate boundary conditions for computational wind engineering models using the k- ϵ model. *Journal of Wind Engineering and Industrial Aerodynamics*, Volym 46&47, p. 145–153.

Rotach, M. W., 1994. Determination of the zero plane displacement in an urban area. *Boundary Layer Meteorology*, 67(1-2), pp. 187-193.

Rotach, M. W., 2001. Simulation of urban-scale dispersion using a Lagrangian stochastic dispersion model. *Boundary-Layer Meteorology*, 99(3), pp. 379-410.

Rotach, M.W., 1993. Turbulence close to a rough urban surface, Part I: Reynolds stress. *Boundary-Layer Meteorology*, 65(1-2), pp. 1-28.

Roth, M., 2000. (2000). Review of atmospheric turbulence over cities. *Quarterly Journal of Royal Meteorological Society*, 126(564), pp. 941-990.

Rusche, H., 2002. Computational fluid dynamics of dispersed two-phase flows at high phase fractions. 2003. Imperial College London (University of London).

Salizzoni, P., Soulhac, L. and Mejean, P., 2009. Street canyon ventilation and atmospheric turbulence. *Atmospheric Environment*, 43(32), pp. 5056-5067.

Schatzmann, M. and Leidl, B., 2011. Issues with validation of urban flow and dispersion CFD models. *Journal of Wind Engineering and Industrial Aerodynamics*, 99(4), pp. 169-186.

Schatzmann, M., Olesen, H. and Franke, J., 2010. Cost 732 model evaluation case studies: Approach and results, Hamburg, Germany: COST Action 732.

Sini J.F., Anquetin, S. and Mestayer, P. G., 1996. Pollutant dispersion and thermal effects in urban street canyons. *Atmospheric Environment*, 30(15), pp. 2659-2677.

Stathopoulos, T. and Storms, R., 1986. Wind environmental conditions in passages between buildings. *Journal of Wind Engineering and Industrial Aerodynamics*, 24(1), p. 19–31.

Stathopoulos, T., Wu, H., Bedard, C., 1992. Wind environment around buildings: a knowledge-based approach. *Journal of Wind Engineering and Industrial Aerodynamics*, 44(1-3), p. 2377–2388.

Theodoridis, G. and Moussiopoulos, N., 2000. Influence of building density and roof shape on the wind and dispersion characteristics in an urban area: a numerical study. *Environment Monitoring and Assessment*, 65(1-2), pp. 407-415.

Thielen, L. Hanjalic, K., Jonker, H., and Manceau, R., 2005. Predictions of flow and heat transfer in multiple impinging jets with an elliptic-blending second-moment closure, *International Journal of Heat and Mass Transfer*, 48.

Tominaga, Y. and Stathopoulos, T., 2007. Turbulent Schmidt numbers for CFD analysis with various types of analysis. *Atmospheric Environment*, 41(37), pp. 8091-8099.

Tominaga, Y. and Stathopoulos, T., 2010. Numerical simulation of dispersion around an isolated cubic building: model evaluation of RANS and LES. *Building and Environment*, 45(10), p. 2231–2239.

Tominaga, Y. and Stathopoulos, T., 2011. CFD modeling of pollution dispersion in a street canyon: Comparison between LES and RANS. *Journal of Wind Engineering and Industrial Aerodynamics*, 99(4), p. 340–348.

Tominaga, Y., Mochida, A., Yoshie, R., Kataoka, H., Nozu, T., Yoshikawa, M. and Shirasawa, T., 2008. AIJ guidelines for practical applications of CFD to pedestrian wind environment around buildings. *Journal of Wind Engineering and Industrial Aerodynamics*, 96(10-11), pp. 1749-1761.

Uehara, K. and Murakami, S., 2000. Wind tunnel experiments on how thermal stratification affects flow in and above urban street canyons. *Atmospheric Environment*, 34(10), p. 1553–1562.

United Nations, Department of Economic and Social Affairs, Population Division (2011). *World Urbanization Prospects: The 2011 Revision, Highlights*.

United Nations, Department of Economic and Social Affairs, Population Division (2014). *World Urbanization Prospects: The 2014 Revision, Highlights (ST/ESA/SER.A/352)*.

United Nations. *Transforming our world: The 2030 agenda for sustainable development*. New York: 2015.

Vardoulakis, S., Fisher, B. and Pericleous, K., 2003. Modeling air quality in street canyons: a review. *Atmospheric Environment*, 37(2), pp. 155-182.

Vieira, C.B., Niceno, B. and Su, J., 2013. Computational simulation of turbulent natural convection in a corium pool. *International Nuclear Atlantic Conference*.

Wedding, J.B., Lombardi, D.J. and Cermak, J.E., 1977. A wind tunnel study of gaseous pollutants in city street canyons. *Journal of Air Pollutant Control Association*, Volym 27, p. 557–566.

Wieringa, J., 1992. Updating Davenport Roughness Classifications. *Journal of Wind Engineering and Industrial Aerodynamics*, 41(1-3), pp. 357-368.

Wilcox, D. C., 1988. Reassessment of the scale-determining equation for advanced turbulence models. *AIAA Journal*, Volym 26, pp. 1299-1310.

Wilson, D.J., 1979. Flow patterns over flat roofed buildings and application to exhaust stack design. *ASHRAE Transactions*, Volym 85, pp. 284-295.

Xie, X. M, Huang, Z. and Wang, J., 2005. Impact of building configuration on air quality in street canyon. *Atmospheric Environment*, 39(25), p. 4519–4530.

Yakhot, V. and Orszag, S. A., 1986. Renormalization group analysis of turbulence. *Journal of Scientific Computing*, 1(1).

Yakhot, V., Orszag, S. A., Thangam, S., Gatski, B., Speziale, C. G., 1992. Development of turbulence models for shear flows by a double expansion technique. *Physics of Fluids*, 4(7), pp. 1510-1521.

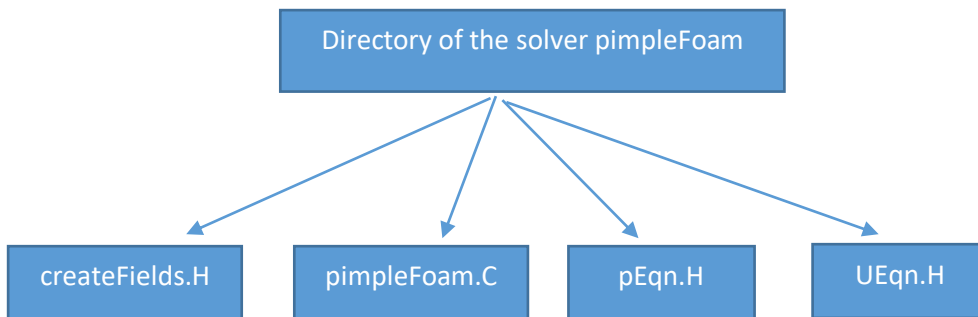
Yang, Y., Gu, M., Chen, S., and Jin, X., 2009. New inflow boundary conditions for modeling the neutral equilibrium atmospheric boundary layer in computational wind engineering. *Journal of Wind Engineering and Industrial Aerodynamics*, 97(2), p. 88–95.

Yassin, M. F., 2011. Impact of height and shape of building roof on air quality in urban street canyons. *Atmospheric Environment*, 45(29), pp. 5220-5229.

Appendix – Implementation of a solver in OpenFoam

OpenFOAM is a code in C++, which can be used to generate executable files (i.e. applications). The applications in OpenFOAM consist of two groups, i.e. solvers and utilities.

A solver commonly consists of a main file and 3 header files.



The variables and parameters is defined in the file createFields.H. pEqn.H contains the equation of pressure and UEqn.H contains the equation of velocity (RANS equation). The main file pimpleFoam.C contains the code related to solving algorithm.

In this study, we need to add an equation of pollutant transport. The hydrodynamics model (RANS equations) is not changed. In order to implement an equation into the code, it is necessary to modify the file createFields.H and pimpleFoam.C. Below are the codes in detail.

1. SGDH approach – pimpleSGDHFoam solver

1.1. The change in the file createFields.H

// add new line

Info<< "Reading transportProperties\n" <<endl;

IOdictionary transportProperties

(

IOobject

(

"transportProperties",

runTime.constant(),

mesh,

IOobject::MUST_READ_IF_MODIFIED,

IOobject::NO_WRITE

)

);

dimensionedScalar Dc

(

"Dc",

dimViscosity,

transportProperties.lookup("Dc")

```
);
```

```
dimensionedScalar Sc
```

```
(
```

```
    "Sc",
```

```
    transportProperties.lookup("Sc")
```

```
);
```

```
// end up new line
```

```
Info<< "Reading field p\n" << endl;
```

```
volScalarField p
```

```
(
```

```
    IOobject
```

```
    (
```

```
        "p",
```

```
        runTime.timeName(),
```

```
        mesh,
```

```
        IOobject::MUST_READ,
```

```
        IOobject::AUTO_WRITE
```

```
    ),
```

```
    mesh
```



```
);
```

```
// add new line
```

```
Info<< "Reading field C\n" << endl;
```

```
volScalarField C
```

```
(
```

```
    IOobject
```

```
    (
```

```
        "C",
```

```
        runTime.timeName(),
```

```
        mesh,
```

```
        IOobject::MUST_READ,
```

```
        IOobject::AUTO_WRITE
```

```
    ),
```

```
    mesh
```

```
);
```

```
// end up new line
```

```
Info<< "Reading field U\n" << endl;
```

```
volVectorField U
```

```
(
```

```
    IOobject
```

```

(
    "U",

    runTime.timeName(),

    mesh,

    IOobject::MUST_READ,

    IOobject::AUTO_WRITE

),

mesh

);

#include "createPhi.H"

label pRefCell = 0;

scalar pRefValue = 0.0;

setRefCell(p, pimple.dict(), pRefCell, pRefValue);

mesh.setFluxRequired(p.name());

singlePhaseTransportModel laminarTransport(U, phi);

autoPtr<incompressible::turbulenceModel> turbulence

(

    incompressible::turbulenceModel::New(U, phi, laminarTransport)

);

#include "createMRF.H"

```

1.2. The change in the file pimpleSGDH.C

```
Info<< "\nStarting time loop\n" << endl;

while (runTime.run())

{

    #include "readTimeControls.H"

    #include "CourantNo.H"

    #include "setDeltaT.H"

    runTime++;

    Info<< "Time = " << runTime.timeName() << nl << endl;

    // --- Pressure-velocity PIMPLE corrector loop

    while (pimple.loop())

    {

        #include "UEqn.H"
```

```

// --- Pressure corrector loop

while (pimple.correct())

{

    #include "pEqn.H"

}


if (pimple.turbCorr())

{

    laminarTransport.correct();

    turbulence->correct();

}

}

// add new line

fvScalarMatrix CEqn

(

    fvm::ddt(C)

    + fvm::div(phi,C)

    - fvm::laplacian(Dc + turbulence->nuEff())/Sc,C)

);

CEqn.solve();

// end up new line

```

```

runTime.write();

Info<< "ExecutionTime = " << runTime.elapsedCpuTime() << " s"
    << " ClockTime = " << runTime.elapsedClockTime() << " s"
    << nl << endl;
}

Info<< "End\n" << endl;

return 0;

```

2. GGDH approach – pimpleGGDHFoam solver

2.1. The change in the file createFields.H

```

// add new line

Info<< "Reading transportProperties\n" << endl;

IOdictionary transportProperties
(
    IOobject

```

```
(
    "transportProperties",
    runTime.constant(),
    mesh,
    IOobject::MUST_READ_IF_MODIFIED,
    IOobject::NO_WRITE
)
);
```

dimensionedScalar Dc

```
(
    "Dc",
    dimViscosity,
    transportProperties.lookup("Dc")
);
```

dimensionedScalar Sc

```
(
    "Sc",
    transportProperties.lookup("Sc")
);
```

// end up new line

```
Info<< "Reading field p\n" << endl;
```

```
volScalarField p
```

```
(
```

```
    IOobject
```

```
    (
```

```
        "p",
```

```
        runTime.timeName(),
```

```
        mesh,
```

```
        IOobject::MUST_READ,
```

```
        IOobject::AUTO_WRITE
```

```
    ),
```

```
    mesh
```

```
);
```

// add new line

```
Info<< "Reading field C\n" << endl;
```

```
volScalarField C
```

```
(
```

```
    IOobject
```

```

(
    "C",

    runTime.timeName(),

    mesh,

    IOobject::MUST_READ,

    IOobject::AUTO_WRITE

),

mesh

);

// end up new line

```

```

Info<< "Reading field U\n" << endl;

```

```

volVectorField U

```

```

(
    IOobject
    (
        "U",

        runTime.timeName(),

        mesh,

        IOobject::MUST_READ,

        IOobject::AUTO_WRITE
    )

```



```

    ),

    mesh

);

#include "createPhi.H"


label pRefCell = 0;

scalar pRefValue = 0.0;

setRefCell(p, pimple.dict(), pRefCell, pRefValue);

mesh.setFluxRequired(p.name());


singlePhaseTransportModel laminarTransport(U, phi);


autoPtr<incompressible::turbulenceModel> turbulence

(

    incompressible::turbulenceModel::New(U, phi, laminarTransport)

);

#include "createMRF.H"

```

2.2. The change in the file pimpleGGDHFoam.C

```
Info<< "\nStarting time loop\n" << endl;

while (runTime.run())
{
    #include "readTimeControls.H"

    #include "CourantNo.H"

    #include "setDeltaT.H"

    #include "RASModel.H"

    runTime++;

    Info<< "Time = " << runTime.timeName() << nl << endl;

    // --- Pressure-velocity PIMPLE corrector loop

    while (pimple.loop())
    {
        #include "UEqn.H"
```

```

// --- Pressure corrector loop

while (pimple.correct())

{

    #include "pEqn.H"

}

if (pimple.turbCorr())

{

    laminarTransport.correct();

    turbulence->correct();

}

}

// add new line

volSymmTensorField fluxTimeScale

(

    0.2*turbulence->mut()/(0.0845*turbulence->k())*turbulence->R()

);

volScalarField alphaEff

(

    "alphaEff",

```

```

        mag(fluxTimeScale)

    );

    fvScalarMatrix CEqn
    (
        fvm::ddt(C)
        + fvm::div(phi,C)
        - fvm::laplacian(Dc+alphaEff,C)
    );

    CEqn.solve();

// end up new line

    runTime.write();

    Info<< "ExecutionTime = " << runTime.elapsedCpuTime() << " s"
    << " ClockTime = " << runTime.elapsedClockTime() << " s"
    << nl << endl;

}

Info<< "End\n" << endl;

return 0;

```

초 록

본 연구에서는 상이한 지형조건의 도시협곡에서의 공기 흐름과 오염확산 양상을 연구하기 위해, 오픈소스 CFD 프로그램인 OpenFOAM 을 기반으로 하는 수치모델을 개발하였다. 수치모의에서 바람유동에 의해 발생하는 오염물질 이송은 운동량 방정식과 연동되는 스칼라 수송 방정식에 의해 기술되며, 운동량 방정식은 RANS(Reynolds Averaged Navier-Stokes) 방정식을 차용하였다. 난류흐름은 다양한 two-equation 난류모형들을 적용하여 본 연구에 적용할 수 있는 실용적이고 효율적인 최적의 난류모형을 선정하였다. 스칼라 수송 방정식에서는 난류 확산항을 기술하는 다음과 같은 두 가지 방법이 있다: Standard Gradient Diffusion Hypothesis(SGDH)와 Generalized Gradient Diffusion Hypothesis(GGDH). 연구 결과, GGDH 방식이 SGDH 방식보다 더 나은 결과를 도출하였으며 각기 다른 실험조건마다 난류 슈미트 수를 조정해주어야 하는 SGDH 방식의 한계를 극복하였다.

수치모델은 다양한 종횡비(도시협곡 내 빌딩의 높이와 너비의 비율)와 지붕 형상(flat, shed, gable, and round)에 대해 수행된 저명한 실험실 실험결과와 비교 및 검증하였다. 수치모델결과와 실험실 실험결과를 비교한 결과, 흐름과 오염물질 분포 양상이 상당히 일치함을 확인할 수 있었다. 또한 수치모델결과는 3 차원 실험조건에서도 실험결과와 합리적인 범위에서

일치하였으며, 이는 본 연구에서 개발된 수치모델이 실제 도시협곡 내 기류와 오염물질 이송을 연구하기 위해 적용될 수 있음을 나타낸다.

마지막으로 본 연구에서 제시되는 수치모델은, 수많은 고층빌딩들을 포함하며 wind shed 가 인근 보행자들과 주변지역의 미세기후에 어떻게 영향을 끼치는지 등 몇 가지 흥미로운 공기역학적 문제들이 내포되어 있는 일본 도쿄의 신주쿠 지역을 대상으로 적용되었다. 본 연구의 수치모델의 결과는 개발된 수치모델이 신주쿠 도시협곡의 실제 공기흐름을 재현할 수 있음을 보여준다.

주요어: 수치모델, 바람유동, 오염물질 이송, 도시협곡, OpenFOAM

학번: 2013-30777.